# 論文 / 著書情報
# Article / Book Information

| | |
|---|---|
| 題目(和文) | 接触熱分解とCO2ガス化プロセスによる電気電子機器廃棄物からの燃料油と有用資源の同時回収 |
| Title(English) | Integrated Recovery of Valuable Resource and Fuel Oil from E-wastes by Catalytic Pyrolysis and CO2 Gasification Process |
| 著者(和文) | 武<br>虎 |
| Author(English) | Hu Wu |
| 出典(和文) | 学位:博士（工学）,<br>学位授与機関:東京工業大学,<br>報告番号:甲第9841号,<br>授与年月日:2015年3月26日,<br>学位の種別:課程博士,<br>審査員:吉川　邦夫,加茂　徹,高橋　史武,時松　宏治,梶谷　史朗 |
| Citation(English) | Degree:,<br>Conferring organization: Tokyo Institute of Technology,<br>Report number:甲第9841号,<br>Conferred date:2015/3/26,<br>Degree Type:Course doctor,<br>Examiner:,,,, |
| 学位種別(和文) | 博士論文 |
| Type(English) | Doctoral Thesis |

**Doctoral Dissertation**

# Integrated Recovery of Valuable Resource and Fuel Oil from E-wastes by Catalytic Pyrolysis and $CO_2$ Gasification Process

**Hu Wu**

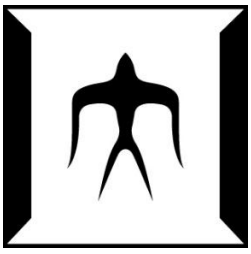

**Department of Environmental Science and Technology**

**Interdisciplinary Graduate School of Science and Engineering**

**Tokyo Institute of Technolog**

# Tables of Contents

# Chapter 1

# General Introduction

## 1.1. Waste Electrical and Electronic Equipment (WEEE)

On the one hand, as the increase and improvement of global economy and technology, the consumption of electrical and electronic equipment dramatically increased worldwide. On the other hand, the lifespan of electrical and electronic equipment also become shorter and shorter. Therefore, in the global, there was about 40 million tons of waste electrical and electronic equipment (WEEE) generated every year, which already become the main stream of the solid waste [1-1]. In addition, WEEE is one of the fastest growing waste streams in the European Union (EU). For instance, 9 million tons of WEEE were generated in 2005, and it was expected to grow to more than 12 million tons by 2020 [1-2]. The United Nations Environment Programme (UNEP) also predicted that an increase of 200-400% in the generation of WEEE in the developing countries from 2010 – 2020 [1-3,1-4]. Taking China for example, it was predicted that by 2020, the old computers will increase by 200 to 400 percent from 2007 levels and the amount of discarded mobile phones will be about 7 times higher by 2020 than that of 2007 levels. Whilst, by 2020, WEEE from old televisions will be 1.5 to 2 times higher than that of 2007 in China. In the case of India, it was predicted that by 2020, the amount of WEEE from discarded computers, mobile phones and televisions will be 5, 18 and 3 times larger than that of 2007 level, respectively [1-1].

According to equipment sorts, WEEE is normally divided into 10 categories in EU, such as refrigerator, washing machine, television, computer, phones et al. According to the EU 10 WEEE categories, the weight percentage of each WEEE collected in EU is listed in Table 1.1 [1-5,1-6],

which indicates that the large household appliances, consumer equipment and IT and telecommunications equipment are the main compositions of the collected WEEE in EU.

Table 1.1 Typical composition and percentage of WEEE collected in EU according to the EU 10 WEEE categories.

| No. | EU WEEE Category (example appliances in parentheses) | wt.% of collected WEEE |
|---|---|---|
| 1 | Large household appliances (refrigerators, washing machines) | 49.07 |
| 2 | Small household appliances (vacuum cleaners, toasters) | 7.01 |
| 3 | IT and telecommunications equipment (phones, laptops) | 16.27 |
| 4 | Consumer equipment (DVD players, televisions) | 21.10 |
| 5 | Lighting equipment (lamps) | 2.40 |
| 6 | Electrical and electronic tools (drills, saws) | 3.52 |
| 7 | Toys, leisure and sports equipment (game consoles) | 0.11 |
| 8 | Medical devices (pulmonary ventilators, dialysis) | 0.12 |
| 9 | Monitoring and control instruments (smoke detector, thermostats) | 0.21 |
| 10 | Automatic dispensers (drink, money dispensers) | 0.18 |

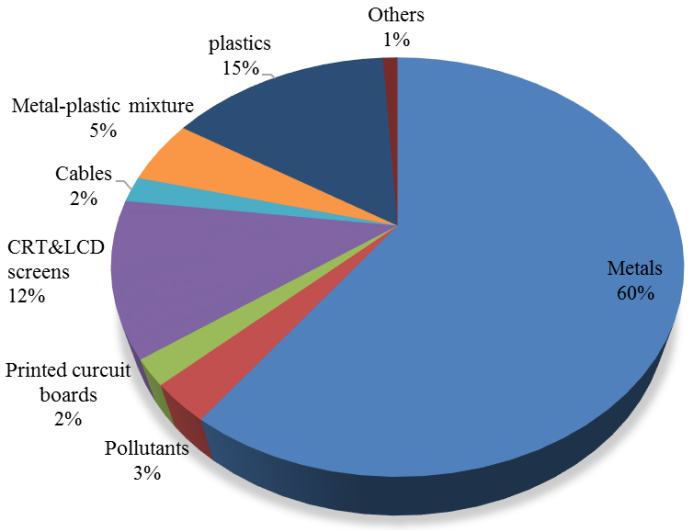


Figure 1.1 Typical material fractions in WEEE, adapted from Widmer et al. [1-6].

The composition of WEEE is quite diverse and differs in products across different categories and countries. Generally, according to material composition sorts, WEEE mainly consisted of five categories of materials: ferrous metals, non-ferrous metals, glass, plastics and others. In general, iron and steel are the most common materials used in electrical and electronic equipment, which account for almost half of the total weight of WEEE. Plastic are the second largest composition by weight, representing about 21 wt.% of WEEE. Whiles, the percentage of non-ferrous metals, including precious and rare metals in WEEE was approximately 13 wt.%, which also contain cupper and it accounts for about 7 wt.% [1-5]. In addition, for different statistical methods and classification method, the percentage of metal, plastic and others fractions are totally different. It was reported by Widmer et al. [1-6] that the metals accounts for 60 wt.% of the total WEEE weight, as shown in Figure 1.1. However, Sodhi and Reimer [1-7], as well as Yang et al. [1-8] reported that WEEE mainly comprised of 40 wt. % metals, 30 wt.% plastics and 30wt.% refractory oxides, as shown in Figure 1.2. In addition, the production, price and distribution of certain main metals used in EEE is shown in Table 1.2. When these EEE was discarded as WEEE, the precious and rare metals contained in these WEEE will be enormous, valuable and worth recycling.

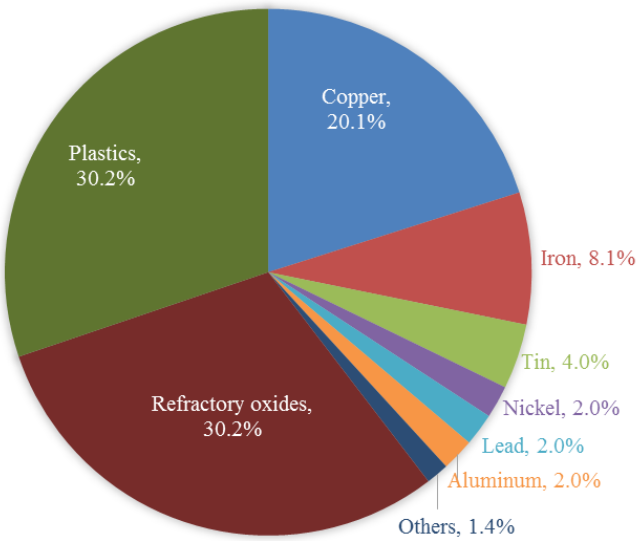


Figure 1.2 The composition of WEEE (Sodhi and Reimer [1-7], Yang, et al.[1-8])

Table 1.2 Value and application of certain main metals used in EEE

| Metal | Primary production | Demand for EEE | Demand/ production | Price | Main application |
|---|---|---|---|---|---|
| | t/y | t/y | % | USD/kg | |
| Ag | 2000 | 6000 | 30 | 430 | Contacts, switches, solders … |
| Au | 2500 | 300 | 12 | 22280 | Bonding wire, integrated circuits… |
| Pd | 230 | 33 | 14 | 11413 | Multilayer, capacitor, connector… |
| Pt | 210 | 13 | 6 | 41957 | Hard disk, themocouple, fuel cell… |
| Ru | 32 | 27 | 84 | 18647 | Hard disk, plasma displays… |
| Cu | 15000000 | 4500000 | 30 | 7 | Cable, wire, connector… |
| Sn | 275000 | 90000 | 33 | 15 | Solders… |
| Sb | 130000 | 65000 | 50 | 6 | Flame retardant, CRT glass… |
| Co | 58000 | 11000 | 19 | 62 | Rechargeable batteries… |
| Bi | 5600 | 900 | 16 | 31 | Solders, capacitor, heat sink… |
| Se | 1400 | 240 | 17 | 72 | Electro-optic, copier, solar cell… |
| In | 480 | 380 | 79 | 682 | LCD glass, solder, semiconductor… |

Furthermore, for various equipment category, the composition was also completely different [1-9]. In the case of the category 2 for small household applications, they contain 40.31 wt.% iron and steel, 36.68 wt.% plastics, 14.01 wt.% aluminum, 6.92 wt.% cupper, 2.08 wt.% other metals and materials. As for the category 3 (IT and telecommunications equipment), they consist of 42.31 wt. % iron and steel, 27.53 wt. % plastics, 19.81 wt. % aluminum, 8.92 wt. % cupper, 0.04 wt. % nickel, 0.01 wt. % silver and others materials. For the category 4 (consumer equipment), they are made up of 36.42 wt.% plastics, 33.90 wt.% iron and steel, 12.14 wt.% aluminum, 6.74 wt.% cupper and others materials. In the case of category 6 (electrical and electronic tools), they comprise 48.03 wt.% plastics, 29.14 wt.% iron and steel, 9.01 wt.% aluminum, 4.90 wt.% cupper

and others. As for the category 7 (toys, leisure and sports equipment), they are made up of 69.82 wt.% plastics, 9.99 wt.% iron and steel, 2.13 wt.% cupper, 1.86 wt.% alumina and others metals and materials [1-9]. Therefore, it could be concluded that the vast majority of WEEE is made up by plastic and the major metals (iron, aluminum, copper), which are valuable and worth recycling resource and feedstock.

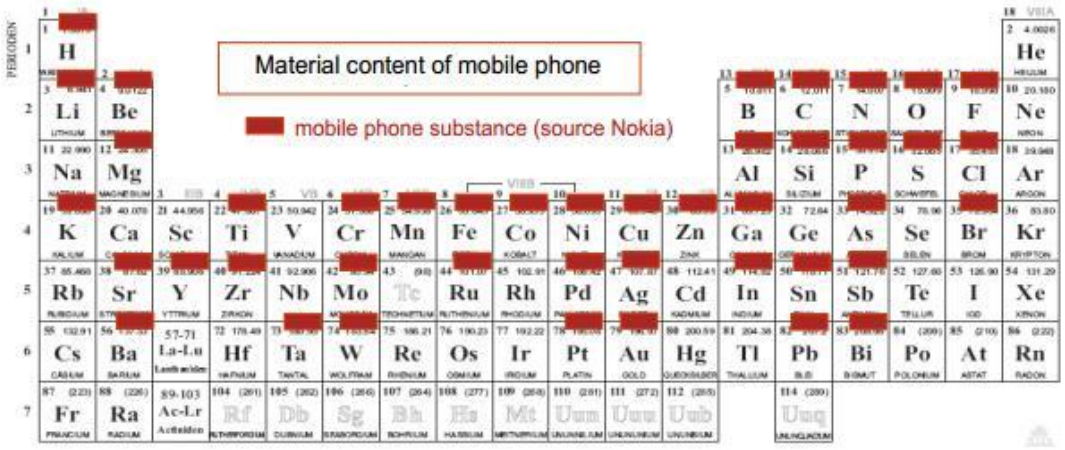


Figure 1.3. The material content of mobile phone (source Nokia)

Furthermore, there are a large amount of rare metals and precious metals contained in the cell phone and print circuit board, as shown in Figure 1.3. And the use of mobile phones has grown rapidly in recent decades. According to the report released by the UNEP and the Secretariat of the Basel Convention, the use of mobile phones has grown exponentially, from the first few users in the 1970s, to 1.76 billion in 2004, and more than 3 billion in April 2008 [1-10]. Worldwide sales of mobile phones reached 294.3 million units in the first quarter of 2008, a 13.6 per cent increase over the first quarter of 2007, according to Gartner, Inc. [1-11]. It was reported by the U.S. Geological Survey that close to 200 million cell phones are deserted every year, collectively containing upwards of 2,000 metric tons of copper, 50 metric tons of silver, 4 metric tons of gold and 2 metric tons of palladium. Indeed, a recent UN report on electronic waste also highlighted the significance of gold extraction. According to the report, 1 metric ton of cell phone handsets could yield 340 grams of gold which is enough to bring in a sizable profit for anyone with the proper resources for handling large-scale recycling and extracting precious metals from mobile

phones [1-3]. Figure 1.4 shows the metal element distribution in the cell phone [1-12]. It also indicated that there are metals densely distributed in printed circuit board of the cell phone. In Japan, WEEE, especially the waste computer and cell phone was called as urban mines. Therefore, in the global, how to conduct effective and low-cost recovery, recycle and reuse of the worth recycled and valuable WEEE have attracted a large amount of attention.

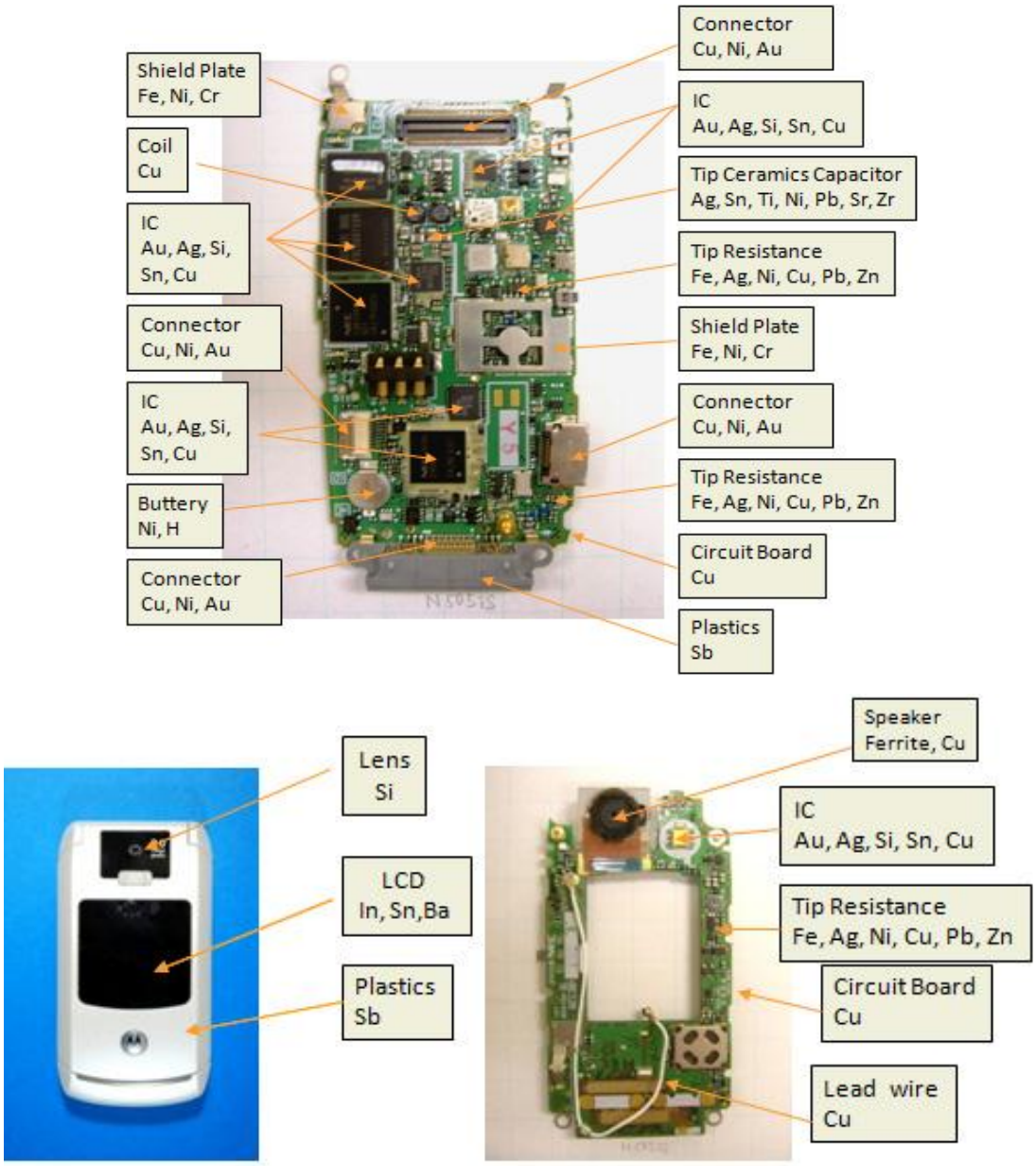


Figure 1.4. Metal elements used in each fraction of cell phone [1-12].

## 1.2. WEEE plastics

As mentioned above, there are not only lots of steel and iron, copper, aluminum, precious and rare metals contained in WEEE, but also a large amount of plastics are contained in WEEE. It was reported by Yang and co-worker [1-8] that WEEE plastics account for about 30 wt.% of the total amount of WEEE, and are important parts of WEEE. In addition, the plastic from WEEE are also an important environmental problems because these plastics commonly contain toxic halogenated flame retardants which may lead to serious environmental pollution and human health issues. It was reported by Eriksson and Jakobsson [1-8,1-13] that brominated flame retardants (BFRs) had certain serious impact on mammals' nervous system and possibly interfered the reproductive system of mammals. Especially, the combustion of certain types of BFRs will result in the formation of more toxic and accumulative products such as lower brominated biphenyl ether congeners and PBDD/Fs [1-8, 1-14].

The complex composition of WEEE makes the effective WEEE recovery very challenging. Different EEE may use different polymer types for their specific purpose such as conforming to environmental requirements or stress intensity criterions. This fact leads to WEEE plastics a complex mix of materials of different, often incompatible, polymer types [1-15,1-16]. Considering only the plastic content of WEEE, it was reported by Martinho and co-workers that EEE (and WEEE of the near future) can be consisted of more than 15 different types of engineering plastics, including acrylonitrile–butadiene styrene (ABS), high-impact polystyrene (HIPS), polypropylene (PP), polystyrene (PS), styrene-acrylonitrile (SAN), polyesters, polyurethane (PU), polyamide (PA), blends of polycarbonate (PC)/ABS and blends of HIPS/poly(p-phenylene oxide) (PPO) [1-17,1-18]. In addition, Figure 1.5 shows typical compositions of WEEE plastics investigated by Freegard et al. [1-15]. Thermoplastics, such as HIPS, ABS, PVC and PC are the most important parts of WEEE plastics. The combination of HIPS and ABS already account for approximate 55% of all WEEE plastics [1-15], whose molecular structure is shown in Figure 1.6. HIPS is a versatile, economical and impact-resistant plastic that is easy to fabricate. HIPS is often specified for low strength structural applications

when the impact resistance, the machinability, and low cost are required. It is frequently used machining pre-production prototypes since it has excellent dimensional stability and is easy to fabricate, paint, and glue. It was commonly used in (1) Consumer products: appliance components, toy, TV and audio-visual equipment parts, recording tape cassettes, bicycle trailer, toys; (2) Automotive industry: Instrument panels and fittings, gasoline tanks; (3) Food services: hot and cold drinking cups; (4) Office products: computer housings. ABS is a terpolymer of acrylonitrile, butadiene and styrene. Usual compositions are about half styrene with the balance divided between butadiene and acrylonitrile. ABS was one of the most widely used thermoplastics today. ABS provides excellent surface appearance, strength and stiffness, toughness and chemical resistance, as well as its processing ease and versatility. It was usually applied in (1) Aerospace applications; (2) Automotive electronics and automotive interior trim; (3) Industrial applications such as electrical housing and computer components; (4) Consumer uses such as TV cabinets, food mixers, telephone sets, vacuum cleaners, LEGO building bricks, razors and refrigerator door liners; (5) Construction applications such as vacuum forming for baths and shower trays and is sometimes preferred to PVC for high and low temperatures. There are also some disadvantages for HIPS and ABS plastics, such as limited weathering resistance; moderate heat, moisture and chemical resistance; Flammable with high smoke generation; relatively high cost; poor resistant to organic solvents et al.

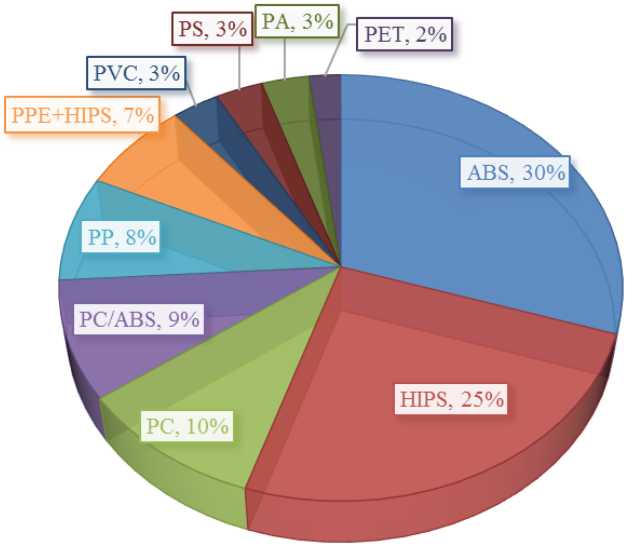


Figure 1.5. Various polymers in WEEE plastics [1-15]

ABS

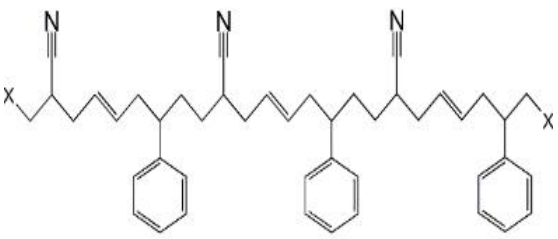

HIPS

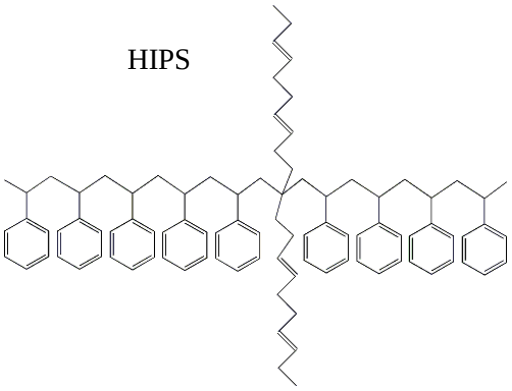

Figure 1.6. The molecular structure of ABS and HIPS

## 1.3. Flame retardants in WEEE plastics

Table 1.3. Properties of five common BFRs: TBBPA, DDO, HBCD and DDE [1-8, 1-12].

| **Brominated flame retardants** | **Chemical structures** | **Bromine percentage (%)** |
|---|---|---|
| Tetrabromobisphenol- A (TBBPA) | 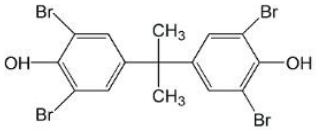 | 58.50 |
| Decabromodiphenyl oxide (DDO) | 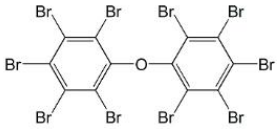 | 83.00 |
| 1,2,5,6,9,10-Hexabromocyclodecane (HBCD) | 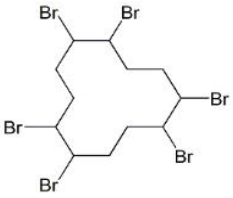 | 74.71 |
| Decabromodiphenyl ethane (DDE) | 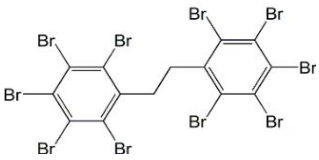 | 82.30 |
| Bistribromophenoxyethane (BTBPE) | 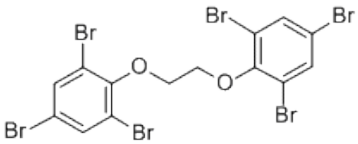 | 69.72 |

Flame retardants are chemicals which are usually added into manufactured materials, such as plastics and textiles, and surface finishes and coatings, in order to prevent, suppress or delay the production of flames to prevent the spread of fire. There are more than 175 different types of flame retardants[1-19] available which include about 27% of halogenated organic compounds [1-8], as well as other types of flame retardants such as organo-phosphorus contained compounds and aluminum hydroxide contained compounds, et al. Halogenated flame retardants are also known as organohalogen flame retardants, which typically contains chlorinated and brominated flame retardants. It was reported that there were 390000 tons of brominated flame retardants (BFRs) sold in 2011, which accounted for 19.7 wt.% of the flame retardants market [1-20]. The BFRs are commonly added into the engineering plastics to reduce their flammability. These plastics containing brominated flame retardants are widely used in EEE, such as printed circuit boards, connectors, plastic covers and cables. Vehlow and co-workers [1-21] reported that there were about 30 wt.% of the plastics used in EEE containing certain flame retardants. In addition, the plastics with halogenated flame retardants take up about 41 wt.% of all flame retarded EEE plastics [1-8].

Table 1.4. Potential Health risks of some BFRs.

| **BFRs** | **Health risks** | **References** |
|---|---|---|
| PBDEs | Cryptorchidism | [1-23] |
| PBDEs | OHCs present in the serum of pregnant women would transfer over the placenta to the infants | [1-24] |
| PBDEs | Diabetes | [1-25] |
| PBDEs | Highest exposure individual scored five less IQ points | [1-26] |
| TBBPA | Current use of TBBPA may be a matter of concern for human health | [1-27] |
| TBBPA | Affected three different proteins involved in important processes of neonatal brain development | [1-28] |
| HBCD | HBCD may disrupt TH-mediated brain development | [1-29] |
| HBCD | HBCD can potentially impact the thyroid system of fish | [1-30] |

At present, there are at least 75 different kinds of BFRs commercially produced. In addition,

the category of BFRs still increases with development of synthesis technology. Tetrabromobisphenol- A (TBBPA), Decabromodiphenyl oxide (DDO), 1,2,5,6,9,10-Hexabromocyclodecane (HBCD) Deca-bromodiphenyl ethane (DDE) and Bistribromophenoxyethane (BTBPE) are the most widely used BFRs, whose chemical structures and bromine percentage are shown in Table 1.3. However, some brominated flame retardants were proved to be persistent, bioaccmulative, and toxic to humans, animals and environment. And then they could lead to neurobehavioral effects and endocrine disruption of humans and animals. Yang and co-workers have summarized the hazards and health risks of some BFRs [1-8], as shown in Table 1.4. Amount the BFRs, brominated diphenyl ethers (DBE) are the most toxic compounds. The use of Deca-BDE in the EU has thus been banned in electrical and electronic applications since 1 July 2008. The Penta- and Octa-BDE formulations have been prohibited to be used in the worldwide [1-22]. However, the harmless of BFRs is still very difficult to be controlled. Consequently, the presence of BFRs in the EEE will also be very serious problem and challenging for the effective recycling of WEEE.

## 1.4. The management and treatment methods of WEEE and WEEE plastics

### 1.4.1 Artificial separation

Figure 1.7. Artificial separation of WEEE in Guiyu of China.

According to government statistics of China, over 25 million TVs, 5.4 million refrigerators, 10 million washing machines, 1 million air conditioners, 12 million computers, 6 million printers and 40 million mobile phones were thrown out in 2009 [1-31]. It was estimated that by 2010, the number of obsolete larger household appliances and PC equipment in China would be as follows [1-32]: Televisions > 58 million units; Refrigerators >9 million units; Washing machines > 11 million units; Air conditioners > 12 million units; PCs > 70 million units. He et al. [1-33] reported an estimated WEEE increase of 13–15% per annum in China [1-5]. In addition, it was estimated that by 2020, the amount of computer and cell phone wastes will become 400% and 600% of those in 2007, respectively.

From 2006, China has become the world's largest manufacturer and exporter of electronic goods. Conversely, China was also the world's largest importer of WEEE. it was reported that 80% of WEEE in the world was exported into Asia, 70% of which was exported into China. It was counted that from 1990 – 2000, the exported WEEE increased from 0.99 million tons to 17.50 million tons [1-34]. Over 700 K people were employed in the WEEE industry in 2007, 98% of which were in the informal recycling sector [1-34]. It has been argued that the comparatively low labor costs and lax environmental and occupational laws make China a prime destination for developed countries export of WEEE. For instance, the labor cost for one worker is just 30 – 100 Yuan RMB. Furthermore, the large demand for low-priced secondary material is also an economic motive for the flow of WEEE from developed countries into China. [1-32].

It was reported by Yang et al. [1-35] that in 2005, there were a total of 503 recyclers estimated to import and recycle 9.55 million tons of mixed metals, cables, motors and other pre-processed products. In the same year, it is reported that in Guiyu, one of the major informal WEEE recycling towns, there were about 30–40 K people involved in WEEE treatment, treating over 1 million tons of WEEE annually. In this informal WEEE recycling company, most of the workers was employed to separate the valuable metals (copper, aluminum, et al) by hands with the simple tools of pliers, chainsaw and knife, as shown in Figure 1.7. Although, the efficiency of this separation methods was very low, when considering the low-cost labor and cheap WEEE resource, as well

as the considerable economic profit from the recycled second-hand metal materials, the separating methods was very popular in the early years in China. This simple recycling method used and the lack of environmental pollution control measures make these recycling activities result in serious environmental pollution and pose significant adverse health risks to workers and nearby residents [1-34]. It was reported that in Guiyu, the proportion of children with lead poisoning over 70 %.

Since 2009, China's Ministry of Commerce has been piloting a home appliance replacement scheme and Chinese government also promulgated certain policies to prevent the illegal import of WEEE from abroad [1-5]. Nevertheless, there are still some small informal recycling company import and recycle the WEEE by the artificial separation methods. Therefore, China government should take more serious policies or regulation to control or prevent this kind of recycling activities to avoid the potential environmental pollution and human's health crisis.

In addition, this artificial separating recycling method not only exists in China but also in other developing countries, such as, India and Africa. Therefore, all of the countries should cooperate and prevent the potential pollution and crisis from WEEE.

### 1.4.2 Land filling and combustion

Land filling of WEEE refers to roughly bury WEEE and WEEE plastic under layers of earth, which was also not a preferred method to recycle WEEE. Because land filling method is not a harmless method. At first, it will occupy a lot of valuable land resources [1-8]. In addition, WEEE plastic was non-biodegradable, it will take hundreds of years to degrade all of WEEE plastics. Last but not the least, it is well known that all landfills leak, which would cause the leakage of harmful materials into soil and pollute the precious underground water. It was reported that, early year, in the UK, government estimates show that we throw away over two million tons of electrical waste each year, mostly into landfill. Therefore the UK government promulgated the WEEE Regulations that aimed to reduce the amount of electrical and electronic waste going to landfill sites and improve recovery and recycling rates of these products [1-36].

Previously, combustion method was also widely applied in the recycling of WEEE to obtain valuable metal resources, as shown in Figure 1.8. Metals can be recovered from WEEE by incinerating the plastic fraction, but in practice this typically carried out without taking any measures to recover the combustion energy. In addition, the main bottleneck of this type of recycling is the possible formation of PBDD/Fs within the incineration process. To control emissions of PBDD/Fs, high temperature ( > 850 ℃) and long residence time ( > 2 s) are required [1-37]. Finally, during the combustion process, the metals are possibly oxidized and hereby will reduce the quality and value of the recycled metals. In addition, the thermal energy from the combustion of WEEE is also very difficult to be collected and used in the small-scale incinerator. Therefore, the combustion method used for the recycling of WEEE also have been prohibited by many developed countries, such as Japan, Germany and USA.


Figure 1.8. Combustion recycling of WEEE in an unsafe conditions.

### 1.4.3 Mechanical recycling of WEEE

Mechanical separation technologies have been widely used in many conventional recycling plants to recover precious metals or base metals from WEEE, because of its high capacity and low cost [1-38]. Most of the mechanical processes are dependent not only on the density of particles but also the size and the shape of particles influence the segregation. According to the difference of mechanical mechanism, the mechanical treatments was mainly divided into 6 kinds,

i.e. the wet shaking table, the jigging, the eddy current separation, the sink-float by heavy medium, the kinetic gravity separation and the magnetic density separation [1-39].

The magnetic density separation (MDS) is utilized in recycling and mineral processing industry since 2007. By changing the magnetization of the liquid, the MDS process provides a good solution for minerals and precious metals concentrating and polymers separation [1-40]. Magnetic fluid was used for recycling of WEEE in 1999 in Germany. Advantages of MDS are the high capacity per hour, low operating costs, environmental impact and suitability to process large amounts of particles with a wide size range. One of the important applications of the MDS in recycling industry is separation of light and heavy non-ferrous products in bottom ash, which provides a promising application of MDS in recycling of WEEE [1-39].

However, the fine pulverization and separation processes required for such methods consume huge amounts of energy, and further processing is needed to utilize the plastic materials separated from WEEE, because each mechanical separation method cannot separate the plastic fraction and the metal fraction completely [1-38, 1-41].

### 1.4.4 Feedstock recycling of WEEE (pyrolysis and gasification)

Feedstock recycling treatment of WEEE aims to convert the organic materials in WEEE plastics into fuels, original monomers or other valuable chemicals by methods such as pyrolysis and gasification. Feedstock recycling is seen as one of the most valuable options in the treatment of WEEE plastics. Pyrolysis, as an important feedstock recycling method, only consumes 10% of the energy content of WEEE plastics.

Pyrolysis has been proposed as a viable processing route for not only converting the organic compounds in WEEE plastics into fuels and chemical feedstock but also separating and recovering the metals from plastic fractions [1-8]. Because of its low cost and easy operation, pyrolysis used for recycling WEEE plastics have been intensively investigated under different feedstocks, operation conditions, reactors, and increasing temperature stages. In addition, there

are a lot of parameters affecting the product distribution from the pyrolysis of WEEE plastics, such as the chemical composition of the plastics, pyrolysis temperature and heating rate, pyrolysis time, reactor type, operating pressure and the presence/absence of catalysts or additives. It is worth noting that when WEEE plastics with brominated flame retardant and $Sb_2O_3$ synergist (Br-HIPS) are pyrolyzed with neither additives nor catalysts, a large amount of brominated compounds, such as $SbBr_3$, HBr and organic brominated compounds, would exist in the oil product [1-42]-[1-47]. The presence of brominated compounds, especially the organic brominated compounds, in the oils would reduce their quality and hinder their reuse [1-43,1-44]. Therefore, lots of debromination methods, effective catalysts and additives in the pyrolysis process of WEEE plastics have been investigated to reduce the bromine content from the oil products [1-8]. Bhaskar et al. synthesized the composite Fe-C and Ca-C additives, which could effectively remove the brominated compounds from the pyrolysis oil products [1-46,1-47]. Terakado and Hirasawa used the metal oxides in the pyrolysis of TBBPA and printed circuit boards containing brominated flame retardants, respectively. They concluded that the addition of metal oxides could effectively suppress the formation of HBr and brominated organic compounds. The above research results indicated that the metal oxides could reduce the bromine content in the pyrolysis oil products by the neutralization reaction [1-48,1-49]. Besides, there were many researches on zeolite catalysts used for the debromination in the pyrolysis of brominated WEEE plastics [1-43,1-44]. Hall et al investigated the catalytic pyrolysis of brominated flame-retarded HIPS and ABS by using HY zeolite and HZSM-5 zeolite, which proved that the zeolite catalysts could effectively catalytically reform the organobrominated compounds and reduce the bromine content in the pyrolysis oils [1-43]. The above research indicated that when the proper catalysts or additives are employed, the low-bromine or bromine-free oil products could be obtained from the catalytic pyrolysis of WEEE plastics.

Gasification was also proposed as a popular method to recovery valuable metals and fuels from WEEE, which have been widely commercialized in converting the biomass and coal into fuel and chemical feedstock. According to the difference of atmosphere, the gasification can mainly be divided into air gasification, steam gasification and $CO_2$ gasification. In our laboratory,

the Shangzhong Zhang seniors conducted the research of steam gasification of epoxy board, phenolic board and PVC in the presence of mixture carbonates ($K_2CO_3$, $Na_2CO_3$ and $Li_2CO_3$) in order to develop an effective and feasible method to recycle plastic fraction and to recover useful metals from WEEE. It was mainly concluded that hydrogen-rich synthetic gas was the major product. And the steam gasification proceeded in two steps, the initial rapid pyrolysis followed by the secondary steam gasification of the char or tar produced in the first pyrolysis stage. The carbonate could accelerate not only the latter steam gasification process, but also improve the initial rapid pyrolysis, as well as preventing the formation of organic brominated compounds. Finally, Zhang et al reported that the steam gasification in the presence of carbonate is expected to be used as an effective and feasible method for converting organic compounds into high quality gaseous products and for the recovery of useful metals from WEEE after gasifying the organic plastic fraction [1-41, 1-50].

## 1.5. Objective of the thesis

The present study is aiming to develop a cost-effective and feasible process and catalysts for integrated recovery of valuable resource and bromine free fuel oil from WEEE by catalytic pyrolysis and $CO_2$ gasification. The specific objectives are shown as following:

First of all, the catalytic impact and debromination performance of low-cost catalysts (red mud, natural zeolite and calcined limestone) in the catalytic pyrolysis of HIPS was investigated. The special attention was paid in the debromination performance and its mechanism for the liquid oil products.

Furthermore, from an industrial implementation point of view, the catalytic effect and debromination performances of zeolites and synthesized iron loaded zeolites in the pyrolysis and catalytic reforming of Br-HIPS were studied.

The feasibility of $CO_2$ gasification as a separation process for char and metal by converting

the char into fuel gas was investigated, especially the $CO_2$ gasification activity of the chars derived from the pyrolysis of WEEE plastic was focused.

The effect of carbonate catalysts ($K_2CO_3$ and $Na_2CO_3$) on $CO_2$ gasification of WEEE plastic chars was also studies in detail.

Finally, the combination of the pyrolysis-catalytic reforming process and $CO_2$ gasification processes was proposed in order to more effectively recycle the WEEE. Briefly, the fuel gas from the pyrolysis-catalytic reforming of WEEE plastic was burned to supply thermal energy for heating the $CO_2$, which could be used for the $CO_2$ gasification of residues derived from the pyrolysis of WEEE in order to obtain the pure metals, as shown in the following Figure 1.9.

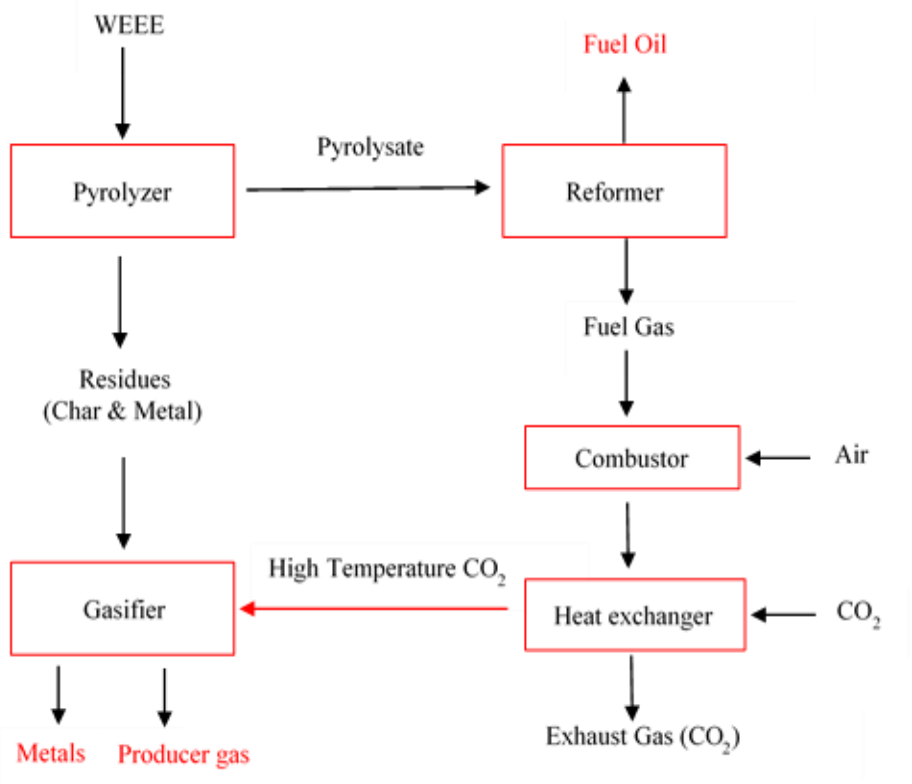


Figure 1.9 the combination of pyrolysis-catalyst reforming process and $CO_2$ gasification process for the recycling of WEEE

## 1.6. Outline of the thesis

The thesis has been divided into 5 chapters. The outlines of each chapter are shown as following:

***Chapter 1. General Introduction***

In this chapter, at first, the compositions, the characteristics, the environmental hazards and the recycle methods of waste electrical and electronic equipments (WEEE) were introduced, respectively. Furthermore, the recent development and research works on the recycling of WEEE, as well as the challenge for implementation, were also reviewed. Special attention was paid to the catalytic pyrolysis and gasification technology for the recycling of WEEE plastics. Finally, the objective and outlines of each chapter of this thesis were presented.

***Chapter 2. Catalytic pyrolysis of brominated high impact polystyrene (Br-HIPS) over red mud, limestone and natural zeolite additives***

In this chapter, the thermal degradation of high impact polystyrene (HIPS) containing brominated flame retardants and antimony trioxide ($Sb_2O_3$) was conducted at different temperatures and in the presence of three additives (red mud, limestone and natural zeolite) in a fixed-bed reactor, respectively. The effect of the pyrolysis temperature on the product yield and the bromine content in the oil product was investigated. It was found that the maximum oil yield was obtained at the pyrolysis temperature of 500℃. The pyrolysis temperature had no significant impact on the bromine reduction in the oil products. The bromine in the flame retardant was mainly transferred into the oil products, where the bromine content was in the range of 7.96-8.56 wt.%. With the aim of removing bromine and antimony from the oils, three additives (red mud, limestone and natural zeolite) were used to investigate their influence on the product yield and composition, especially on the bromine and antimony removal ability from the oil products. In this study, it was found that all of the additives could significantly lower the bromine and antimony contents in the oil products and the red mud was the most effective, which is attributed to the fact that,

on the one hand, red mud played a cracking catalyst effect on destroying the organobrominated compounds; On the other hand, it could work as a sorbent to fix HBr formed by the Br-HIPS degradation. In addition, the distribution and fate of bromine and antimony in the residues were also studied by the SEM-EDX and XRD analysis in details. There were lots of metal bromides existing in the pyrolysis residues, which indicated that bromine removal from the oil products was mainly attributed to the formation of metal bromides.

***Chapter 3. Fuel oil production from two-stage pyrolysis-catalytic reforming of brominated high impact polystyrene using zeolite and iron oxide loaded zeolite catalysts***

The experiments of two-stage pyrolysis and catalytic reforming of high impact polystyrene (HIPS) containing brominated flame retardants and antimony trioxide ($Sb_2O_3$) were conducted in the presence of four zeolite catalysts in order to remove the bromine content from the derived oil products. The four catalysts used were natural zeolite (NZ), iron oxide loaded natural zeolite (Fe-NZ), HY zeolite (YZ) and iron oxide loaded HY zeolite (Fe-NZ). The effect of catalyst types on the product yield, the gas and oil product composition and the debromination efficiency of the oil products were evaluated in details. The results showed that the loading of iron oxides reduced the pore size and surface areas of natural zeolite and HY zeolite. Regardless of the presence of catalysts, the single-ring aromatic compounds were the main components of the oil products, such as ethylbenzene, toluene, styrene and cumene etc.. Meanwhile, when YZ and Fe-YZ were used, the two-ring and multi-ring aromatic compounds in the oils, as well as the yield of gas products, significantly increased at the expense of valuable single-ring aromatic compounds. Furthermore, in the term of the debromination performance of the oil products, Fe-NZ and Fe-YZ were better than NZ and YZ, duo to the loading of iron oxide, which could react with derived HBr and then remove more bromine from the oil products. Finally, the life time, the deactivation and the regeneration of catalysts were also evaluated in this chapter. It was found that the deactivation of the catalysts was attributed to the coking and the reduction of $Fe_2O_3$. In addition, the regenerated catalyst almost have the comparable activity and effect for the catalytic decomposition of Br-HIPS.

## *Chapter 4. The $CO_2$ gasification kinetic study of WEEE plastic char derived from medium temperature pyrolysis by thermogravimetric analyzer*

In this chapter, in order to effectively utilize the char without oxidizing the metal contents, the isothermal $CO_2$ gasification characteristics of three chars derived from pyrolysis of WEEE plastics were firstly studied by using a thermogravimetric analyzer (TGA) within the temperature range of 850−1050°C. Phenolic board (PB), brominated high impact polystyrene (HIPS) and acrylonitrile butadiene styrene (ABS) are widely used for the electric and electronic equipment and were employed as model WEEE plastics for the char sample production in this study. The effects of their physicochemical properties and gasification temperature on the WEEE plastic chars conversion rate, the reactivity indexes and the gasification rate were investigated in detail. The random pore model (RPM), the extended random pore model (eRPM) and the shifted extended random pore model (s-eRPM) have been employed to fit with the $CO_2$ gasification rate curve of WEEE plastic chars. The kinetic parameters and the correlation coefficients ($R^2$) were evaluated by RPM, eRPM and s-eRPM, respectively. It was found that the $CO_2$ gasification reactivity of PB char was the highest, followed by that of HIPS char and the gasification reactivity of ABS char was the lowest, which have a close relationship with their pore and carbon crystal structure properties. In addition, it was found that the RMP could fit well with the gasification reaction rate of HIPS char whose maximum reaction rate appears at the char conversion of approximate 0.4. Nevertheless, as for PB char and ABS char, their maximum gasification rate presented at char conversion of around 0.8 and 0.2, respectively. And it was observed that eRMP and s-eRPM could predict their gasification rate of PB char and ABS char very well with a higher $R^2$, respectively. Finally it was found that the addition of carbonate catalyst could obviously increase the gasification rate and the reactivity index of the char samples. At 850 °C, the addition of 10wt.%$K_2CO_3$, 5wt.%$K_2CO_3$ 5wt.%$Na_2CO_3$, 10wt.%$Na_2CO_3$ into HIPS char could increase the reactivity index 10, 2.8 and 6.7 times, respectively. According to eRPM and Arrhenius curve, the addition of 10 wt.% $K_2CO_3$, 10 wt.% $Na_2CO_3$, 5 wt.% $K_2CO_3$ + 5 wt.% $Na_2CO_3$ carbonate catalysts could reduce the activation energy of HIPS char from 145.94 KJ/mol to 78.50, 125.00, 98.23 KJ/mol, respectively.

## *Chapter 5. Conclusions and recommendations*

The principal results achieved in this research are summarized. The proposals and comments for the future study were also provided.

## References


[1-1] UNEP, United Nations Environment Programme 1, Press Release, Urgent Need to Prepare Developing Countries for Surge in e-Wastes, 2010, February 22, 2010, available at: http://www.unep.org/Documents.Multilingual/Default.asp?DocumentID=612&ArticleID=647.

[1-2] B. Robinson, E-waste: an assessment of global production and environmental impacts, Sci. Total Environ. 408 (2009) 183–191.

[1-3] UNEP, United Nations Environmental Programme Recycling – From e-Waste to Resources – Final Report, Sustainable Innovation and Technology Transfer Industrial Sector Studies, 2009, pp. 2009.

[1-4] Lina, K., H. & Chiang, H., L. (2014). Liquid oil and residual characteristics of printed circuit board recycle by pyrolysis. *Journal of Hazardous Materials*, **271**, 258-265.

[1-5] Ongondo, F., O., Williams, I., D. & Cherrett T., J. (2011). How are WEEE doing? A global review of the management of electrical and electronic wastes. *Journal of Hazardous Materials*, **31**, 714-730.

[1-6] Widmer, R., Oswald-Krapf, H., Sinha-Khetriwal, D., Schnellmann, M. & Böni, H. (2005). Global perspectives on e-waste. *Environmental Impact Assessment Review*, **25 (5)**, 436–458.

[1-7] Sodhi, M., S. & Reimer, B. (2001). Models for recycling electronics end-of-life products. OR Spektrum 23, 97–115.

[1-8] Yang, X., N., Sun, L., S., Xiang, J., Hu, S. & Su, S. (2013). Pyrolysis and dehalogenation of plastics from waste electrical and electronic equipment (WEEE): A review. *Waste Management*, **33**, 462–473.

[1-9] Haig, S., Morrish, L., Morton, R. & Wilkinson, S. (2012). Electrical product material composition. http://www.wrap.org.uk/sites/files/wrap/Electrical%20product%20material%20composition%20overview.pdf

[1-10] Mobile phone disposal discussed at UN hazardous waste meeting in Bali, 23 June 2008. http://www.un.org/apps/news story.asp? News ID=27121 & Cr=waste & Cr1= management.

[1-11] Gartner Says Worldwide Mobile Phone Sales Increased 14 Percent in First of 2008, Gartner May 28, 2008. http://www.gartner.com/it/page.jsp?id=680207.

[1-12] National Institute for Materials Science (NIMS). Special report about rare metal and rare ash. http://www.nims.go.jp/research/elements/rare-metal/urban-mine/index.html

[1-13] Eriksson, P. & Jakobsson, E. (2001). Brominated flame retardants: a novel class of developmental neurotoxicants in our environment. *Environmental Health Perspectives*, 109, 903–908.

[1-14] Morris, P., J., Quensen 3rd, J., F., Tiedje, J., M. & Boyd, S.A. (1992). Reductive debromination of commercial polybrominated biphenyl mixture Firemaster BP6 by anaerobic microorganisms from sediments. *Applied and Environment Microbiology*, **58**, 3249–3256.

[1-15] Freegard, K., Morton, R., Coggins, C., Hearn, G., Froes, D. & Alger, M. (2005). Develop a process to separate brominated flame retardants from WEEE polymers Interim Report 1. www.wrap.org.uk.

[1-16] Schlummer, M., Gruber, L., Maurer, A., Wolz, G. & Eldik, R. (2007). Characterization of polymer fractions from waste electric and electronic equipment (WEEE) and implications for waste management. *Chemosphere*, **67**, 1866–1876.

[1-17] Martinho, G., Pires, A., Saraiva, L. & Ribeiro, R. (2012). Composition of plastics from waste electrical and electronic equipment (WEEE) by direct sampling. *Waste Management*, **32**, 1213–1217.

[1-18] Vilaplana, F. & Karlsson, S. (2008). Quality concepts for the improved use of recycled polymeric materials: a review. *Macromol. Mater. Eng.*, **293**, 274–297.

[1-19] Birnbaum, L.S., Staskal, D.F., 2003. Brominated flame retardants: cause for concern? Environmental Health Perspectives 112, 9–17.

[1-20] The flame retardants market. Global consumption of flame retardants in plastic by types. http://www.flameretardantsonline.com/web/en/106/7ae3d32234954e28e661e506e284da7f.htm.

[1-21] Vehlow, J., Bergfeldt, B., Hunsinger, H., Jay, K., Mark, F.E., Tange, L., Drohmann, D. & Fisch, H. (2000). Recycling of bromine from plastics containing brominated flame retardants in state-of-the-art combustion facilities. <www.apme.org>.

[1-22] Adrian, C., Stuart, H., Mohamed A.,E., A., Nadeem, A., Robin, J., Dorte, H. & Cynthia, A., W. (2011). Novel brominated flame retardants: A review of their analysis, environmental fate and behaviour. *Environment International*, **37**, 532–556.

[1-23] Main, K., M., Kiviranta, H., Virtanen, H.E., Sundqvist, E., Tuomisto, J.T., Tuomisto, J., Vartiainen, T., Skakkebaek, N.E., Toppari, J., 2007. Flame retardants in placenta and breast milk and cryptorchidism in newborn boys. Environmental Health Perspectives 115,

1519–1526.

[1-24] Meijer, L., Weiss, J., Van Velzen, M., Brouwer, A., Bergman, Å. & Sauer, P.J.J., 2008. Serum concentrations of neutral and phenolic organohalogens in pregnant women and some of their infants in The Netherlands. Environmental Science and Technology 42, 3428–3433.

[1-25] Lim, J., Lee, D., Jacobs Jr., D.R., 2008. Association of brominated flame retardants with diabetes and metabolic syndrome in the U.S. population, 2003–2004. Diabetes Care 31, 1802–1807.

[1-26] Herbstman, J.B., Sjödin, A., Kurzon, M., Lederman, S.A., Jones, R.S., Rauh, V., Needham, L.L., Tang, D., Niedzwiecki, M., Wang, R.Y., Perera, F., 2010. Prenatal exposure to PBDEs and neurodevelopment. Environmental Health Perspectives 118, 712–719.

[1-27] Van der Ven, L.T.M., Van de Kuil, T., Verhoef, A., Verwer, C.M., Lilienthal, H., Leonards, P.E.G., Schauer, U.M.D., Cantón, R.F., Litens, S., De Jong, F.H., Visser, T.J., Dekant, W., Stern, N., Håkansson, H., Slob, W., Van den Berg, M., Vos, J.G., Piersma, A.H., 2008. Endocrine effects of tetrabromobisphenol-A (TBBPA) in Wistar rats as tested in a one-generation reproduction study and a subacute toxicity study. Toxicology 245, 76–89.

[1-28] Viberg, H., Eriksson, P., 2011. Differences in neonatal neurotoxicity of brominated flame retardants, PBDE 99 and TBBPA, in mice. Toxicology 289, 59–65.

[1-29] Ibhazehiebo, K., Lwasaki, T., Xu, M., Shimokawa, N., Koibuchi, N., 2011. Brainderived neurotrophic factor (BDNF) ameliorates the suppression of thyroid hormone-induced granule cell neurite extension by hexabromocyclododecane (HBCD). Neuroscience Letters 493, 1–7.

[1-30] Palace, V., Park, B., Pleskach, K., Gemmill, B., Tomy, G., 2010. Altered thyroxine metabolism in rainbow trout (Oncorhynchus mykiss) exposed to hexabromocyclododecane (HBCD). Chemosphere 80, 165–169.

[1-31] Xinhua News Agency, 2010b. New Rule to Manage E-waste. Available from: http://news.xinhuanet.com/english2010/china/2010-06/07/c13336556.htm

[1-32] Li, J., Tian, B., Liu, T., Liu, H., Wen, X., Honda, S. (2006). Status quo of e-waste management in mainland China. *Journal of Material Cycles and Waste Management*, **8 (1)**, 13–20.

[1-33] He K., T., Li, L. & Ding W., Y. (2008). Research on recovery logistics network of waste electronic and electrical equipment in China. In: Industrial Electronics and Applications, 2008. ICIEA 2008. 3rd IEEE Conference, 1797–1802.

[1-34] Yu, J., L., Ju, M., T. & Williams, E. (2009). Waste electrical and electronic equipment

recycling in China: practices and strategies. In: 2009 IEEE International Symposium on Sustainable Systems and Technology. ISSST, Tempe, Arizona, USA, May 18–20.

[1-35] Yang, J., Lu, B. & Xu, C. (2008). WEEE flow and mitigating measures in China. *Waste Management*, **28 (9)**, 1589–1597.

[1-36] The WEEE Regulations: a brief introduction. http://www.out-law.com/page-10692

[1-37] Mark, F.E., Dresch, H., Bergfeld, B., Dima, B., Grüttner, W., Kleppmann, F., Kramer, K., Lehner, T., Vehlow, J., 2006. Large scale demonstration of the treatment of electrical and electronic shredder residue. Plastics Europe. <www.plasticseurope.org>.

[1-38] Cui, J. & Forssberg, E. (2003). Mechanical recycling of waste electric and electronic equipment: a review. Journal of Hazardous Materials, 99, 243-263.

[1-39] Hu, B., Giacometti, L., Dinaio, F. & Rem, P. (2011). Recycling of WEEE by Magnetic Density Separation, the Sixth International Conference on Waste Management and Technology.

[1-40] Bakker, E., J., Rem, P., C. & Fraunholcz, N. (2009). Upgrading mixed polyolefin waste with magnetic density separation. *Waste Management*, **29**, 1712-1717.

[1-41] Zhang S., Z., Yoshikawa K., Nakagome, H. & Kamo, T. (2013). Kinetics of the steam gasification of a phenolic circuit board in the presence of carbonates. *Applied Energy*, **101**, 815–821.

[1-42] Jakab, E., Uddin, Md.A., Bhaskar, T. & Sakata Y. (2003) Thermal decomposition of flame-retarded high impact polystyrene. *J. Anal. Appl. Pyrolysis*, **68-69**, 83-99.

[1-43] Hall, W.J. & Williams, P.T. (2008) Removal of organobromine compounds from the pyrolysis oils of flame retarded plastics using zeolite catalysts. *J. Anal. Appl. Pyrolysis*, **81**, 139–147.

[1-44] Hall, W.J., Miskolczi, N., Onwudili, J. & Williams, P.T. (2008) Thermal Processing of Toxic Flame-Retarded Polymers Using a Waste Fluidized Catalytic Cracker (FCC) Catalyst. *Energy & Fuels*, **22**, 1691–1697.

[1-45] Miskolczi, N., Hall, W.J., Angyal, A., Bartha, L. & Williams, P.T. (2008) Production of oil with low organobromine content from the pyrolysis of flame retarded HIPS and ABS plastics. *Journal of Analytical and Applied Pyrolysis*, **83**, 115-123.

[1-46] Bhaskar, T., Matsui T., Azhar Uddin, Md., Kaneko, J., Muto, A. & Sakata, Y. (2003) Effect of $Sb_2O_3$ in brominated heating impact polystyrene (HIPS-Br) on thermal degradation and debromination by iron oxide carbon composite catalyst (Fe-C) *Applied Catalysis B: Environmental*, **43**, 229–241.

[1-47] Bhaskar, T., Matsui, T., Kaneko, J., Uddin, Md. A., Muto, A. & Sakata, Y. (2002) Novel calcium based sorbent (Ca-C) for the dehalogenation (Br, Cl) process during halogenated mixed plastic (PP/PE/PS/PVC and HIPS-Br) pyrolysis. *Green Chemistry*, **4**, 372–375.

[1-48] Terakado, O., Ohhashi, R. & Hirasawa, M. (2011) Thermal degradation study of tetrabromobisphenol A under the presence metal oxide: Comparison of bromine fixation ability. *J. Anal. Appl. Pyrolysis*, **91**, 303–309.

[1-49] Terakado, O., Ohhashi, R. & Hirasawa, M. (2013) Bromine fixation by metal oxide in pyrolysis of printed circuit board containing brominated flame retardant. *J. Anal. Appl. Pyrolysis*, **103**, 216–221.

[1-50] Zhang S., Z., Yoshikawa K., Nakagome, H. & Kamo, T. (2011). Steam gasification of epoxy circuit board in the presence of carbonates. Materials Cycles Waste Management, 14, 294 - 300.

# Chapter 2

# Catalytic pyrolysis of brominated high impact polystyrene (Br-HIPS) over red mud, limestone and natural zeolite additives

## 2.1. Introduction

Waste electrical and electronic equipment (WEEE) are currently considered to be one of the fastest growing solid waste streams in the world. According to a report of UNEP (2009) about the recycling from WEEE to resources, 40 million tons of WEEE were generated and discharged annually in the world and it was expected an alarming growth per year in the future [2-1]. It was well known that there are lots of valuable metals and plastics contained in WEEE, which are worthy recyclable feedstock and could be converted into important mineral resources, fuel and chemical feedstock if recycled properly. On the other hand, WEEE also contained certain dangerous and hazardous substances, such as toxic metals and brominated flame retardants, which will pose considerable environmental pollution and health risks if treated inadequately [2-2, 2-3]. Therefore, how to scientifically and cost-effectively reuse, recycle and recover WEEE has drawn plenty of attentions through the world.

WEEE plastics, which account for about 30% of the total weight of WEEE, are worthwhile recyclable parts of WEEE [2-2]. One of the most popular plastics widely used in electrical and electronic equipment (EEE) is high-impact polystyrene (HIPS), because of its low cost and excellent impact resistance and machinability properties. HIPS is a composite material composed of a polystyrene phase and a dispersed polybutadiene rubber phase [2-4]. Polybrominated compounds and antimony trioxide ($Sb_2O_3$), as synergistic flame retardants, are frequently added

to HIPS to reduce its flammability [2-5]. Because of the presence of brominated flame retardants (BFRs), the traditional methods of dealing with WEEE plastics, such as land-filling and incineration, will produce secondary pollution on the ecological environment and endanger human health, as well as being a waste of resource [2-2]. For instance, the direct incineration of WEEE plastics containing brominated flame retardant will produce some highly toxic brominated dioxins and dibenzofurans [2-6]. With a view to the environmental protection and saving non-regeneration resources, feedstock recycling technologies have been proposed as a viable processing route for converting WEEE plastics into useful fuels and chemical feedstock.

The pyrolysis and the catalytic pyrolysis are the most widely used feedstock recycling technologies for the conversion of WEEE plastics into valuable chemicals and fuel oil. Because of its low cost and easy operation, pyrolysis used for recycling WEEE plastics have been intensively investigated under different feedstocks, operation conditions, reactors, and increasing temperature stages [2-2]. However, there were lots of organic brominated compounds remaining in the pyrolysis oils, which would reduce the quality and hinder the reuse of them. Compared with the thermal pyrolysis, the catalytic pyrolysis not only reduces the degradation temperature, but also obtains comparatively high-grade oil fuel without bromine. A wide range of catalysts have been tested for upgrading the quality and debromination of the pyrolysis oil derived from WEEE plastics and brominated flame retardants, such as zeolites [2-7, 2-8], FCC catalysts [2-9], metallic oxides [2-10]-[2-12], etc. For example, Hall and Williams [2-7] investigated the catalytic pyrolysis of brominated flame-retarded HIPS and ABS by using HY Zeolite and HZSM-5 Zeolite, which could effectively remove the organobromines from the pyrolysis products. Terakado and Hirasawa [2-11,2-12] used the metal oxides in the pyrolysis of TBBPA and printed circuit boards including brominated flame retardants, respectively. They concluded that the addition of metal oxides could suppress the formation of HBr and brominated organic compounds.

However, from a practical industrial application point of view, the use of expensive catalysts, such as commercial HY and HZSM-5 zeolites, would increase the operation cost, due to a large amounts of catalyst demand and the deactivation of catalysts in a large continuously operating

plant. Ali et al. [2-13] indicated that the main factor is the catalyst cost for the economic comparison of catalytic cracking and thermal cracking technologies. In addition, Cardona et al. [2-14] concluded that a plastic waste pyrolysis process could only be supported if the catalyst cost was practically zero [2-15]. Therefore, it is necessary to develop the low-cost catalysts or additives for pyrolysis of WEEE plastic and debromination of brominated flame retardant.

Red mud, a solid waste product of the bauxite processing through the Bayer process, is mainly composed of $Fe_2O_3$, $Al_2O_3$, $SiO_2$ and $TiO_2$. Because of its special physicochemical properties, such as a high content of $Fe_2O_3$, a high surface area, the sintering resistance and a low cost, red mud have been used as catalysts for the hydrodechlorination and hydrogenation reactions [2-16]-[2-18]. In addition, it was found that, in the presence of $Al_2O_3$, $SiO_2$ and $TiO_2$, the red mud with certain acidity could contribute to the catalytic cracking of plastic wastes [2-15]. Limestone, as a common natural mineral, was also widely employed as a catalyst or an additive in the pyrolysis and gasification of biomass and plastic for the dehalogenation and tar removal [2-10,2-19]. The natural zeolite was also widely studied as catalysts for the catalytic pyrolysis of biomass and plastic to upgrade the liquid product due to its large surface area, acidity and sintering resistance property [2-20, 2-21].

To our knowledge, there were few reported works on the use of red mud, limestone and natural zeolite for the WEEE plastic pyrolysis [2-22, 2-23]. In this chapter, thermal degradation of HIPS containing BFRs and $Sb_2O_3$ was carried out at different temperatures with the presence of three additives (red mud, limestone and natural zeolite) in a fixed-bed reactor. The influence of the pyrolysis temperature on the product yield and bromine distribution in the oil products was evaluated systematically. In addition, the effect of three additives (red mud, limestone and natural zeolite) on the yields and compositions of products were investigated in details. Furthermore, the special attention was paid to study the content and distribution of bromine and antimony in the oils and residues, respectively, when the additives were used.

## 2.2. Experimental

### 2.2.1. Materials

The feedstock sample was high-impact polystyrene (HIPS) containing brominated flame retardant and antimony trioxide as a synergist. The brominated flame retardant was decabromo diphenyl ethane (DDE). The high-impact polystyrene consists of polystyrene backbone chain and rubbery polybutadiene chains. The sample will be referred to as Br-HIPS. In order to mix the Br-HIPS sample with an additive uniformly, the pellet-type Br-HIPS sample was ground and sieved to obtain the powder Br-HIPS sample with a diameter smaller than 0.5mm. The color of the sample powder was white. The proximate analysis and ultimate analysis of the Br-HIPS sample was presented in Table 2.1. And the photo of Br-HIPS sample and molecular structure of HIPS are shown in Figure 2.1.

Table 2.1. Proximate analysis and ultimate analysis of the Br-HIPS sample

| **Proximate analysis** | **wt.%** | **Ultimate analysis** | **wt.%** |
|---|---|---|---|
| Moisture | 0.00 | C | 78.61 |
| Volatile matter | 98.13 | H | 7.11 |
| Fixed carbon | 0.34 | O | 0.75 |
| Ash | 1.53 | N | 0.10 |
| | | Br | 9.30 |
| | | Sb | 3.77 |
| | | Ti | 0.36 |

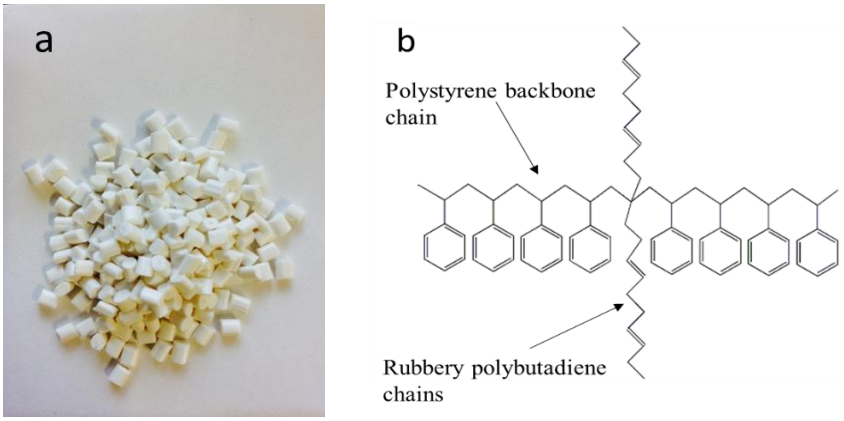


Figure 2.1. The photo of Br-HIPS samples (a) and the molecular structure of HIPS (b)

The additives employed in this chapter were red mud, natural zeolite and limestone, which were obtained from the local companies of Indonesia. Before the experiments, three additives were ground, sieved and then dried at 110 ℃ over the night. The red mud and natural zeolite were calcined at 500 ℃ for 2 hours to remove the organic impurities while the natural limestone was calcined at 900 ℃ for 4 hours to obtain CaO from the limestone. There were no any other activation operation was done for calcined red mud, natural zeolite and limestone. The additives will be referred to as RM, NZ and CL, respectively. Their chemical components and BET surface area are shown in Table 2.2, and the photos of three catalyst used in this Chapter are shown in Figure 2.2.

Table 2.2. Chemical components and BET surface area of RM, NZ and CL (wt.%) (dry basis)

| **Additives** | **$Fe_2O_3$** | **$SiO_2$** | **$Al_2O_3$** | **CaO** | **$TiO_2$** | **$Na_2O$** | **MgO** | **Others[a]** | **BET surface area ($m^2/g$)** |
|---|---|---|---|---|---|---|---|---|---|
| RM | 51.30 | 13.00 | 13.90 | 3.31 | 10.40 | 4.93 | 0.00 | 3.16 | 21.26 |
| CL | 0.00 | 0.97 | 0.42 | 97.60 | 0.00 | 0.00 | 0.32 | 0.69 | 7.49 |
| NZ | 3.58 | 77.30 | 9.62 | 5.32 | 0.64 | 0.69 | 0.00 | 2.85 | 60.16 |

[a] By difference.

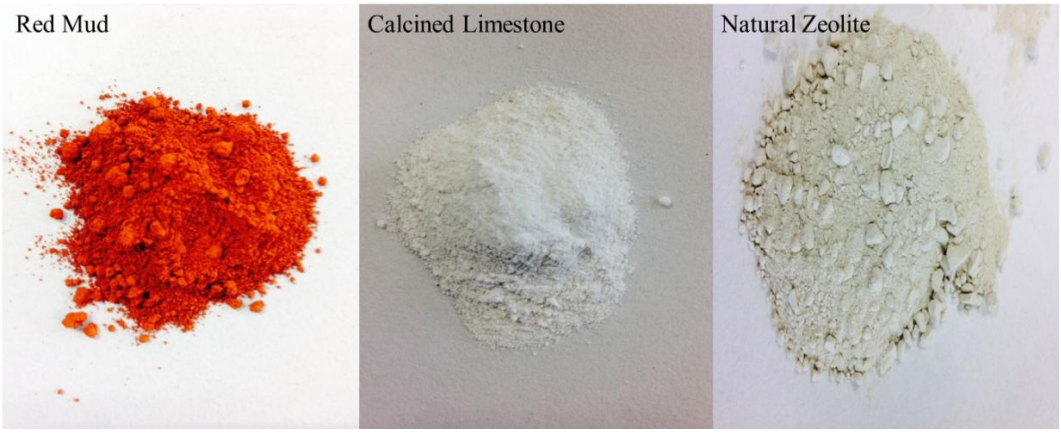


Figure 2.2. The photos of red mud, calcined limestone and natural zeolite additives

### 2.2.2 Experimental setup

Figure 2.3 is the schematic diagram of the experimental apparatus. The pyrolysis reactor was made of quartz. The inner diameter and inner height are 50 mm and 280 mm, respectively. In the thermal pyrolysis experiments without additive, the powder sample was fed into the reactor and was pyrolyzed over a range of temperature (450-550 ℃) under the carrier gas of $N_2$ with a flow rate of 50 mL/min. When the additives were used, 40 g samples and 8g of each additive (20 wt.%) were mixed well, respectively, and fed into the reactor, which was heated to 500 ℃ at a heating rate of 50 ℃/min. In the all experiments, after the reactor temperature reached the target temperature, it was held at this temperature for 2 hours and was then cooled quickly. The oil product was condensed in an oil collector, which was cooled by dry ice and ethanol mixture solution. In order to capture HBr, the gaseous products were scrubbed with 1 mol/L NaOH solution in the second trap before being collected in a tedlar bag for the off-line gas component analysis. The each experimental facility part was connected by silicon tubes. In order to ensure the repeatability of experiments, each experiment was repeated at least two times until similar results were obtained from the same conditions.

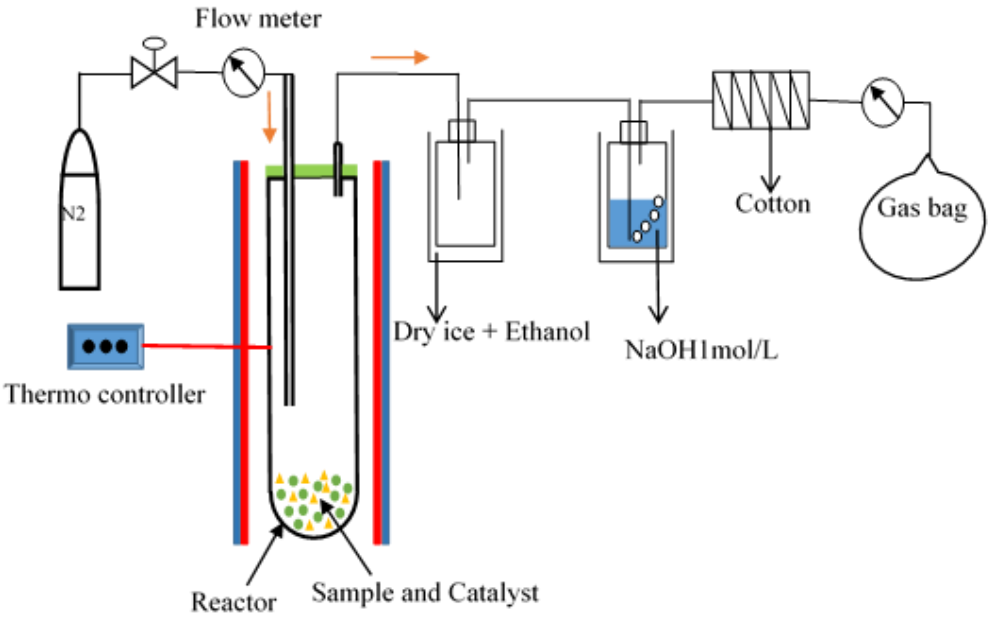


Figure 2.3. Schematic diagram of the pyrolysis apparatus.

## 2.2.3. Analytical methods

The CHN element analysis was conducted by using a Micro Corder JM 10 Elemental Analyzer. The bromine contents of the sample and pyrolysis products were determined by using air combustion coupled with ion chromatography according to JIS K 7392. In general, a sample of about 10 mg was weighed and ignited slowly in a quartz combustion tube at 950 ℃ with air at a flow rate of 1.5 L $min^{-1}$. The combustion products were collected into 30 mL of a 40 mM potassium hydroxide solution in which 20 μL of 3% hydrogen peroxide was added for reducing $Br_2$ to HBr. The resulting brominated solution was then detected by Dionex ICS-1100 ion chromatography fitted with a *Shodex* IC *S1-904E* column. The accuracy of this method was evaluated by analyzing a standard reference material with known bromine contents. The amount of antimony in the Br-HIPS sample and the oil products were determined by the inductively coupled plasma mass spectrometry (ICP-MS). The solution for the ICP-MS analysis was prepared by digesting 10 mg of sample or product in the mixed concentrated nitric and sulfuric acid in a sonicator for 3 hours in 200 ℃. After digestion, the solution was diluted with distilled water to 50 ml for the ICP-MS analysis. The antimony and bromine contents in the pyrolysis residues were measured by a scanning electron microscopy with energy disperse X-ray analysis (SEM-EDX). The surface morphology structures of RM, LS and NZ were observed by the SEM and shown in Figure 2.4.

The chemical compositions of the additives were determined by an energy dispersive X-ray fluorescence spectrometer (XRF) (Rayny EDX-700, Shimadzu Co., Japan)) under vacuum mode for precise measurement. Powder X-ray diffraction (XRD) analysis were carried out for the verification of the crystallinity of the additives. XRD measurements were performed using a Rigaku UltimalV diffractometer with the CuKα radiation ($\lambda$ =1.540) at 40kV and 40 mA. The XRD patterns were accumulated in the range of 5–80° 2θ every 0.02° (2θ) with the counting time of 1 s per step. The phase identification was obtained by the comparison with those included in the Joint Committee of Powder Diffraction Standards (JCPDS) database. The XRD patterns of three additives were presented in Figure 2.5. The surface structure property was analyzed by the

SEM. Surface area and textural properties of the used additives were determined by $N_2$ physical adsorption at 77 K, applying the Brunauer–Emmett–Teller (BET) method, using a Micromeritics Tristar 3020 equipment. And the surface area of the additives (RM, LS and NZ) used for this study was shown in Table 2.2.

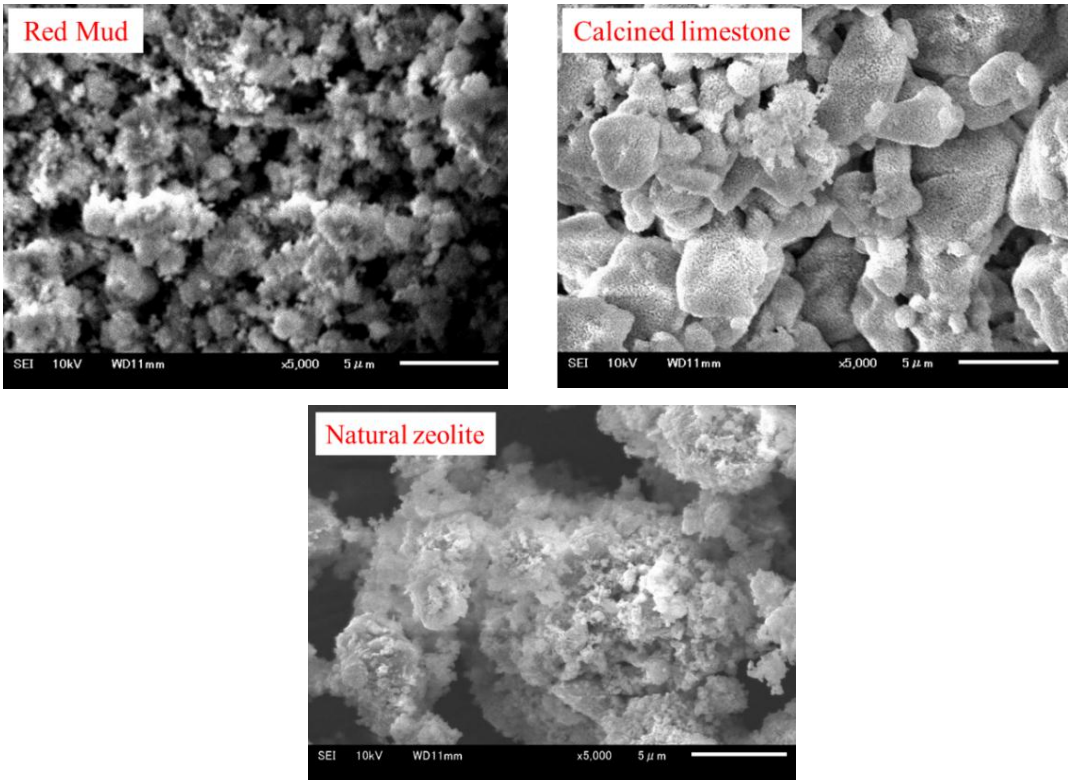


Figure 2.4. SEM micrographs (5,000X) of RM, CL and NZ.

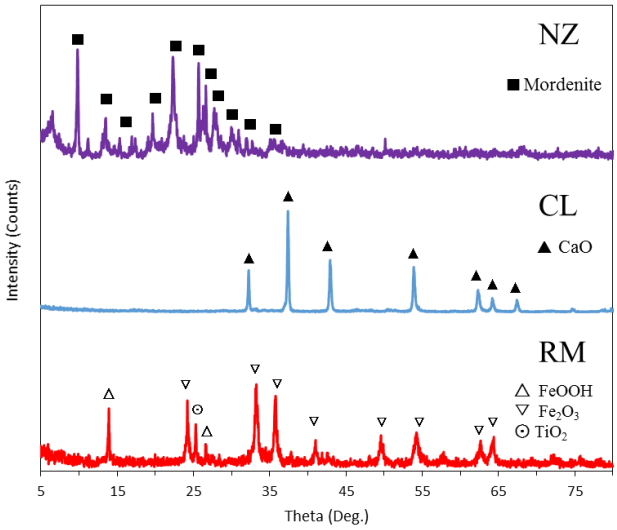


Figure 2.5. The XRD patterns of RM, CL and RM.

The yield of the oil product was measured by the weight difference of the silicon tube and the oil collector after and before the experiments. The yield of the solid product was determined by the weight difference of the reactor after and before the experiments. The yield of the gas product was calculated by subtracting the weight of the solid and oil products from the total weight of the sample.

The composition of the oil product was analyzed by a gas chromatograph coupled with a mass spectrometer (GC-MS) (Agilent 6890N, GC-MSD 5973N). The column was an HP5 (5% Ph-Me-Siloxane) capillary column, 30 m length with 0.25 mm diameter and 0.25 μm film thickness. Helium was used as the carrier gas. The injector temperature was 250 ℃. The temperature program used was the initial temperature of 40 ℃ for 10 minutes followed by the heating rate of 5 ℃ /min to 300 ℃ and held at 300 ℃ for 20 minutes. The ion source and Quadrupole temperatures were 230 ℃ and 150 ℃, respectively. The organobrominated compound in the oil products were measured by the gas chromatograph fitted with electron capture detectors (GC-ECD). In addition, the liquid pyrolysis products were further characterized using Fourier Transform Infrared Spectroscopy (FT-IR) with a JIR-SPX200 FT-IR spectrometer. The oil samples were mixed with KBr and pelletized. Then, it was scanned from 400 to 4000 $cm^{-1}$ with the resolution of 4 $cm^{-1}$.

The composition of the produced gases in the experiments was measured by a micro gas chromatograph fitted with a thermal conductivity detector (GC-TCD) (Agilent Micro 3000), and the yield of each component was calculated by the following equation.

$$m_i = M_i \times \frac{C_i}{C_{N_2}} \times \frac{V_{N_2}}{22.4} \tag{2.1}$$

Where $m_i$ is the yield of the gas $i$ in the gas products, $M_i$ is the molar mass of each gas product; $C_i$ is the concentration of the gas $i$ in the gas products; $C_{N2}$ is the concentration of $N_2$ in the gas products; $V_{N2}$ is the $N_2$ flow rate × the flow time.

## 2.3. Results and discussion

### 2.3.1 TGA results

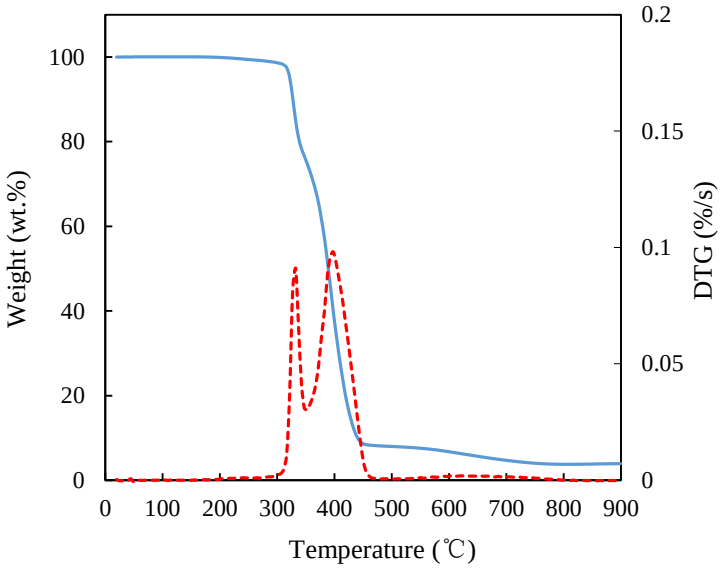


Figure 2.6. TGA and DTG curve of Br-HIPS at 5 ℃ /min

In order to investigate the thermal decomposition property of Br-HIPS, the thermogravimetric analysis (TGA) was conducted with a thermogravimetric analyzer (Shimadzu D50). 10 mg of HIPS-Br sample was loaded into the alumina crucible and heated from the ambient temperature to 900 ℃ with a heating rate of 5 ℃ /min. The flow rate of the carrier gas ($N_2$) was 150 mL/min. The TGA and DTG curves of Br-HIPS were shown in Figure 2.6. The TGA curves indicated that the decomposition of Br-HIPS mainly occurred between 310 and 450 ℃, followed by a stable mass reduction at higher temperatures. The DTG curve obviously illustrated that the pyrolysis of Br-HIPS mainly included two distinct decomposition stages from 310 to 350 ℃ and from 360 to 450 ℃, respectively. This result corresponds to the previous reported works [2-5,2-10] that the first decomposition stage was attributed to the presence of $Sb_2O_3$ as a synergist, which will reacted with BFRs and partial polystyrene by the dehydrogenation and debromination reactions, as presented in Figure 2.7. The decomposition of the majority of Br-HIPS took place in the second stage by the β-scission reaction [2-20]. Furthermore, the Br-HIPS pyrolysis residues

were about 7 wt.% and 2 wt.% at 600 and 900 ℃, respectively, which indicated that the remaining residue could be further decomposed at a higher temperature. These thermogravimetric analysis results could be used for determining the suitable pyrolysis temperatures for the following experiments in the fixed bed reactor.

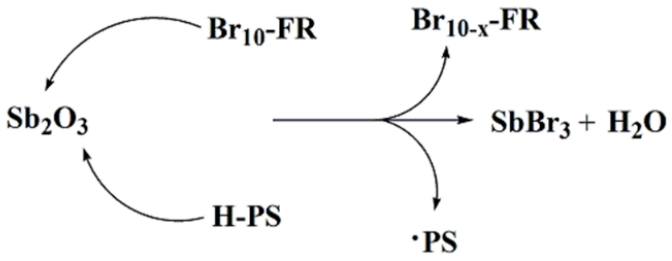


Figure 2.7. First-stage degradation mechanism of Br-HIPS proposed by Bhaskar et al, [2-5].

### 2.3.2 The effect of the pyrolysis temperature on the product yields and the bromine content in the produced oils

It is well known that the reaction temperature is an essential parameter for both the plastic pyrolysis degradation and the catalyst activation [2-24]. Therefore, a preliminary study of Br-HIPS pyrolysis at different temperatures was conducted in an attempt to investigate the impact of the pyrolysis temperature on the product yield and the bromine content in the oil products. The effect of the pyrolysis temperature on the product yield is shown in Figure 2.8. It indicated that as the increase of the pyrolysis temperature from 450 ℃ to 500 ℃, the yield of the oil and gaseous products increased, accompanied by the decrease of the yield of the solid residue, which was attributed to the intense cracking of Br-HIPS under the higher pyrolysis temperature resulting in a higher conversion ratio of samples into the gaseous and liquid products [2-25,2-26]. When the pyrolysis temperature increased from 500 ℃ to 550 ℃, the yield of the gaseous product increased at the expense of the liquid product and the solid residue, which implied that a higher pyrolysis temperature would further convert some liquid products into small-molecular gaseous products. However, the change was slight, which indicated that the pyrolysis temperature of 500 ℃ was high enough for the thermal degradation of Br-HIPS. The maximum oil product yield (84.4 wt. %) was obtained at the pyrolysis temperature of 500 ℃.

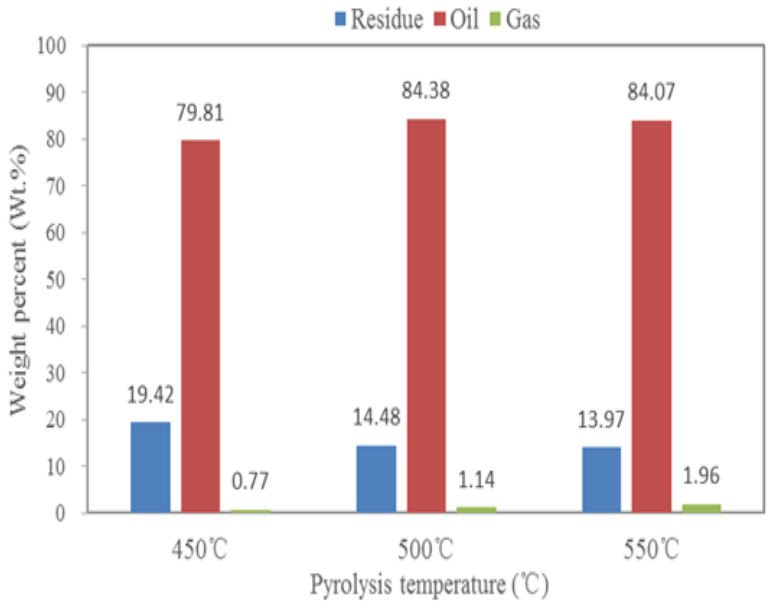


Figure 2.8. Effect of the pyrolysis temperature on the product yield.

The total bromine content in the pyrolysis oils was measured using a bomb calorimeter equipped with an ion chromatograph (JIS K 7392), and the result is shown in Table 2.3. This result clearly shows that there was a high bromine content in each oil product, which means large amounts of bromine was transferred to the oil products during the pyrolysis of Br-HIPS. With the increase of the pyrolysis temperature, the bromine content increased slightly. When the pyrolysis temperature was 550 ℃, 77.4 wt. % of the total bromine in the Br-HIPS sample was transferred into the oil products. Furthermore, it should be mentioned that there are some solid precipitates existed in the oil phase. Because $Sb_2O_3$ might react with HBr derived from the thermal degradation of BFRs and then generate $SbBr_3$ with a low boiling point, which easily evaporated from the reactor and condensed in the oil product faction, hereby resulting in the high bromine contents in the oil products, as shown in Figure 2.7.

Table 2.3. Total bromine contents in the oil derived from the pyrolysis of Br-HIPS

| | **450 ℃** | **500 ℃** | **550 ℃** |
|---|---|---|---|
| Br in oil (wt. %)[a] | 7.96 | 8.21 | 8.56 |
| Yield of bromine in the oil[b] | 68.31 | 74.49 | 77.38 |

[a] Br in oil (wt. %) = mass of bromine in oil (g) /mass of oil (g) ×100;
[b] Yield of Br (%) = mass of Br in oil/ mass of Br in plastic ×100.

The total bromine content in the oil products contained the organobrominated and inorganic brominated compounds, such as antimony bromide. As for the organobromine content in the pyrolysis oils, it was determined by the GC-ECD analysis, which only responds to organo-halogenated compounds, in terms of the organobrominated compounds in this chapter. In each analysis, the same volume of oils was injected and analyzed at the same GC conditions [2-27]. Therefore, the chromatographs can be generally compared with each other to reveal the variation of the organobrominated compounds by the number, size and intensity of ECD peaks. Figure 2.9 shows the results of the GC-ECD analysis of the oil products obtained at different pyrolysis temperatures. It apparently illustrated that a large amount of organobrominated compounds also existed in the pyrolysis oil. As the increase of the pyrolysis temperature, the intensity of the ECD peak increased, especially the peaks in the later retention time increase significantly. It illustrated that the high temperature will contribute to the production of certain large molecule brominated organic compounds, which was attributed to the more intensive cracking reaction and the bromine addition reaction.

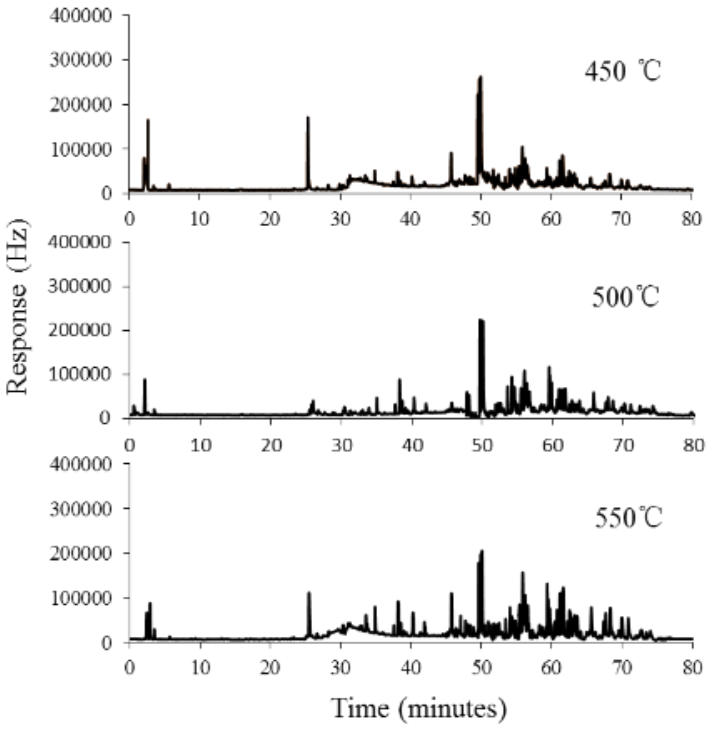


Figure 2.9. GC-ECD chromatograms of the oils produced by the pyrolysis of Br-HIPS at different temperatures

### 2.3.3 Effect of additives on the pyrolysis of Br-HIPS

#### 2.3.3.1 Effect of additives on the gas and oil products.

As stated above, a high total bromine content and lots of organobrominated compounds retained in the oil products, and the effect of pyrolysis temperature on them was limited. Therefore, the effective catalysts or additives were essential for the debromination to obtain valuable oil products. RM, CL and NZ were industrial solid wastes or natural mineral. Because of their low-cost, high metal oxides content and catalytic cracking properties, they were frequently applied as catalysts or additives for the catalytic pyrolysis of biomass and plastics [2-15, 2-19, 2-20, 2-28, 2-29].

In this chapter, in order to investigate the effect of RM, CL and NZ additives on the degradation of Br-HIPS and the debromination characteristic, the pyrolysis experiments were carried out in presence of each additive at the pyrolysis temperature of 500 ℃. Because of the reaction of the additives and the evolved HBr, the accurate mass balance and the product yields of Br-HIPS degradation were difficult to be calculated. As for the gaseous products, they were measured by the GC-TCD and the results were listed in Table 2.4. It was found that when the Br-HIPS sample was pyrolyzed without additives, propene and propane were the main gaseous products. When CL was used in the reaction system, there was no obvious change in the gaseous product, compared with that of thermal pyrolysis. When the Br-HIPS sample was pyrolyzed with RM and NZ, respectively, the yields of gaseous products increased significantly, especially in the case of NZ. It was presumably because of the zeolite property (acidity and large surface area) of RM and NZ, which could exert a catalytic cracking effect during the pyrolysis of Br-HIPS and promoted the yields of gaseous products. In addition, it should be mentioned that the bromine content in the gas products was almost zero, regardless of the presence or absence of each additive. This result was consistent with the results reported by other researchers [2-9].

Table 2.4. Main components of gas and oil products (wt.%/sample mass)

| Main gaseous products | Thermal | +RM | +CL | +NZ |
|---|---|---|---|---|
| Hydrogen | 0.02 | 0.00 | 0.00 | 0.05 |
| Methane | 0.15 | 0.29 | 0.16 | 0.27 |
| Ethene | 0.14 | 0.35 | 0.15 | 0.49 |
| Ethane | 0.16 | 0.43 | 0.18 | 0.60 |
| Propene | 0.21 | 0.49 | 0.22 | 0.64 |
| Propane | 0.17 | 0.65 | 0.14 | 0.69 |

The oil products evolved from the pyrolysis of Br-HIPS in the absence and presence of additives were analyzed by GC-MS, and the main components of them were also listed in Table 2.5. It illustrated that toluene, ethylbenzene, styrene and 1,3-diphenylpropane were the main components in oil products, over 50 wt. % of Br-HIPS sample weight. It was in well agreement with the previous findings [2-7,2-10,2-27], which was a consequence of the structure property and the thermal degradation property of the HIPS matrix. In addition, in the case of without additives, the ethylbenzene, cumene and 1,3-diphenylpropane were the main components of the oil products while the small amount of styrene existed in the oil. It was attributed to the presence of $Sb_2O_3$ that reacted with HBr derived from the decomposition of BFRs to produce $SbBr_3$ with an acidity nature, which played a catalytic role to convert the styrene and α-methylstyrene into ethylbenzene and 1,3-diphenylpropane by the intermolecular H transfer and the intermolecular carbanion.

However, when the additives were added, the yield of styrene increased a lot, accompanied by the decrease of ethylbenzene and 1,3-diphenylpropane. On the one hand, it partially originated from the fact that the main components of these three additives were metal oxides, such as $Fe_2O_3$ and CaO, which would exert basic-catalytic impact on the degradation of HIPS to form carboanions by the H abstraction, resulting in the increase of styrene in the oil products [2-20]. On the other hand, the existence of metal oxides in the additives would inhibit the formation of $SbBr_3$ due to the competing reaction with HBr generated by the degradation of BFRs. In addition,

owing to the pore property, the additives also could capture the produced volatile $SbBr_3$, subsequently reducing its amount in the oil.

Table 2.5. Main components of oil products (wt.%/sample mass)

| **Main oil components** | Thermal | +RM | +CL | +NZ |
|---|---|---|---|---|
| *Single ring compounds* | | | | |
| Toluene | 6.96 | 3.16 | 3.78 | 3.39 |
| Ethylbenzene | 28.60 | 11.80 | 11.03 | 16.20 |
| Styrene | 0.48 | 25.10 | 31.17 | 19.69 |
| Cumene | 4.29 | 2.42 | 1.96 | 3.86 |
| Methylstyrene | 0.92 | 1.47 | 3.05 | 1.37 |
| *Two ring compounds* | | | | |
| Diphenylpropane | 18.02 | 8.98 | 6.93 | 11.43 |
| diphenyl-butene | 4.44 | 1.03 | 1.49 | 2.29 |
| Methyl-naphthalene | 0.14 | 0.10 | 1.32 | 1.37 |
| Methyl-phenylindan | 0.47 | 1.86 | 0.79 | 2.60 |
| Multi ring compounds | | | | |
| Benzylnaphthalene | 0.92 | 1.19 | 0.89 | 1.41 |
| Anthracene | n.d.[a] | 1.01 | 0.87 | 1.49 |
| Ethenylanthracene | 0.28 | 0.41 | 0.22 | 0.83 |
| Triphenylbenzene | 0.85 | 0.47 | 0.60 | 0.35 |
| *Brominated compounds* | | | | |
| (1-Bromoethyl)benzene | 2.75 | 0.53 | 0.51 | 0.97 |
| Methylbenzyl bromide | 0.47 | n.d. | n.d. | 0.10 |
| Dibromoanthracene | 0.11 | 0.15 | 0.15 | 0.24 |

[a] Not detected.

In addition, when the Br-HIPS sample was pyrolyzed in the presence of RM, CL and NZ, respectively, the amount of styrene in the oil products was obviously different. It was probably caused by the differences in the composition and the surface area of additives, as shown in Table 2.1. In the case of RM, it was mainly attributed to the fact that red mud also contained the $SiO_2$, $Al_2O_3$ and $TiO_2$ components and forms the Si-O-T units (T = Si or Al), which makes RM to have

zeolite nature (Brønsted acid) and play catalytic action to increase the amount of ethybenzene by further hydrogenation of styrene [2-30]. As for NZ, a high ratio of $Al_2O_3$ and $SiO_2$ in NZ will also improve the acidity of NZ. Therefore, the oil derived from the pyrolysis of Br-HIPS and NZ contained smaller amounts of styrene and larger amounts of ethylbenzene. Besides, the high amounts of 2-methylnaphthalene, anthracene and 9-ethenylanthracene compounds in the oil were detected due to the Diels-Alder reaction, which was proposed by Koo et al. [2-31]. It also illustrated the stronger acidity of NZ than other two additives.

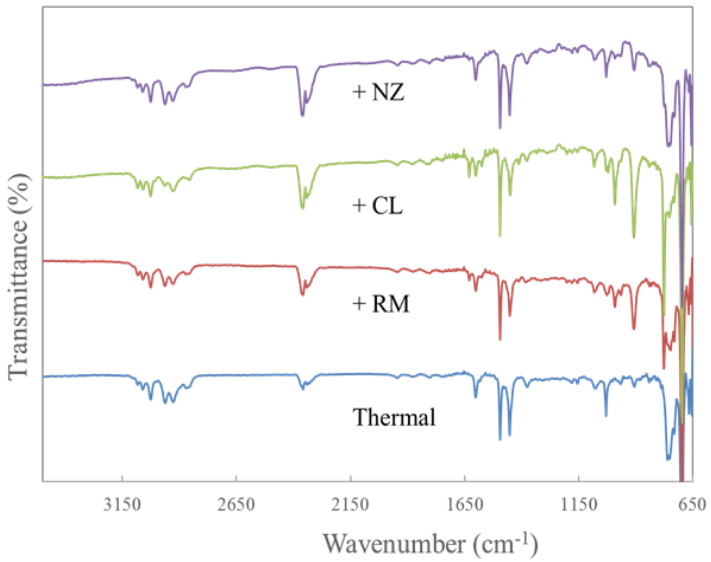


Figure 2.10. FT-IR spectra of oil products evolved from the pyrolysis of Br-HIPS without additive, with RM, CL and NZ additives. (thin film/KCl)

For the purpose of verifying the molecular structure and the organic functional groups, the oil products were further characterized by FT-IR analysis and the result is presented in Figure 2.10. Generally, the band in the 3150-3000 $cm^{-1}$ range is associated with the vibration of C-H bond in the aromatic ring. The strong band observed in the interval of 900-675 $cm^{-1}$ were assigned of C-H out-of-plane vibration of the mono-substituted aromatic ring, which further confirmed the aromatic characteristics of the oil products. Additionally, the vibration bands in the region of 3000-2900 $cm^{-1}$ correspond to the C-H asymmetric stretching of $CH_3$, $CH_2$ and CH groups. The vibration bands at 992 and 906 $cm^{-1}$ are the typical vibration mode of $CH=CH_2$ in the vinyl compounds and the bands at 1450 $cm^{-1}$ are ascribed to the asymmetric bending vibration of ethyl

groups. The aliphatic functional groups observed in the FTIR spectra are probably attributed to the alkyl groups attached to the aromatic rings.

Comparing the FTIR spectra of the oil products derived from Br-HIPS pyrolysis in the absence and presence of additives, it was observed that the vibration bands at 992 and 906 $cm^{-1}$, corresponding to $CH=CH_2$ bonds in the vinyl compounds, in the oil from the Br-HIPS pyrolysis with additives are more intensive than that of oil from the Br-HIPS pyrolysis without additives. Whereas, the bands at 1450 $cm^{-1}$ are ascribed to the asymmetric bending vibration of ethyl groups and become weaker than that when no additive was used. The above variations corroborated with the GC-MS analytical results that when additives were used, the amount of ethylbenzene decreased, accompanied by the increase of styrene. In addition, it should be noted that the bond vibration bands at 1030 $cm^{-1}$ were typical of aryl-bromines [2-9,2-27] and when the additives were used, the intensity of this band became weakened, which was also well associated with those obtained by the GC-MS analysis.

### 2.3.3.2 Effect of additives on bromine and antimony contents in the oil products

The total bromine and antimony contents in the pyrolysis oils were determined using a bomb calorimeter equipped with an ion chromatograph and ICP-MS after digestion of oil samples, respectively. The bromine and antimony contents of each oil product were listed in Table 2.6. It was apparent that the additives played a positive role in the removal of bromine and antimony contents from the pyrolysis oils. At the same pyrolysis temperature of 500 ℃, the bromine content of 8.21wt.% in the pyrolysis oil of Br-HIPS degradation without additives was reduced dramatically to 0.84wt.%, 0.91wt.% and 3.47wt.%, when RM, CL and NZ were used as the additive, respectively. RM was more effective than the other two additives in the respect of bromine removal, which was attributed to the fact that, on the one hand, $Fe_2O_3$ in the red mud would react with HBr derived from the degradation of BFRs and hinder the formation of volatile $SbBr_3$, on the other hand, the zeolite property of RM [2-15] could catalytically degrade the organobromine compounds. The effect of NZ on the bromine removal was weakest. It was mainly due to the fact that $Al_2O_3$ and $SiO_2$ were the main components, which could not react with bromine

radicals derived from the degradation of BFRs. Therefore, it illustrated that the reaction between bromine and metal oxides was the dominant mechanism of the bromine fixation when the additives were used. In addition, the antimony content of the oil product was measured and the result is also shown in Table 2.6. When additives were employed, the antinomy content in the oils was also reduced a lot. The main reasons were already explained in the section 3.3.1.

Table 2.6. Total bromine and antimony contents in the oil products derived from the pyrolysis of Br-HIPS with and without additives at the temperature of 500 ℃

| | **Thermal** | **+RM** | **+CL** | **+NZ** |
|---|---|---|---|---|
| Br in oil (wt. %) [a] | 8.21 | 0.84 | 0.91 | 3.47 |
| Sb in oil (wt. %) [b] | 1.84 | 0.35 | 0.52 | 0.69 |

[a] Br in oil (wt. %) = mass of bromine in oil (g) /mass of oil (g) ×100;

[b] Sb in oil (wt.%) = mass of antimony in oil (g) /mass of oil (g) ×100.

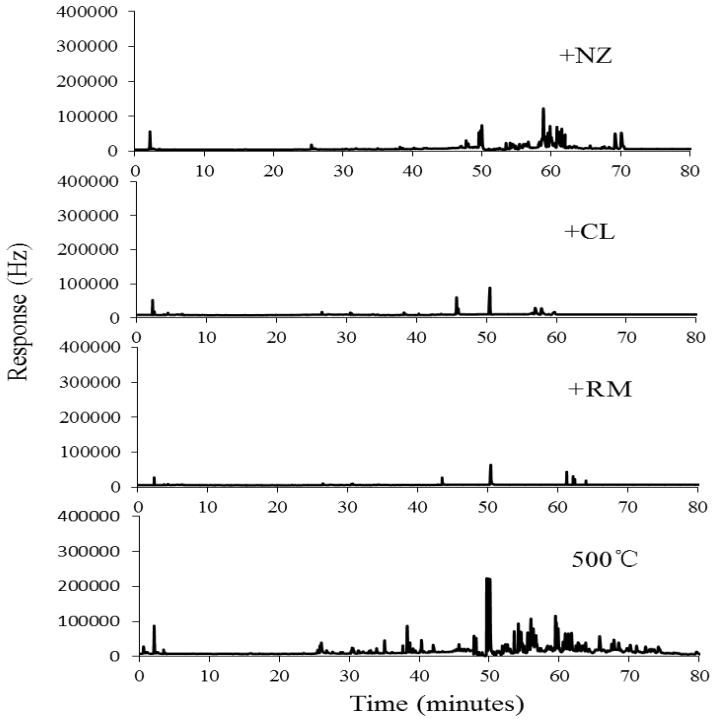


Figure 2.11. GC-ECD chromatographs of the oils produced from the pyrolysis of Br-HIPS without and with additives at the temperature of 500 ℃.

The main purpose of using the additives was to remove the organobromine from the pyrolysis oils and obtained the clean oil products. The organobromine compounds in the oils were

analyzed by the GC-ECD and the results are presented in Figure 2.11. When the Br-HIPS sample was pyrolyzed with NZ, certain portion of the organobromine compounds still retained in the pyrolysis oil. Meanwhile, when RM and CL were applied, the intensity of ECD peaks apparently reduced dramatically. It implied that RM and CL could also effectively suppress the formation of organobrominated compounds and produce the valuable oil products.

### 2.3.4 Pyrolysis residues

When the Br-HIPS sample was pyrolyzed in the presence of additives, both bromine and antimony contents in the oils decreased dramatically. The bromine in the flame retardants is converted to not only HBr and the brominated organic compounds but also metal bromides left in the residues. However, because of very heterogeneous and intermingled nature of the residues, it was impossible to take representative sampling to analyze precise contents of Br and Sb in the residues [2-9]. Therefore, the residues were qualitatively analyzed by the SEM-EDAX and XRD in order to determine and compare the additive change, residue compositions and bromine and antimony distributions in the residues. The results are presented in Figure 2.12 and Figure 2.13, respectively. In the EDAX pattern, when Br-HIPS was pyrolyzed in the absence of additives, the residue was found to contain carbon, titanium, bromine and antimony. The carbon can be caused by char formation. Only few of bromine and antimony was left in the residues. And from the XRD pattern, neither $Sb_2O_3$ nor $SbBr_3$ crystal was identified in the residues in Figure 2.13, whilst only the $TiO_2$ crystal was observed, which is commonly employed as an additive in plastics [2-9]. It was attributed to the reaction between $Sb_2O_3$ with HBr, derived from the BFRs decomposition, thereby generating the volatile $SbBr_3$ [2-32, 2-33]. Therefore, major parts of antimony and bromine were found in the oil products rather the chars when Br-HIPS was pyrolyzed without catalysts [2-5, 2-10].

In the case of Br-HIPS and RM pyrolysis, there were lots of bromine and antimony elements were observed in the residues from the EDAX pattern. When compared with XRD pattern of RM in Figure 2.5, the peaks of $Fe_2O_3$ and FeOOH disappeared or weakened while the additional peaks of $FeBr_2$, $Sb_4O_5Br_2$, $SbBr_3$ and $Sb_2O_3$ were detected. $FeBr_3$ was not identified in the residues,

which owes to that $FeBr_3$ decomposes above 200 ℃ to form $Br_2$ and $FeBr_2$ [2-2, 2-11,2-12]. In addition, it was found that certain amount of $Fe_2O_3$ was reduced into $Fe_3O_4$ by the hydrogenation reaction.

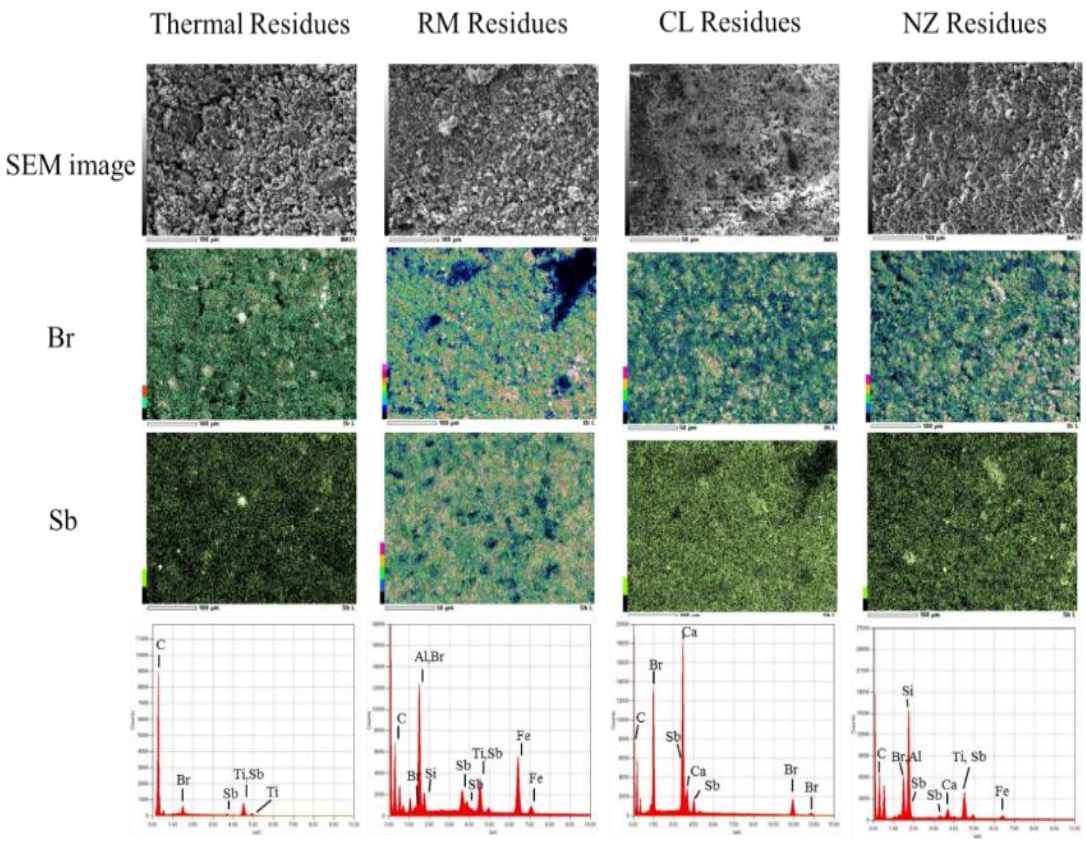


Figure 2.12. SEM and EDX analysis of the residues derived from the pyrolysis of Br-HIPS sample without and with RM, CL and NZ, respectively.

When Br-HIPS was pyrolyzed with CL, as shown in Figure 2.12, lots of bromine and antimony were also detected in the residues. From the XRD pattern, it was found that the peaks of CaO became weaker while the new peaks of $CaBr_2$ and $CaBr_2(H_2O)_6$ were observed in the pattern. The existence of $CaBr_2(H_2O)_6$ was attributed to the hygroscopic nature of $CaBr_2$ [2-11,2-12]. In addition, the $Sb_2O_3$ were detected, which further confirmed the presence of lots of antimony existing in the residues.

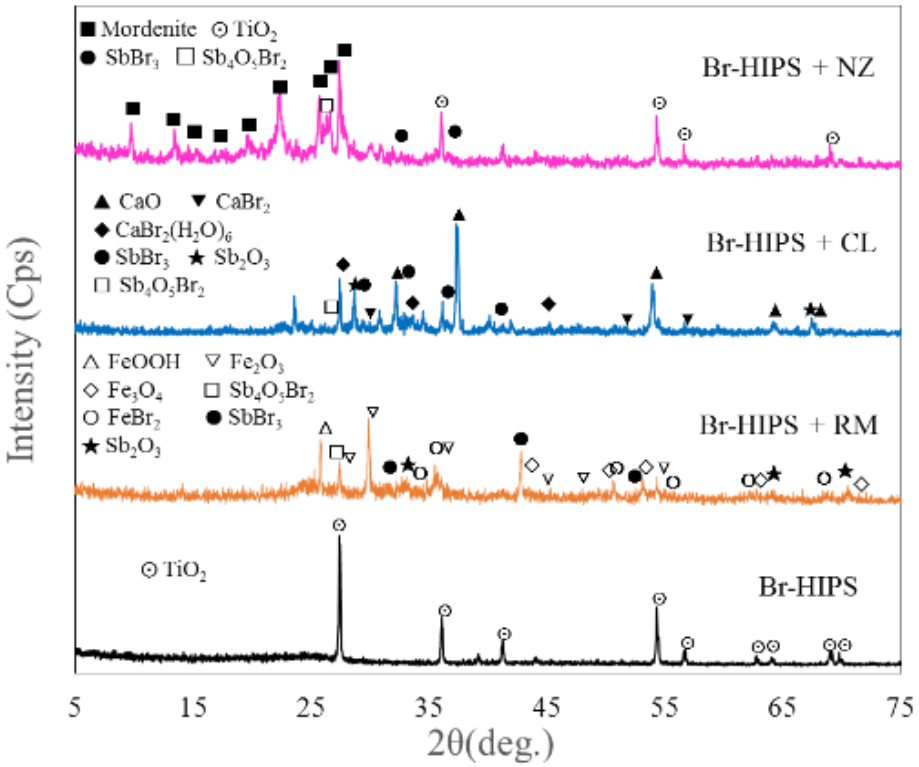


Figure 2.13. XRD patterns of residues derived from the pyrolysis of Br-HIPS sample without and with RM, CL and NZ, respectively.

As for the residues of Br-HIPS and NZ pyrolysis, no reflection characteristic of metal bromides was presented in the XRD pattern, except for $SbBr_3$ and $Sb_4O_5Br_2$. It was related to the fact that natural zeolite is mainly composed of $SiO_2$ and $Al_2O_3$, which would not react with evolved HBr. The amount of other metal oxides, such as CaO and $Fe_2O_3$, is few in NZ and then produced metal bromide species with too small particle sizes on the surface of the residue to be identified by the XRD method. As for NZ, the fixation of bromine and antimony was mainly associated with the physical adsorption of $SbBr_3$ and $Sb_4O_5Br_2$ on the surface of NZ [2-9]. When compared with that of RM and CL, the bromine fixation ability of NZ was weaker and then the bromine and antimony content in the oils were relatively higher.

## 2.4. Summary

In this chapter, the pyrolysis of high impact polystyrene containing BFRs and $Sb_2O_3$ was carried out in the absence and presence of three additives (red mud, calcined limestone and natural

zeolite) in a fixed bed reactor. In the pyrolysis of Br-HIPS without additives, with the increase of the pyrolysis temperature from 450 ℃ to 550 ℃, the yield of the residue decreased while the yield of the gas increased slightly. The yield of the oil product was dependent upon the pyrolysis temperature, and the maximum oil yield (84.4 wt.%) was obtained at the pyrolysis temperature of 500 ℃. In the pyrolysis of Br-HIPS with the additives, it was found that red mud and natural zeolite could increase the yield of the gaseous product because of their zeolite property. In addition, the use of additives, especially red mud and calcined limestone, could increase the amount of styrene at the expense of ethylbenzene and 1,3-diphenylpropane. Furthermore, the additives could also upgrade the oil products by reducing the total bromine content, organobrominated compounds and antimony content in the oil products significantly. Red mud was the most effective additives used in this chapter. Because, on the one hand, red mud played a cracking catalyst effect on destroying the organobrominated compounds. On the other hand, it could work as a sorbent to fix HBr formed by the Br-HIPS degradation. The bromine fixation abilities of red mud and calcined limestone were similar with each other and better than that of natural zeolite, which implied that the reaction between bromine and metal oxides was the dominant mechanism of the bromine fixation. Additionally, from the XRD and SEM-EDAX analysis of the residues, it was found that there were lots of metal bromides compounds existing in the residues, which further confirmed the above bromine fixation mechanism.

## References


[2-1] United Nations Environment Programme [UNEP] year book 2009, new science and developments in our changling environment. http://www.unep.org/yearbook/2009/

[2-2] Yang, X. N., Sun, L., S., Xiang, J., Hu, H., & Su, S. (2013). Pyrolysis and dehalogenation of plastics from waste electrical and electronic equipment (WEEE): A review. Waste Management, 33, 462–473.

[2-3] Ongondo, F., O., Williams, I., D., & Cherrett, T., J. (2011). How are WEEE doing? A global review of the management of electrical and electronic wastes. Waste Management, 31, 714–730.

[2-4] Bhaskar, T., Matsui, T., Uddin, M., A., Kaneko, J., Mutoa, A., & Sakata, Y. (2003).Effect of $Sb_2O_3$ in brominated heating impact polystyrene (HIPS-Br) on thermal degradation and debromination by iron oxide carbon composite catalyst (Fe-C). Applied Catalysis B: Environmental, 43, 229-241.

[2-5] Jakab, E., Uddin, M., A., Bhaskar, T., & Sakata, Y. (2003). Thermal decomposition of flame-retarded high-impact polystyrene. Journal of Analytical and Applied Pyrolysis, 68-69, 83-89.

[2-6] Ni, M., J., Xiao, H., X., Chi, Y., Yan, J., H., Buekens, A., Jin, Y., Q., & Lu, S., Y. (2012). Combustion and inorganic bromine emission of waste printed circuit boards in a high temperature furnace. Waste Management, 32, 568–574.

[2-7] Hall, W., & Williams, P., T. (2008). Removal of organobromine compounds from the pyrolysis oils of flame retarded plastics using zeolite catalysts. Journal of Analytical and Applied Pyrolysis, 81, 139-147.

[2-8] Bozi, J., & Blazsó, M. (2009). Catalytic modification of pyrolysis products of nitrogen-containing polymers over Y zeolites. Green Chemistry, 11, 1638–1645.

[2-9] Hall, W., J., Miskolczi, N., Onwudili, J., & Williams, P., T. (2008). Thermal Processing of Toxic Flame-Retarded Polymers Using a Waste Fluidized Catalytic Cracker (FCC) Catalyst. Energy & Fuels, 22, 1691–1697.

[2-10] Jung, S., H., Kim, S., J., & Kim, J., S. (2012). Fast pyrolysis of a waste fraction of high impact polystyrene (HIPS) containing brominated flame retardants in a fluidized bed reactor: The effects of various Ca-based additives (CaO, $Ca(OH)_2$ and oyster shells) on the removal of bromine. Fuel, 95, 514-520.

[2-11] Terakado, O., Ohhashi, R., & Hirasawa, M. (2011). Thermal degradation study of tetrabromobisphenol A under the presence metal oxide: Comparison of bromine fixation ability. Journal of Analytical and Applied Pyrolysis, 91, 303–309.

[2-12] Terakado, O., Ohhashi, R., & Hirasawa, M. (2013). Bromine fixation by metal oxide in pyrolysis of printed circuit board containing brominated flame retardant. Journal of Analytical and Applied Pyrolysis, 103, 216–221.

[2-13] Ali, S., Garforth, A., A., Harris, D., H., Rawlence, D., J., & Uemichi, Y. (2002). Polymer waste recycling over "used" catalysts. Catalysis Today, 75, 247–255.

[2-14] Cardona, S., C. & Corma, A. (2000). Tertiary recycling of polypropylene by catalytic cracking in a semibatch stirred reactor Use of spent equilibrium FCC commercial catalyst. Applied Catalysis B: Environmental, 25, 151–162.

[2-15] López, A., Marco, I., D., Caballero, B., M., Laresgoiti, M., F., Adrados, A. & Aranzabal, A. (2011). Catalytic pyrolysis of plastic wastes with two different types of catalysts: ZSM-5 zeolite and Red Mud. Applied Catalysis B: Environmental, 104, 211–219.

[2-16] Sushil, S., & Batra, V., S. (2008). Catalytic applications of red mud, an aluminium industry waste: A review. Applied Catalysis B: Environmental, 81, 64–77.

[2-17] Ordóñez, S., Sastre, H., & Díez, F., V. (2001). Characterisation and deactivation studies of sulfided red mud used as catalyst for the hydrodechlorination of tetrachloroethylene. Applied Catalysis B: Environmental, 29, 263–273.

[2-18] Álvarez, J., Ordóñez, S., Rosal, R., Sastre, H., V. & Díez, F., V. (1999). A new method for enhancing the performance of red mud as a hydrogenation catalyst. Applied Catalysis A: General, 180, 399-409.

[2-19] Hinz, B., Hoffmockel, M., Pohlmann, K., Schädel, S., Schimmel, I., & Sinn, H. (1994). Dehalogenation of pyrolysis products. Journal of Analytical and Applied Pyrolysis, 30, 35-46.

[2-20] Lee, S., Y., Yoon, J., H., Kim, J., R., & Park, D., W. (2001). Catalytic degradation of polystyrene over natural clinoptilolite zeolite. Polymer Degradation and Stability, 74, 297–305.

[2-21] Lee, S., Y., Yoon, J., H., Kim, J., R., & Park, D., W. (2002). Degradation of polystyrene using clinoptilolite catalysts. Journal of Analytical and Applied Pyrolysis, 64, 71–83.

[2-22] Yanik, J., Uddin, M., A., Ikeuchi, K., & Sakata, Y. (2001). The catalytic effect of Red Mud on the degradation of poly (vinyl chloride) containing polymer mixture into fuel oil. Polymer Degradation and Stability, 73, 335–346.

[2-23] Vasile, C., Brebu, M., A., Totolin, M., Yanik, J., Karayildirim, T., & Darie, H. (2008). Feedstock Recycling from the Printed Circuit Boards of Used Computers. Energy & Fuels, 22, 1658–1665.

[2-24] Park, E., S., Kang, B., S., & Kim, J., S. (2008). Recovery of Oils with High Caloric Value and Low Contaminant Content by Pyrolysis of Digested and Dried Sewage Sludge Containing Polymer Flocculants. Energy & Fuels, 22, 1335–1340.

[2-25] Aguado, J., Serrano, D. P., Miguel, G. S., Castro, M. C., & Madrid, S. (2007). Feedstock recycling of polyethylene in a two-step thermo-catalytic reaction system. Journal of Analytical and Applied Pyrolysis, 79, 415-423.

[2-26] Syamsiro, M., Wu, H., Komoto, S., Cheng, S., Noviasri, P., Prawisudha, P., & Yoshikawa, K. (2013). Co-Production of Liquid and Gaseous Fuels from Polyethylene and Polystyrene in a Continuous Sequential Pyrolysis and Catalytic Reforming System. Energy and Environment Research, 3, 2.

[2-27] Miskolczi, N., Hall, W., J., Angyal, A., Bartha, L., & Williams, P., T. (2008). Production of oil with low organobromine content from the pyrolysis of flame retarded HIPS and ABS plastics. Journal of Analytical and Applied Pyrolysis, 83, 115–123.

[2-28] Yathavan, B., K., & Agblevor, F., A. (2013). Catalytic Pyrolysis of Pinyon−Juniper Using Red Mud and HZSM‑5. Energy & Fuels, 27, 6858-6865.

[2-29] Zhang, L., Zhang, B., Yang, Z., Q., & Yan, Y., F. (2014). Pyrolysis behavior of biomass with different Ca-based additives. RSC Advances, 4, 39145–391555.

[2-30] Wang, S., B., Ang, H., M., & Tadé, M., O. (2008). Novel applications of red mud as coagulant, adsorbent and catalyst for environmentally benign processes. Chemosphere, 72, 1621–1635.

[2-31] Koo, J., K., Kim, S., W., & Seo, Y., H. (1991). Characterization of aromatic hydrocarbon formation from pyrolysis of polyethylene-polystyrene mixtures. *Resources, Conservation and Recycling, 5*, 365-382.

[2-32] Rzyman, M., Grabda, M., Oleszek-Kudlak, S., Shibata, E., & Nakamura, T. (2010). Studies on bromination and evaporation of antimony oxide during thermal treatment of tetrabromobisphenol A (TBBPA). Journal of Analytical and Applied Pyrolysis, 88, 14–21.

[2-33] Grause, G., Karakita, D., Kameda, T., Bhaskar, T., & Yoshioka, T. (2012). Effect of heating rate on the pyrolysis of high-impact polystyrene containing brominated flame retardants: fate of brominated flame retardants. Journal of Material Cycles and Waste Management, 14, 259–265.

# Chapter 3

# Fuel oil production from two-stage pyrolysis-catalytic reforming of brominated high impact polystyrene using zeolite and iron oxide loaded zeolite catalysts

## 3.1. Introduction

Pyrolysis has been proposed as a viable processing route for not only converting the organic compounds in WEEE plastics into fuels and chemical feedstock but also separating and recovering the metals from plastic fractions [3-1]-[3-3]. Noteworthy, when HIPS added with brominated flame retardant and $Sb_2O_3$ synergist (Br-HIPS) is pyrolyzed with neither additives nor catalysts, a large amount of brominated compounds, such as $SbBr_3$, HBr and organic brominated compounds, would exist in the oil product [3-4]-[3-9]. The presence of brominated compounds, especially the organic brominated compounds, in the oils would reduce their quality and hinder their reuse [3-5, 3-6]. Therefore, lots of debromination methods, effective catalysts and additives in the pyrolysis process of WEEE plastics have been investigated to reduce the bromine content from the oil products [3-1]. Bhaskar et al. synthesized the composite Fe-C and Ca-C additives, which could effectively remove the brominated compounds from the pyrolysis oil products [3-8, 3-9]. Terakado and Hirasawa used the metal oxides in the pyrolysis of TBBPA and printed circuit boards containing brominated flame retardants, respectively. They concluded that the addition of metal oxides could effectively suppress the formation of HBr and brominated organic compounds. The above research results indicated that the metal oxides could reduce the bromine content in the pyrolysis oil products by the neutralization reaction [3-10, 3-11]. Besides, there were many researches on zeolite catalysts used for the debromination in the pyrolysis of brominated WEEE

plastics [3-5, 3-6]. Hall et al investigated the catalytic pyrolysis of brominated flame-retarded HIPS and ABS by using HY zeolite and HZSM-5 zeolite, which proved that the zeolite catalysts could effectively catalytically reform the organobrominated compounds and reduce the bromine content in the pyrolysis oils [3-5]. The above research indicated that when the proper catalysts or additives are employed, the low-bromine or bromine-free oil products could be obtained from the catalytic pyrolysis of WEEE plastics.

However, the usage of expensive commercial zeolite catalysts would improve the cost of the process, due to the high amounts of catalyst which would be necessary in a continuous operating plant. Ali and co-worker [3-12] concluded that the catalyst cost (type and amount) is a key factor when it comes to compare the catalytic cracking with thermal cracking technology economics; for this reason, the study on deactivation, regeneration and reuse of catalysts in the catalytic pyrolysis of WEEE plastics is of the most interest from an industrial implementation point of view [3-13].

Additionally, in the practical operation, the impurities (such as metals) in WEEE and lots of cokes produced on the catalysts, would easily make the catalyst deactivate, which will increase the usage amount of catalysts and operating cost [3-14]. Two-stage combined pyrolysis and catalytic reforming process is proposed to be used for the pyrolysis recycling of WEEE plastics in this chapter. In the first stage, plastics are pyrolyzed for the purpose of depolymerization and decomposition. In the second stage, the pyrolysate of the plastics is reformed by the catalysts into valuable bromine-free liquid oil and gas. This pyrolysis and catalytic reforming process have the following merits. It is more practical for the recycling of raw WEEE plastics, which normally contain some impurities and metals that may deactivate the catalyst easily in the single catalytic pyrolysis process [3-15]. In addition, the residues and catalysts are separated, which has a potential to recycle the residues and metals, as well as to regenerate the catalyst, respectively.

Therefore, in the present chapter, the performance of small-scale two-stage combined pyrolysis and catalytic reforming reaction system used for the pyrolysis recycling of Br-HIPS was investigated at both the pyrolysis and reforming temperature of 500 ℃. Natural zeolite (NZ) and

commercial HY zeolite (YZ), as well as synthesized iron oxide loaded natural zeolite (Fe-NZ) and iron oxide loaded HY zeolite (Fe-YZ) were selected as the catalysts. The effect of catalyst types on the product yield, the gas and oil product composition and the debromination efficiency of the oil products were evaluated in details. In addition, the detail debromination mechanism will be discussed. Finally, the catalytic performance of the deactivated and regenerated Fe-NZ catalysts were also investigated in order to evaluate its effectiveness systematically.

## 3.2. Experimental

### 3.2.1. Materials

The feedstock sample was HIPS containing brominated flame retardant and $Sb_2O_3$ as a synergist. The brominated flame retardant was decabromo diphenyl ethane (DDE). The sample will be referred to as Br-HIPS. The samples were rectangular; with a size of 2 mm width and 3 mm length. The proximate analysis and ultimate analysis of the Br-HIPS sample are shown in Table 3.1. And the photos of Br-HIPS sample used in this chapter and the molecular structure of HIPS are presented in Figure 3.1.

Table 3.1. Proximate analysis and ultimate analysis of the Br-HIPS sample

| **Proximate analysis** | **wt.%** | **Ultimate analysis** | **wt.%** |
|---|---|---|---|
| Moisture | 0.00 | C | 78.61 |
| Volatile matter | 98.13 | H | 7.11 |
| Fixed carbon | 0.34 | O | 0.75 |
| Ash | 1.53 | N | 0.10 |
| | | Br | 9.30 |
| | | Sb | 3.77 |
| | | Ti | 0.36 |

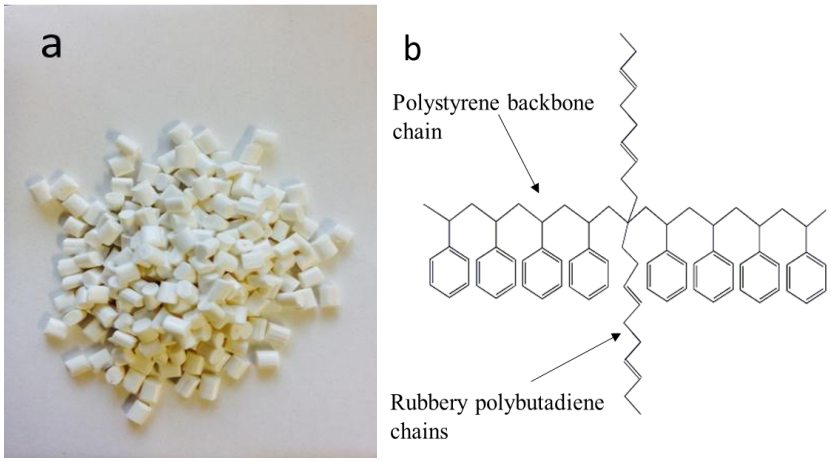


Figure 3.1. The photo of Br-HIPS samples (a) and the molecular structure of HIPS (b)

The catalysts were natural zeolite (NZ), iron oxide loaded natural zeolite (Fe-NZ), HY zeolite (YZ) and iron oxide loaded HY zeolite (Fe-YZ). NZ and YZ catalysts were provided by the Nitto Funka Trading Company and Zeolyst International Company, respectively. Fe-NZ and Fe-YZ catalysts were prepared by the wetness impregnation method with 10 wt.% iron oxide loading referred to the mass of catalysts. The addition of iron oxide was controlled through the concentration of the precursor solution. Firstly, NZ and YZ catalysts were outgassed for 1 hour under vacuum. Then, the desired amount of iron nitrate ($Fe(NO_3)_3\ 9H_2O$) was dissolved in deionized water, to which a predetermined weight of NZ and YZ was added. This solution was continuously stirred at the temperature of 60 ℃ for 24 hours. Subsequently, the suspension was stirred in a rotary vacuum evaporator at the temperature of 60 ℃ until the water was completely evaporated. The catalysts were then dried at 110 ℃ for 24 hours. The dry-based catalyst was calcined at 550 ℃ in air for 4 hours at a heating rate of 5 ℃ /min [3-16]-[3-19]. After that, the catalysts were kept in the vacuum vessel for the future experiments. The mechanism and method of preparation of Fe-Zeolite catalysts are briefly shown in Figure 3.2, which illustrates that the loading of Fe ion on the zeolite catalysts are mainly contributed to the ion exchange and pore adsorption mechanisms. As for the regeneration of spent Fe-NZ catalysts, the spent Fe-NZ catalysts were calcined in air in a muffle furnace at the temperature of 550 ℃ for 4 hours. The photos of the parent and synthesized zeolite catalysts used in this chapter are shown in Figure 3.3. It was found that after the loading of $Fe_2O_3$, the color of the synthesized zeolite catalysts became

red. It also confirmed that the loading of $Fe_2O_3$ on the zeolite catalysts were achieved.

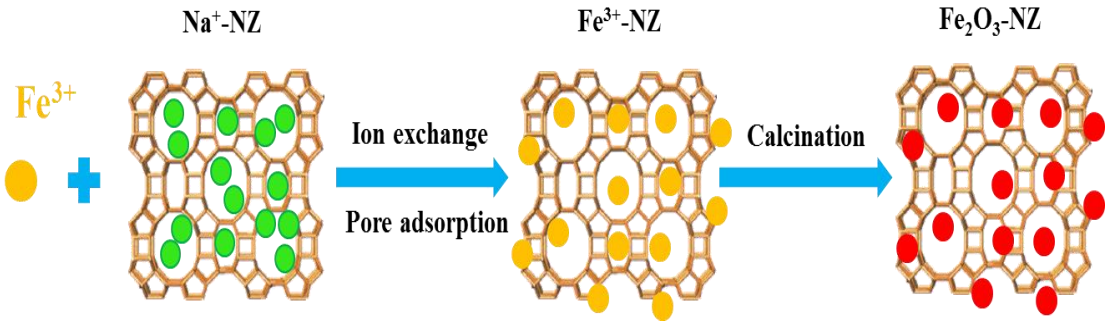


Figure 3.2. The preparation of Fe-Zeolite by impregnation method


Figure 3.3. The photos of NZ, Fe-NZ, YZ and Fe-YZ catalysts used.

### 3.2.2. Experimental setup and procedures

The experimental apparatus was composed of a pyrolyzer, a packed-bed catalytic reformer, a condenser, two condensate samplers and a gas scrubbing bottle, as shown in Figure 3.4. The

pyrolyzer and the reformer were made of stainless steel (SUS316) and covered with an electric heater. The inner diameter and inner height of the pyrolyzer are 30 mm and 280 mm, respectively. The dimensions of the reformer is 25 mm (diameter) ×200mm (height). The reaction temperatures in both the pyrolyzer and the reformer were controlled by K-type thermocouples and heaters. During the experiments, 50 g Br-HIPS sample and 10 g each catalyst (20 wt% of the sample) were fed into the pyrolyzer and the reformer, respectively. Subsequently, the pyrolyzer and the reformer were heated to 500 ℃ at a heating rate of 50 ℃/min under the $N_2$ carrier gas with a flow rate of 50 ml/min. In all experiments, the reactor temperature was held at the target temperature for 2 hours. The oil product was condensed in two oil collectors, which were cooled by ice water solution. In order to capture HBr, the gaseous products were scrubbed with 50 ml 0.1 mol/L NaOH solution in the third trap before being collected in a tedlar bag. Additionally, the photo of the reactor used in this chapter is shown in Figure 3.5.

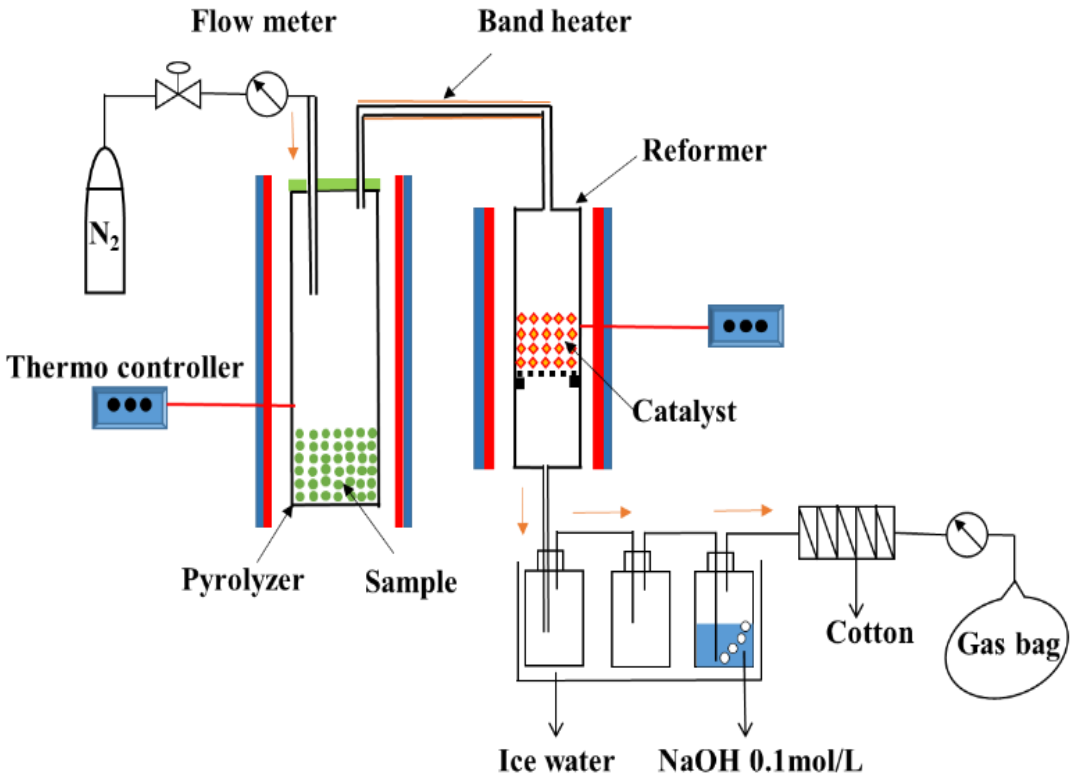


Figure 3.4. Schematic diagram of the pyrolysis and catalytic reforming apparatus.

Figure 3.5**.** The photo of the pyrolysis and the catalytic reforming reactor.

### 3.2.3. Analytical methods

The elemental analysis was conducted by using a Micro Corder JM 10 Elemental Analyzer. The bromine content was determined by an air combustor coupled with Dionex ICS-1100 ion chromatography fitted with a *Shodex* IC *S1-904E* column according to JIS K 7392. The amounts of antimony and titanium were determined by the inductively coupled plasma mass spectrometry (ICP-MS). The antimony and bromine contents in the cokes were measured by a scanning electron microscopy with energy disperse X-ray analysis (SEM-EDX).

The crystalline structures of the four catalysts were characterized by a powder X-ray diffraction (XRD) analysis. XRD measurements were performed using a Rigaku Ultimal V diffractometer with the CuKα radiation (λ = 1.540) at 40kV and 40 mA. Besides, the surface structure was characterized by the scanning electron microscopy (SEM). The surface area and textural properties of the used catalysts were determined by $N_2$ physical adsorption at 77 K, applying the Brunauer–Emmett–Teller (BET) method, using the Micromeritics Tristar 3020 equipment.

The weights of the char and coke were determined by the weight differences of the pyrolyzer and the reformer after and before the experiments, respectively. The weight of the oil product was measured by the weight difference of the oil collectors after and before the experiments. The weight of the gas product was calculated by subtracting the weight of the char, coke and oil products from the total weight of the sample.

The composition of the oil product was analyzed by the gas chromatograph coupled with a mass spectrometer (GC-MS) (Shimadzu QP-2010). The column was an Rtx-5MS capillary column (30 m length, 0.25 mm id, 0.25 μm film thickness). Helium was used as the carrier gas. The injector temperature was 300 ℃. The temperature program used was the initial temperature of 40 ℃ for 10 minutes followed by the heating rate of 5 ℃ /min to 300 ℃ and held at 300 ℃ for 10 minutes. The ion source and Quadrupole temperatures were 230 ℃ and 150 ℃, respectively. The composition of the produced gases in the experiments was measured by a micro gas chromatograph fitted with a thermal conductivity detector (GC-TCD) (Agilent Micro 3000), and the yield of each component was calculated by the following equation.

$$m_i = M_i \times \frac{C_i}{C_{N_2}} \times \frac{V_{N_2}}{22.4} \tag{3.1}$$

Where $m_i$ is the yield of the gas $i$ in the gas products, $M_i$ is the molar mass of each gas product; $C_i$ is the concentration of the gas $i$ in the gas products; $C_{N2}$ is the concentration of $N_2$ in the gas products; $V_{N2}$ is the $N_2$ flow rate ×the flow time.

## 3.3. Results and discussion

### 3.3.1. Catalyst characterization

The parent NZ and YZ catalysts and the catalysts obtained by incorporation of iron oxide loadings (Fe-NZ and Fe-YZ) were characterized by SEM, XRD and BET to determine the effect of the iron oxide addition on the catalyst properties. The $N_2$ adsorption isotherms and the pore

structure properties of the catalysts are shown in Figure 3.6 and Table 3.2, respectively. It can be clearly found that the surface area, the pore volume and the average pore diameter decreased after the iron oxide loaded on NZ and YZ. It may be attributed to the part of $Fe_2O_3$ distributed on the outer surface of NZ and YZ to reduce their outer surface area. The others are transferred into the pores of the catalysts so that the pore diameter and the volume also reduced.

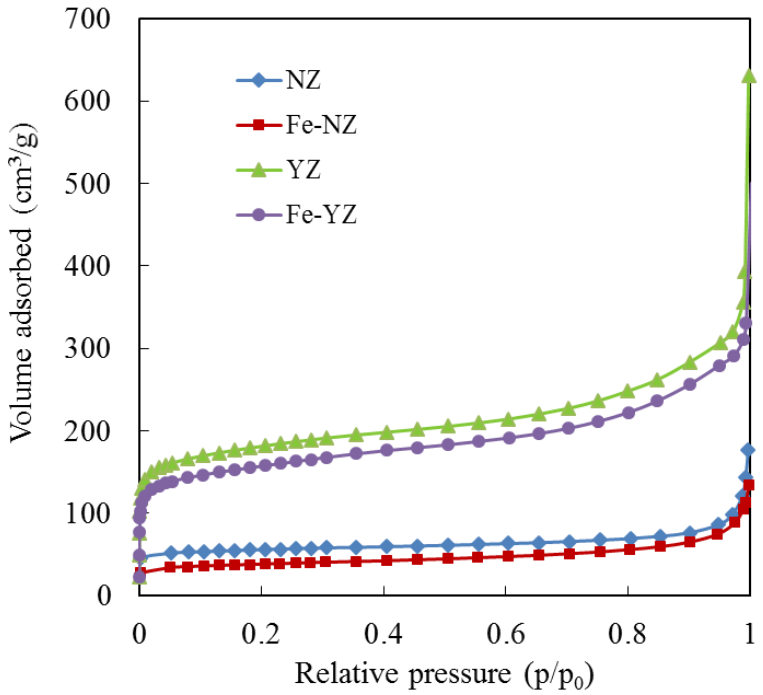


Figure 3.6. $N_2$ adsorption isotherms at 77 K of NZ, Fe-NZ, YZ and Fe-YZ catalysts

Table.3.2. Pore structure properties of NZ, Fe-NZ, YZ and Fe-YZ catalysts

| **Catalysts** | **BET surface area ($m^2/g$)** | **Pore volume ($cm^3/g$)** | **Average pore diameter (nm)** |
|---|---|---|---|
| NZ | 167.91 | 0.226 | 5.60 |
| Fe-NZ | 119.02 | 0.187 | 4.85 |
| YZ | 613.32 | 0.488 | 3.84 |
| Fe-YZ | 507.34 | 0.418 | 3.58 |

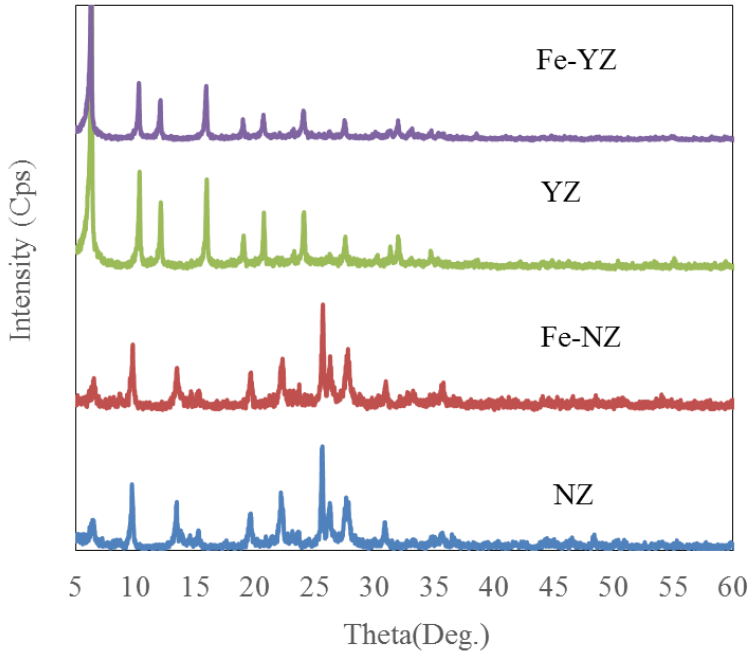


Figure 3.7. XRD patterns of NZ, Fe-NZ, YZ and Fe-YZ catalysts.

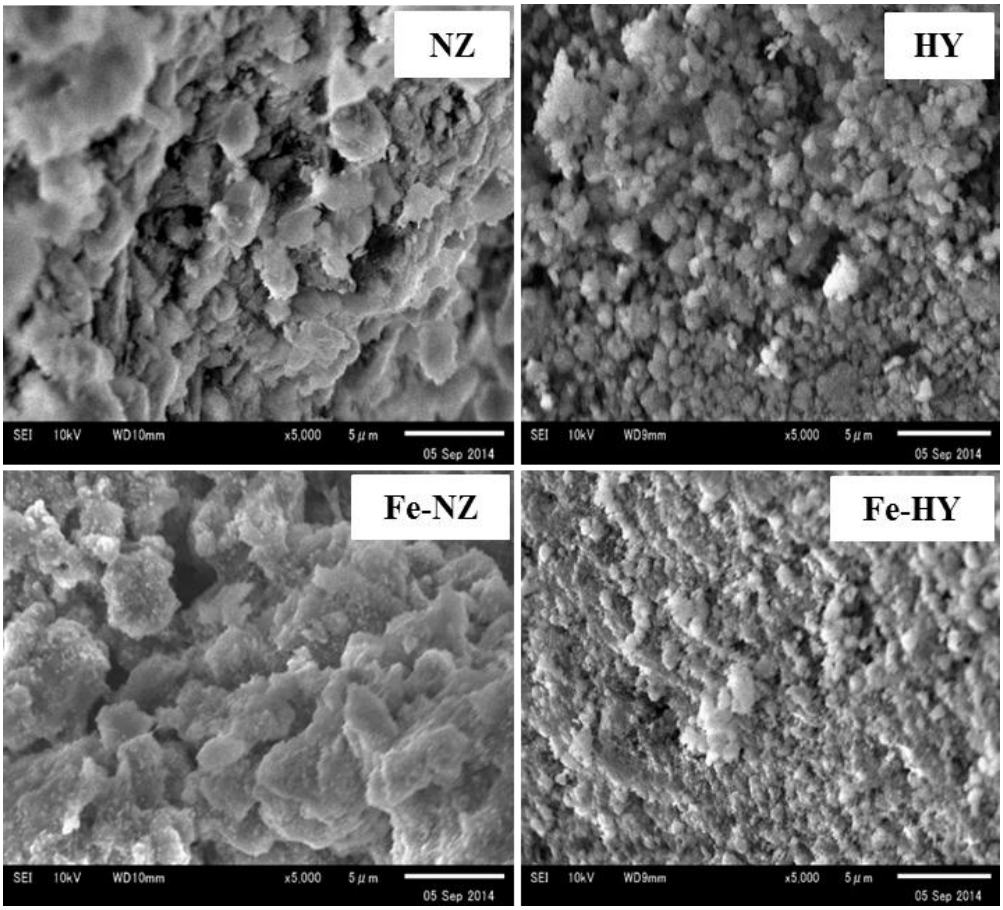


Figure 3.8. SEM photographs (5000X) of NZ, YZ, Fe-NZ and Fe-YZ catalysts

The parent catalysts and the impregnated catalysts are verified by XRD, which is presented in Figure 3.7. According to the PDF card of the standard diffraction datum, the XRD pattern of NZ and YZ indicated their MOR structure and FAU structure, respectively. The Fe wetness impregnation procedure seemed not to affect their crystallinity. The iron oxide peak designated at 2θ value of 33˚was not observed in the Fe loaded NZ and YZ catalysts. Hence, it indicated that Fe was highly dispersed in the zeolite matrix and the loaded iron oxide with too small particle sizes on the surface of the zeolites was difficult to be identified by the XRD method. It should be noted that the XRD diffraction bands shifted slightly to higher d values (inter-planar spacing) for the iron-substituted catalysts. It originated from an increase in the lattice parameters for the Fe loaded NZ and YZ zeolite catalysts, which indicated the fact that the iron oxides were successfully incorporated into NZ and YZ catalysts [3-20].

Figure 3.8 shows the SEM images of NZ, YZ, Fe-NZ and Fe-YZ catalysts for the surface characteristic analysis. From these characterizations, the porous and textural surface structure of NY and YZ catalysts could be observed. Additionally, YZ catalyst was consisted of small uniform crystals, while NY catalyst was formed by different size particles and crystals with different shapes and morphology. After the loading of iron oxide, the surfaces of both Fe-NZ and Fe-YZ became rougher and some large particles can be observed on Fe-NZ and Fe-YZ as a result of the agglomeration produced by the deposited iron oxides. Consequently, the result could confirm the reduction of the surface areas of Fe-NZ and Fe-YZ after the iron oxide loading

### 3.3.2. The effect of the reforming temperature on the oil yield and Br content in oil products

It is well known that the reforming temperature exerts great influence on the activity of catalyst and then will affect the product yield and composition. Therefore, in this Chapter, the pyrolysis and catalytic reforming of Br-HIPS experiments were further conducted at the reforming temperature of 450 ºC, 500 ºC and 550 ºC, respectively. In the presence of Fe-NZ catalyst, the effect of the reforming temperature on the oil product yield and the Br content in the oil products was investigated and the results are shown in the following Figure 3.9.

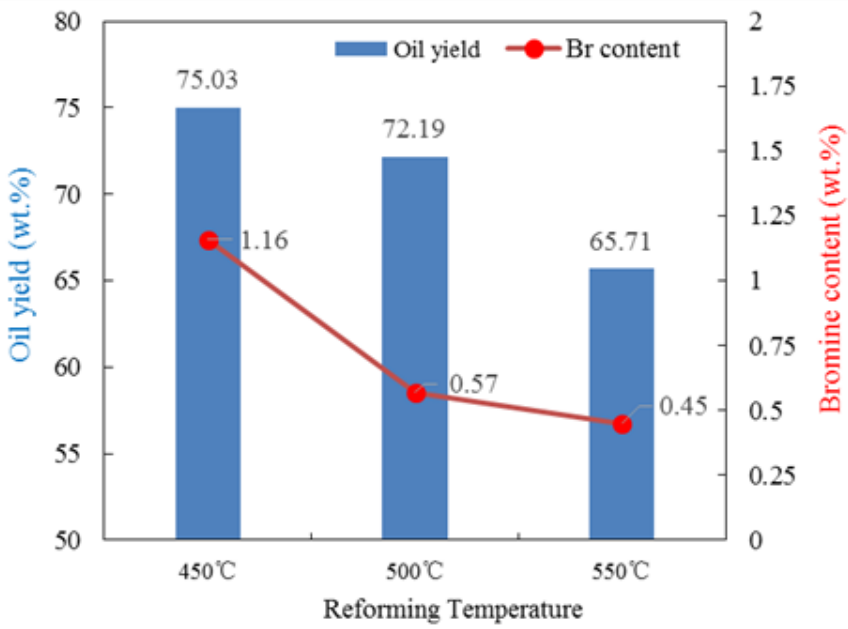


Figure 3.9. The effect of reforming temperature on the oil yield and Br content in the oil products.

It is found that both of the oil yield and the Br content in the oil product decreased with the increase of the reforming temperature. The reduction of the oil yield was attributed to the fact that the increase of the reforming temperature promotes the activity of Fe-NZ catalyst and then can further catalytically convert the oil products into gas products and coke. In addition, it is found that, at 450 $^{o}$C, the Br content in the oil products was the highest, it means that for the natural zeolite, 450 $^{o}$C is not high enough to catalytically degrade the brominated compounds. Furthermore, it was reported by Terakado and co-workers [3-10] that higher temperature could improve the reaction between HBr and metal oxide and then further reduce the amount of HBr. Therefore, in this study, with consideration of both the oil yield and the lower bromine content, the 500 $^{o}$C was chosen in the following experiments in order to compare the effect of different type catalysts on the production yield and compositions, as well as their debromination performance.

### 3.3.3. The effect of the catalyst types on the product yield and the product compositions

In the thermal pyrolysis of Br-HIPS, there would be lots of bromine content existing in the oil products, as reported [3-4]-[3-9]. The existence of brominated compounds in the oil products, especially the organic brominated compounds, would lower the oil quality and hinder reuse of the oil products, in this chapter, the two-stage combined pyrolysis and catalytic reforming of Br-HIPS was carried out to investigate the effect of NZ, Fe-NZ, YZ and Fe-YZ catalysts on the degradation of Br-HIPS and the debromination characteristics. The pyrolysis and catalytic reforming experiments were carried out in the absence and presence of NZ, Fe-NZ, YZ and Fe-YZ catalysts at the pyrolysis temperature of 500℃ and the reforming temperature of 500℃, respectively. In this system, Br-HIPS was thermally decomposed in the pyrolyzer, and then the pyrolysate flowed into the reformer, as shown in Figure 3.4. The product yield distribution was presented in Figure 3.10, which indicated that when Br-HIPS was pyrolyzed in the absence of the catalyst, the char, oil and gas yields were 15.9 wt.%, 82.9 wt.% and 1.2 wt.%, respectively. When the Br-HIPS was pyrolyzed in the presence of NZ, Fe-NZ, YZ and Fe-YZ, respectively, the oil yield decreased from 82.9 wt.% to 73.6 wt.%, 72.2 wt.%, 56.9 wt.% and 59.9 wt.%, respectively, while the coke yields increased to 5.5 wt.%, 8.4 wt.%, 16.8 wt.% and 15.4 wt.% from 0.0 wt.%, respectively. And the gas yields increased from 1.2 wt.% to 5.2 wt.%, 3.5 wt.%, 10.2 wt.% and 8.3 wt.%, respectively. On one hand, it was primarily related to the fact that these four zeolite catalysts possess the Lewis and Brønsted acidity and the catalytic activity [3-21]-[3-24]. Thus, they could catalytically reform the pyrolysate derived from the pyrolyzer and converted oil products into gases and coke. On the other hand, the increase of the coke yield was also attributed to the fact that the zeolite catalysts with the pore property could capture the inorganic brominated compounds, such as $SbBr_3$ [3-5], which originally would be transferred into the oil products. The detail debromination mechanism will be discussed in the section 3.3.

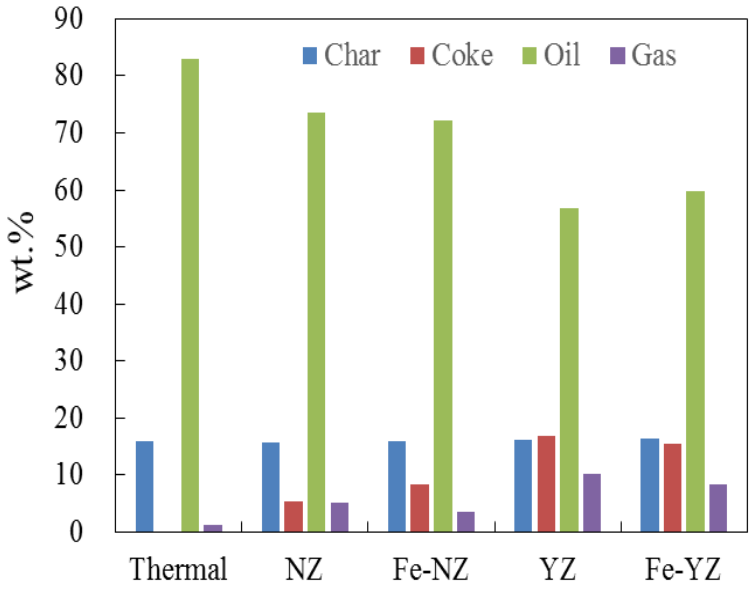


Figure 3.10. Effect of the catalyst types on the product yield.

In addition, the maximum gas yield was achieved by using the YZ catalyst due to the strongest acidity and the largest surface area of YZ catalyst, compared with the other three catalysts (Table 3.2). Furthermore, when Fe-NZ and Fe-YZ catalysts were used, it was found that the gas yield became lower than that case of NZ and YZ usage, respectively. It is most likely attributed to the fact that iron oxide particles in NZ and YZ catalysts can not only reduce their surface areas and the pore sizes, but also would lower the acidity and the activity of the parent catalysts. The reason could be attributed to the de-aluminization process during the calcination, which reduced the acid site density or it could be the partial exchange between iron ions with $H^+$ of the acidic zeolite [3-22]. As for the char yield, there was no obvious change regardless of whether catalysts were used or not. It might be originated from the fact that the thermal degradation of Br-HIPS mainly occurred in the pyrolyzer and the yield of char was only affected by the pyrolysis temperature.

The effect of the catalysts on the composition of the oil and gas products were investigated by GC-TCD and GC-MS, as shown in Table 3.3 and Table 3.4, respectively. As for the composition of the gas products, it was found from Table 3.3 that they are mainly composed of hydrocarbons from $C_1$ (methane), $C_2$ (ethane and ethene) and $C_3$ (propane and propene), along

with small quantities of hydrogen. It can be seen that $C_2$–$C_3$ gases were the main fractions of gas products both in absence and presence of the catalysts. In general, the use of catalysts enhanced the amount of each gas composition, especially $C_2$ and $C_3$ gas fractions, which might be related to the shape selectivity of these catalysts (pore size). This significant increase in the gas yield in the presence of YZ, which was also reported by others [3-5], suggested the strong cracking ability of this catalysts, which was a consequence of its higher porosity and stronger acidity than the other catalysts. Furthermore, the use of iron oxide loaded catalysts (Fe-NZ and Fe-YZ) reduced the production of $C_2$ and $C_3$ fractions compared to the parent zeolite catalysts (NZ and YZ). It further confirmed that the loading of iron oxide would weaken the cracking ability of the parent zeolite catalysts. It is worth mentioning that all catalysts enhanced the hydrogen production, which was most likely attributed to the hydrogen abstraction that took place during the aromatization reactions [3-6].

The oil products evolved from the pyrolysis of Br-HIPS in the absence and presence of catalysts were analyzed by GC-MS, and the main components are listed in Table 3.4. It indicated that the single-ring aromatic compounds were the major components of the oil products with or without the catalysts, such as toluene, styrene, cumene, ethylbenzene and xylenes etc., which is attributed to the structure property of HIPS polymer matrix. Whereas, when no catalyst was used, the amount of styrene monomer in the oil product was very small. In general, when polystyrene or high impact polystyrene without flame retardants is pyrolyzed, styrene monomer is often obtained as the main oil component, which is mainly due to its characteristics of the free radical mechanism, namely the β-scission followed by the depolymerization [3-25]-[3-28]. The low yield of the styrene monomer in the oil products may be originated from the flame retardant inhibiting the formation of styrene monomers due to the interaction between the polymer radicals and the flame retardants [3-4,3-29]. When NZ and YZ catalysts were used, the yields of the styrene monomer became lower. The reason for this could be that NZ and YZ catalysts, especially YZ, showed a high catalytic efficiency on the cracking, the isomerization and the aromatization due to the acidic property and the micropore crystalline structure [3-30]. Additionally, when the iron oxide loaded catalysts (Fe-NZ and Fe-YZ) were applied, the

concentration of styrene greatly increased, while the concentrations of ethlybenzene decreased. The distinct increase of the styrene content in the presence of the iron oxide loaded catalysts may be attributed to the fact that the degradation of the styrene backbone of HIPS took place after the anionic mechanism to form carbanion, as shown in Figure 3.11 [3-26].

Noteworthy, when Br-HIPS was pyrolyzed in the absence of a catalyst, 50.3 wt.% single-ring aromatic compounds was obtained in the oil products. When YZ and Fe-YZ catalysts were used, the amount of valuable single-ring aromatic compounds decreased from 50.3 wt.% to 20.6 wt.% and 27.1 wt.% while the production of two-ring aromatic compounds and multi-ring aromatic compounds significantly increased. However, when Br-HIPS was pyrolyzed in the presence of NZ and Fe-NZ catalysts, the single-ring aromatic compounds only reduced from 50.3 wt.% to 39.9 wt.% and 44.5 wt.% while the two-ring aromatic compounds and multi-ring aromatic compounds slightly increased. Williams et al. [3-24] reported that there were a large number of polycyclic aromatic hydrocarbons (PAH) in the pyrolysis oil of polystyrene that had been pyrolyzed in the presence of ZSM-5. Hall et al. [3-5] also observed that when Br-HIPS was pyrolyzed with HY-zeolite, the production of PAH in the oil products was obviously enhanced. Williams et al. [3-24] proposed that the formation of PAH in the polystyrene pyrolysis oil was attributed to the Diels-Alder reaction. Furthermore, the above results also indicated that YZ and Fe-YZ were more active than NZ and Fe-NZ in the case of the catalytic cracking while NZ and Fe-NZ catalysts did not greatly alter the pyrolysis products and therefore preserved the valuable single-ring aromatic compounds.

Table 3.3. Main components of the gas products determined by GC-TCD

| **Main gas components** | **Thermal** | **NZ** | **Fe-NZ** | **YZ** | **Fe-YZ** |
|---|---|---|---|---|---|
| $H_2$ | 0.05 | 0.15 | 0.07 | 0.23 | 0.17 |
| $CH_4$ | 0.16 | 0.59 | 0.43 | 0.86 | 0.77 |
| $C_2$ | 0.32 | 1.53 | 0.98 | 2.86 | 2.75 |
| $C_3$ | 0.38 | 1.81 | 1.06 | 3.91 | 2.38 |

Table 3.4. Main components of the oil products determined by GC-MS (% area). (wt.%/sample mass)

| **Main oil components** | **Thermal** | **NZ** | **Fe-NZ** | **YZ** | **Fe-YZ** |
|---|---|---|---|---|---|
| ***Total single ring compounds*** | *50.32* | *39.88* | *44.48* | *20.63* | *27.08* |
| Toluene | 6.78 | 4.9 | 4.57 | 2.05 | 3.43 |
| Styrene | 4.21 | 3.26 | 12.93 | 1.67 | 9.31 |
| Cumene | 2.64 | 3.96 | 4.69 | 2.35 | 2.78 |
| Ethylbenzene | 20.21 | 14.46 | 6.93 | 7.35 | 2.23 |
| Xylenes | 6.73 | 5.96 | 6.86 | 1.74 | 2.37 |
| Allylbenzene | 2.48 | 2.12 | 1.5 | 0.65 | 1.03 |
| Propylbenzene | 2.91 | 1.05 | 1.76 | 1.43 | 1.94 |
| Methylstyrene | 3.11 | 1.61 | 1.23 | 1.02 | 1.48 |
| Indane | 0.13 | 1.31 | 2.22 | 1.45 | 1.34 |
| Diehtylbenzenes | 1.12 | 1.25 | 1.79 | 0.92 | 1.17 |
| ***Total two ring compounds*** | *11.88* | *13.15* | *9.6* | *15.13* | *12.54* |
| Biphenyl | 0.21 | 0.77 | 0.54 | 1.03 | 0.87 |
| Naphthalene | 1.13 | 1.72 | 1.09 | 2.31 | 1.96 |
| Methylnaphthalenes | 0.89 | 1.74 | 1.56 | 2.99 | 2.06 |
| Bibenzyl | 0.6 | 0.51 | 0.43 | 1.85 | 1.33 |
| Diphenylpropane | 8.53 | 6.67 | 4.81 | 4.54 | 4.29 |
| Ethylnaphthalenes | 0.2 | 0.98 | 0.63 | 1.49 | 1.12 |
| Dimethylnaphthalenes | 0.32 | 0.76 | 0.54 | 0.92 | 0.91 |
| ***Total multi ring compounds*** | *2.68* | *4.32* | *3.22* | *8.61* | *5.71* |
| Phenylnaphthalenes | 0.43 | 0.92 | 0.87 | 1.87 | 1.01 |
| Anthracene | 0.91 | 1.06 | 0.62 | 2.01 | 1.56 |
| Ethenylanthracenes | 0.21 | 0.67 | 0.52 | 1.78 | 0.94 |
| Terphenyls | 0.42 | 0.74 | 0.46 | 0.98 | 0.87 |
| Triphenylbenzene | 0.71 | 0.93 | 0.75 | 1.97 | 1.33 |
| ***Total Brominated compounds*** | *2.99* | *1.71* | *0.24* | *0.48* | *0.11* |
| (Bromoethyl)benzene | 1.24 | 0.78 | 0.17 | 0.11 | 0.11 |
| Methylbenzyl bromide | 0.94 | 0.75 | 0.07 | 0.14 | n.d. |
| Bromoanthracene | 0.56 | n.d[a] | n.d. | 0.09 | n.d. |
| Dibromoanthracene | 0.25 | 0.18 | n.d. | 0.14 | n.d. |

[a] not detected

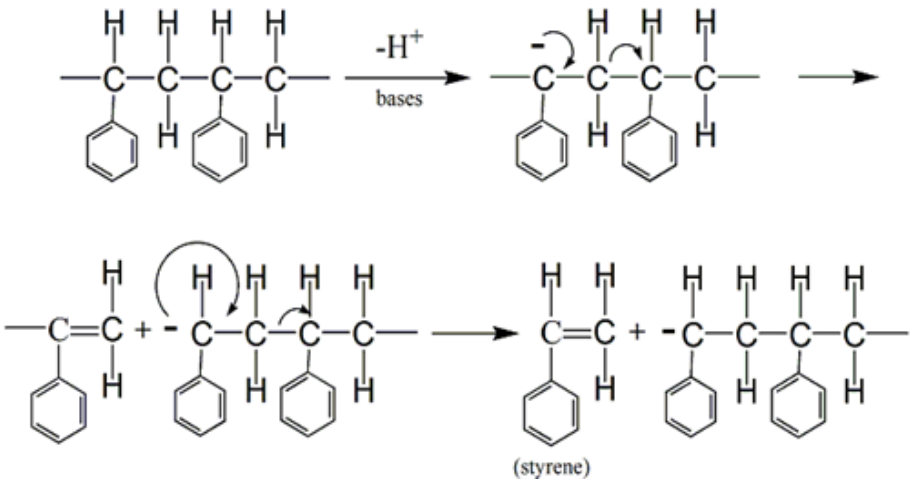


Figure 3.11. Base-catalyzed mechanism for polystyrene proposed by Ukei et al [3-26].

### 3.3.4. The effect of the catalysts on the bromine and antimony content in the oil products.

The total bromine and antimony contents in the pyrolysis oils were determined using a bomb calorimeter equipped with an ion chromatograph and ICP-MS after digestion of oil samples, respectively, as shown in Figure 3.12. During the pyrolysis of Br-HIPS, HBr, $SbBr_3$, $Br_2$ and certain organic brominated compounds were produced. It should be worth mentioning that the brominated compounds (such as HBr) in the gas products was not determined by the ion chromatograph. The similar results have been reported by Hall et al [3-5, 3-6]. Additionally, Figure 3.12 obviously indicated that there was a high bromine content (7.6 wt.%) in each oil product, which means that large amounts (68.1 wt.%) of bromine was transferred to the oil products during the pyrolysis of Br-HIPS without catalysts. This demonstrated that the effective catalysts or additives were essential for removing bromine in an attempt to obtain bromine free oil products. When NZ and YZ catalysts were used, the bromine content in the oils decreased to 2.0 wt.% and 1.4 wt.%, respectively. This significant decrease of the bromine content in the oil by YZ catalyst was a consequence of its higher porosity and stronger acidity, contributing to capture $SbBr_3$ and catalytically crack the organobrominated compounds [3-5,3-6]. When Fe-NZ and Fe-YZ were used, the bromine content in the oils decreased from 7.6 wt.% to 0.7wt.% and 0.6 wt.%, respectively. It indicated that after the iron oxide loading, the debromination

performance of Fe-NZ and Fe-YZ got improved, which was possibly attributed to the neutralization reaction of loaded iron oxide with HBr derived from the degradation of Br-HIPS [3-28]. The neutralization reaction can be shown as following.

$$Fe_2O_3 + 6HBr \rightarrow 2FeBr_3 + 3H_2O \quad (3.2)$$

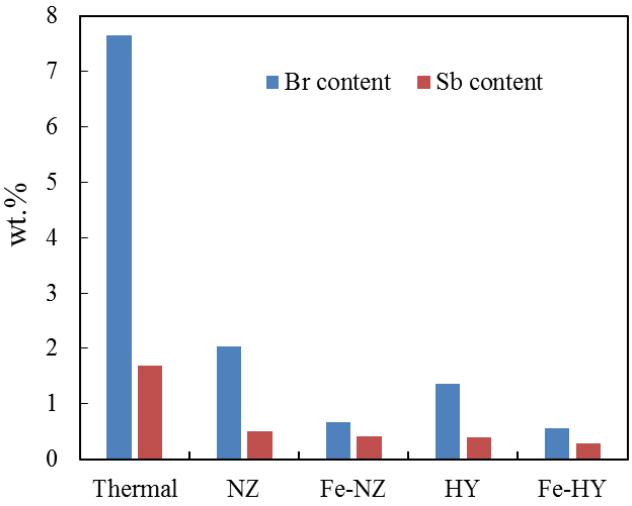


Figure 3.12. The bromine and antimony content in the oil products

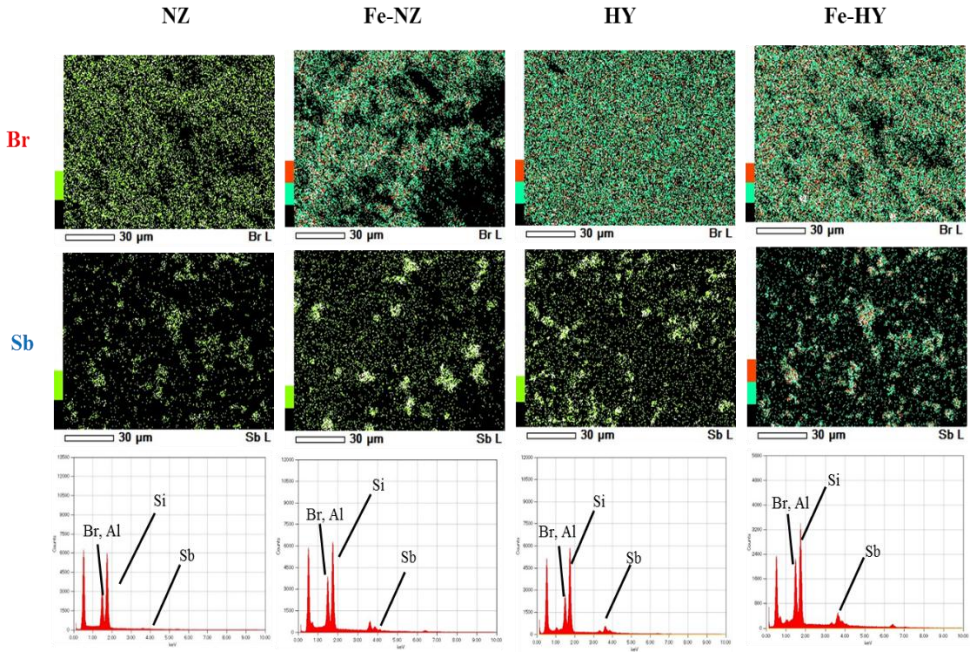


Figure 3.13. EDX and element map analysis of spent NZ, Fe-NZ, YZ and Fe-HYcatalysts

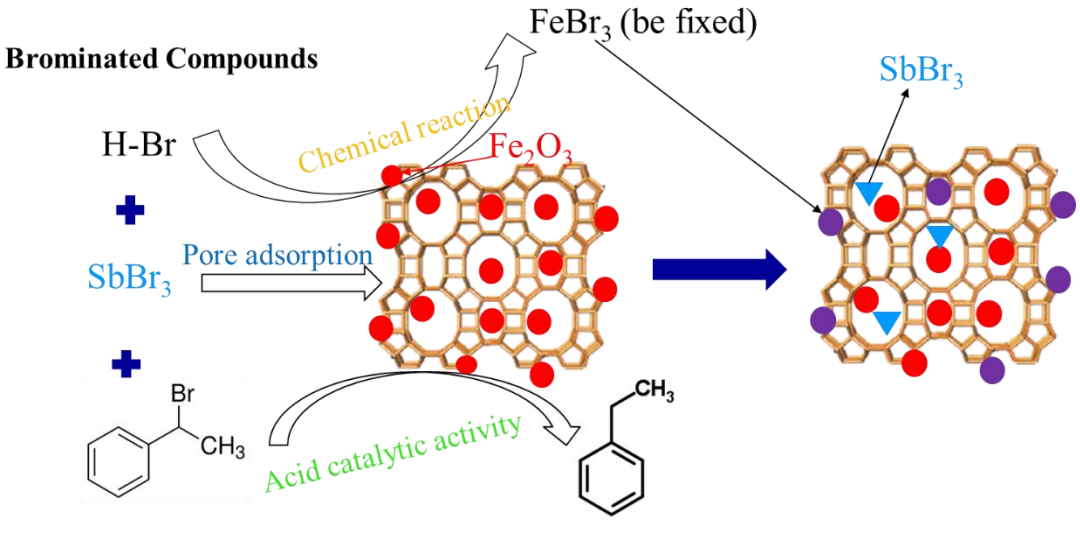


Figure 3.14. The proposed debromination mechanism

$Fe_2O_3$ was fixed on the surface and in the pore of Fe-NZ and Fe-YZ. Consequently, the solid-phase product $FeBr_3$ also could be easily captured by Fe-NZ and Fe-YZ. As for Fe-NZ and Fe-YZ, the main debromination mechanism could be summarized as the capture of $FeBr_3$ and $SbBr_3$, as well as the catalytic reforming of the organobrominated compounds, which originated from their porosity, iron oxide loading and acidity, as shown in Figure 3.14. In addition, the EDX analysis of spent NZ, Fe-NZ, YZ and Fe-YZ were carried out to confirm the above debromination mechanism and compare the debromination performance of each catalyst. From Figure 3.12 and Figure 3.13, it is obviously demonstrated that the bromine removal ability of Fe-YZ was better than that of Fe-NZ. However, in the view of the cost reduction of the catalyst and preservation of the valuable single-ring aromatic compounds in the oil product, Fe-NZ was more effective and feasible for the feedstock recycling of Br-HISP by the pyrolysis process.

In addition, with regard to Br distribution in the products, it was also investigated and the results are shown in Table 3.5. As mentioned above, in the case of thermal pyrolysis of Br-HIPS, most of Br was transferred into the oil products while in the presence of catalysts, especially the Fe-NZ and Fe-HY, Br contents in the oil products were significantly removed. From Table 3.5, it can be found that when the catalysts were used, most of Br was fixed by the catalysts. For instance, when the Br-HIPS was pyrolyzed and catalytically reformed in the presence of Fe-HY,

50.12 wt.% Br was fixed in the catalysts. Moreover, it was found that the total Br mass balance does not reach 100 wt.%, which was attributed to the fact that on the one hand, it is difficult to collect all products, because some of which exists in the reactor and the connecting tube. Therefore, the bromine content in this fraction is difficult to be determined. On the other hand, when the catalysts were used, it was reported by Hall and co-worker [3-5,3-6] that the bromine content of the residue and the catalyst was very difficult to be measured because they have very heterogeneous and intermingled nature. Therefore, it is possible that there are some loss during the measurement of bromine content in the residues and catalysts. Terakado et al. [3-10] also mentioned that the evaluation of bromine content in the pyrolysis residue through ash content in the elementary analysis is an error source for the loss of Br mass balance.

Table 3.5 Br distribution in the products

| **Br distribution (Wt.%)** | **Thermal** | **NZ** | **Fe-NZ** | **HY** | **Fe-HY** |
|---|---|---|---|---|---|
| Br in residue | 5.96 | 6.21 | 6.56 | 7.01 | 6.39 |
| Br in catalyst | 0.0 | 30.49 | 47.38 | 35.13 | 50.12 |
| Br in oil | 68.06 | 16.05 | 4.21 | 8.32 | 2.98 |

Furthermore, with regard to the debromination mechanism, Terakado and co-workers [3-10, 3-11] used the metal oxides ($Fe_2O_3$, CaO, ZnO et al) in the pyrolysis of TBBPA and printed circuit boards containing brominated flame retardants, respectively. They concluded that the addition of metal oxides could effectively suppress the formation of HBr and brominated organic compounds because of the chemical reaction with metal oxides. In addition, Hall et al. [3-5] investigated the catalytic pyrolysis of brominated flame-retarded HIPS and ABS by using HY zeolite and HZSM-5 zeolite, which proved that the zeolite catalysts could effectively catalytically reform the organobrominated compounds because of the catalytic reforming and physical pore adsorption of $SbBr_3$. Furthermore, in Chapter 2, from the comparison of the debromination performance of three additives (red mud, natural zeolite and calcined limestone) and the XRD analysis, it could be proposed that the mechanism of bromine removal from oil product was attributed to the zeolite pore property and acidity, as well as the reaction with the iron oxide. Therefore, in this Chapter,

in the case of the $Fe_2O_3$ loaded natural zeolite and HY zeolite, the same debromination mechanisms were proposed that the mechanism of bromine removal from oil product was attributed to the zeolite pore property and acidity, as well as the reaction with the iron oxide.

### 3.3.5. The catalytic performance of spent and regenerated catalysts on the oil yield and debromination.

The surface morphology structure characteristics of fresh, spent and regenerated Fe-NZ catalysts were observed by the SEM and is shown in Figure 3.15. It illustrated that the surface of fresh Fe-NZ consisted of many relatively uniform and small particles. As for the spent Fe-NZ, quite higher and bigger particles can be observed as a consequence of agglomeration produced by the deposited coke and $FeBr_3$ or $FeBr_2$ and $SbBr_3$. On the contrary, the SEM photograph of the regenerated zeolite is very similar to that of the fresh one, which imply that it recovers its textural appearance after the regeneration process. This result is consistent with the previous reports made by López and Bozi, respectively [3-15, 3-30].

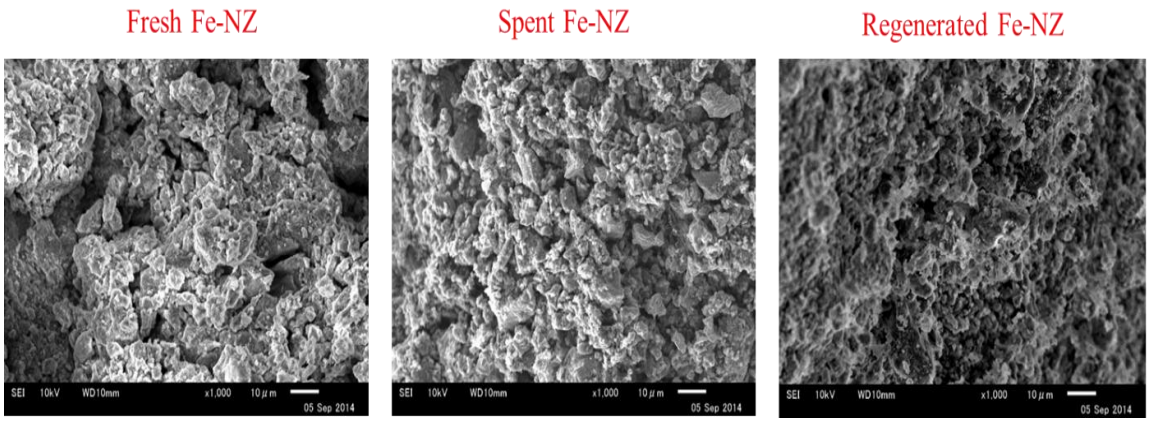


Figure 3.15. The surface SEM photographs of fresh, spent and regenerated catalysts

The pore structure properties of the fresh, spent and regenerated Fe-NZ catalysts are listed in Table 3.6. Compared with the fresh Fe-NZ catalyst, the BET surface area of spent Fe-NZ catalyst decreased from 119.02 $m^2/g$ to 73.14 $m^2/g$ while its pore volume also decreased from 0.167 $cm^3/g$ to 0.102 $cm^3/g$. This face may be explained by the coke formation during the catalytic pyrolysis, which would aggregate on the surface and in the pore of catalyst, subsequently reduced

the BET surface area and pore volume of Fe-NZ catalyst. It was reported by Castaño and co-workers that the severity of the shape selectivity of the zeolite controls not only product distribution but also coke deposition. Coke precursors with aromatic nature tend to grow, up to a point where they have steric hindrance. The growth in larger-pore zeolites is mainly aromatic, giving rise to polyaromatic structures that remain in the cages of the pore network [3-31]. Therefore, the coking on the surface of zeolite is easier to occur in the case of catalytic pyrolysis of polystyrene whose main products are the aromatic compounds, which could easily result in the formation of polyaromatic compounds and coke precursors. Additionally, as mentioned above, during the pyrolysis of Br-HIPS, there are certain amount of $SbBr_3$ produced, which would be captured by the Fe-NZ. Thereby, it also lead to the reduction of the BET surface area and pore volume of catalysts. After the regeneration, it was found that the BET surface are and the pore volume of the regenerated Fe-NZ catalysts are comparative with that of the fresh one. It illustrated that after the regeneration, the pore structure property could be almost recovered.

Table 3.6. Pore structure properties of fresh, spent and regenerated Fe-NZ catalysts

| **Catalysts** | **BET surface area ($m^2/g$)** | **Pore volume ($cm^3/g$)** | **Average pore diameter (nm)** |
|---|---|---|---|
| Fresh Fe-NZ | 119.02 | 0.167 | 5.62 |
| Spent Fe-NZ | 73.14 | 0.102 | 4.23 |
| Regenerated Fe-NZ | 112.56 | 0.161 | 5.58 |

The pyrolysis and catalytic reforming experiments were also conducted in the presence of spent and regenerated Fe-NZ catalysts, respectively. Because, in this study, main attention was paid to the amount and quality of oil products, the effects of spent and regenerated Fe-NZ catalysts on the oil yield and bromine content in the oil products were investigated and compared with that of thermal pyrolysis and when fresh Fe-NZ catalyst was employed. The result is presented in Figure 3.16, which indicates that when the spent Fe-NZ catalyst was used, compared with that of fresh Fe-NZ used, the yield of oil products increased while the bromine content in the oil product also obviously increased. It was attributed to the fact that, as discussed above, the formation of coke and the capture of the produced $SbBr_3$ would block and reduce the BET surface area and

pore volume, and then would reduce the activity of Fe-NZ and decrease the amount of the loaded $Fe_2O_3$. Therefore, the cracking ability of Fe-NZ significantly decreased and resulted in the increase of the yield of oil products. In addition, the reduction of the capture ability and the amount of $Fe_2O_3$ would also lead to the decrease of the debromination performance. There are the main reasons which could be explained the fact that the bromine content in the oil faction increased, which lead to the increase of the yield of oil products owing to more produced organic and inorganic brominated compounds were transferred into the oil product faction instead of being captured by the spent Fe-NZ. In the case of regenerated Fe-NZ, it was found that when the regenerated Fe-NZ catalyst was used, the yield of the oil product and the bromine content in the oil product were almost similar with those when the fresh Fe-NZ catalyst was employed. It illustrated that after the regeneration process, the produced coke could totally burned out and be completely removed. In addition, the captured $FeBr_3$ or $FeBr_2$ could be converted into the $Fe_2O_3$ again, which play an important role in the fixation of the brominated compounds. Consequently, the above result indicated that the debromination and the catalytic cracking performance of the regenerated Fe-NZ were comparative with those of fresh Fe-NZ. Therefore, the synthesized Fe-NZ catalyst was cost-effective and recyclable for the production of valuable and low bromine content oil products from the pyrolysis and catalytic reforming of Br-HIPS.

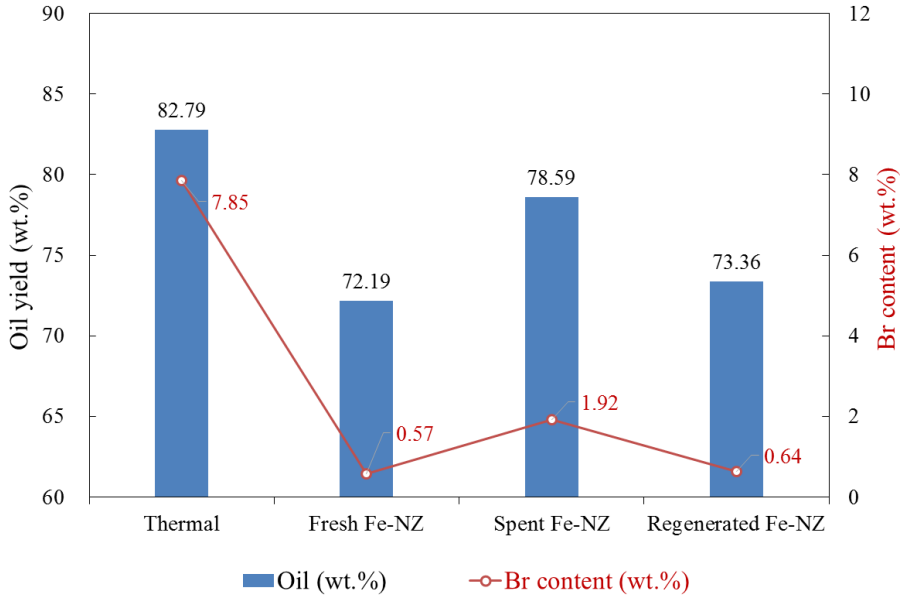


Figure 3.16. The effect of different catalyst on the oil yield and Br content

## 3.4. Summary

The effect of NZ, Fe-NZ, YZ and Fe-NZ catalysts on the product yield, the gas and oil product composition and the debromination efficiency of the oil products were investigated in the two-stage combined pyrolysis and catalytic reforming reactor at both pyrolysis and reforming temperatures of 500 ℃. It could be concluded from the present study that the amount of bromine in the oil product could effectively be reduced in the presence of the catalysts. The loading of $Fe_2O_3$ on zeolite, such as Fe-NZ and Fe-YZ could enhance the debromination performance, where the bromine content in the oils decreased from 7.6 wt.% to 0.7wt.% and 0.6 wt.%, respectively. Compared with Fe-HY, Fe-NZ did not greatly alter the pyrolysis products and therefore preserved the valuable single-ring aromatic compounds. Consequently, Fe-NZ was more effective and feasible for the feedstock recycling of Br-HISP by the pyrolysis process. The mechanism of bromine removal from the oil product was mainly attributed to the zeolite pore capture of produced $SbBr_3$ and $FeBr_3$, the catalytic reforming of the organobrominated compounds, as well as the neutralization reaction of the iron oxide with HBr derived from the decomposition of Br-HIPS. As for the spent Fe-NZ, the debromination performance become weaker, which was attributed to the formation of coke and the reduction of the amount of $Fe_2O_3$. Whilst, the debromination performance of regenerated Fe-NZ was comparative with that of fresh Fe-NZ. It illustrated that the synthesized Fe-NZ catalyst was cost-effective and recyclable for the production of valuable and low bromine content oil products from the pyrolysis and catalytic reforming of Br-HIPS.

## References


[3-1] Yang, X.N., Sun, L.S., Xiang, J., Hu, S. & Su, S. (2013) Pyrolysis and dehalogenation of plastics from waste electrical and electronic equipment (WEEE): A review. *Waste Management*, **33**, 462-473.

[3-2] Martinho, G., Pires, A., Saraiva, L. & Ribeiro, R. (2012) Composition of plastics from waste electrical and electronic equipment (WEEE) by direct sampling. *Waste Management*, **32**, 1213–1217.

[3-3] Ongondo, F.O., Williams, I.D. & Cherrett, T.J. (2011). How are WEEE doing? A global review of the management of electrical and electronic wastes. *Waste Management*, **31**, 714-730.

[3-4] Jakab, E., Uddin, Md.A., Bhaskar, T. & Sakata Y. (2003) Thermal decomposition of flame-retarded high impact polystyrene. *J. Anal. Appl. Pyrolysis*, **68-69**, 83-99.

[3-5] Hall, W.J. & Williams, P.T. (2008) Removal of organobromine compounds from the pyrolysis oils of flame retarded plastics using zeolite catalysts. *J. Anal. Appl. Pyrolysis*, **81**, 139–147.

[3-6] Hall, W.J., Miskolczi, N., Onwudili, J. & Williams, P.T. (2008) Thermal Processing of Toxic Flame-Retarded Polymers Using a Waste Fluidized Catalytic Cracker (FCC) Catalyst. *Energy & Fuels*, **22**, 1691–1697.

[3-7] Miskolczi, N., Hall, W.J., Angyal, A., Bartha, L. & Williams, P.T. (2008) Production of oil with low organobromine content from the pyrolysis of flame retarded HIPS and ABS plastics. *Journal of Analytical and Applied Pyrolysis*, **83**, 115-123.

[3-8] Bhaskar, T., Matsui T., Azhar Uddin, Md., Kaneko, J., Muto, A. & Sakata, Y. (2003) Effect of $Sb_2O_3$ in brominated heating impact polystyrene (HIPS-Br) on thermal degradation and debromination by iron oxide carbon composite catalyst (Fe-C) *Applied Catalysis B: Environmental*, **43**, 229–241.

[3-9] Bhaskar, T., Matsui, T., Kaneko, J., Uddin, Md. A., Muto, A. & Sakata, Y. (2002) Novel calcium based sorbent (Ca-C) for the dehalogenation (Br, Cl) process during halogenated mixed plastic (PP/PE/PS/PVC and HIPS-Br) pyrolysis. *Green Chemistry*, **4**, 372–375.

[3-10] Terakado, O., Ohhashi, R. & Hirasawa, M. (2011) Thermal degradation study of tetrabromobisphenol A under the presence metal oxide: Comparison of bromine fixation ability. *J. Anal. Appl. Pyrolysis*, **91**, 303–309.

[3-11] Terakado, O., Ohhashi, R. & Hirasawa, M. (2013) Bromine fixation by metal oxide in pyrolysis of printed circuit board containing brominated flame retardant. *J. Anal. Appl.*

*Pyrolysis*, **103**, 216–221.

[3-12] Alia, S., Garfortha, A.,A., Harrisb, D.,H., Rawlencec, D.,J.& Uemichid. Y., (2002). Polymer waste recycling over "used" catalysts. *Catalysis Today*, **75**, 247–255.

[3-13] López, A., Marco, I., D., Caballero, B.,M., Adrados, A. & Laresgoiti, M., F., (2011). Deactivation and regeneration of ZSM-5 zeolite in catalytic pyrolysis. *Waste Management*, **31**, 1852-1858.

[3-14] Castano, P., Elordi, G., Olazar, M., Aguayo, A.T., Pawelec, B. & Bilbao, J. (2011) Insights into the coke deposited on HZSM-5, Hβ and HY zeolites during the cracking of polyethylene. *Applied Catalysis B: Environmental*, **104**, 91-100.

[3-15] Park, Y., Namioka, T., Sakamoto, S., Min, T.J., Roh, S.A. & Yoshikawa, K. (2010) Optimum operating conditions for a two-stage gasification process fueled by polypropylene by means of continuous reactor over ruthenium catalyst. *Fuel Processing Technology*, **91**, 951-957.

[3-16] Valle, B., Gayubo, A., G., Aguayo A., T., Olazar, M. & Bilbao, J. (2010) Selective Production of Aromatics by Crude Bio-oil Valorization with a Nickel-Modified HZSM-5 Zeolite Catalyst. *Energy & Fuels*, **24**, 2060-2070.

[3-17] Liang, G., F., Cheng, H., Y., Li, W., He, L., M., Yu, Y., C. & Zhao, F., Y. (2012). Selective conversion of microcrystalline cellulose into hexitols on nickel particles encapsulated within ZSM-5 zeolite. *Green Chemistry*, **14**, 2146.

[3-18] Botasa, J., A., Serranoa, D., P., Garcíac, A., Vicentea, J. de & Ramosa, R. (2012). Catalytic conversion of rapeseed oil into raw chemicals and fuels over Ni- and Mo-modified nanocrystalline ZSM-5 zeolite. *Catalysis Today*, **195**, 59-70.

[3-19] Pedrosa, A., M., G., Souza, M., J., B., Melo, D., M., A. & Araujo., A., S. (2006). Cobalt and nickel supported on HY zeolite: Synthesis, characterization and catalytic properties. *Materials Research Bulletin*, **41**, 1105–1111.

[3-20] Joshi, P.N., Awate, S.V. & Shiralkar, V.P. (1993) Partial isomorphous substitution of $Fe^{3+}$ in the LTL framework, *J. Phys. Chem.* **97**, 9749–9753.

[3-21] Adam, F., Wong, J.T. & Ng, E.P. (2013). Fast catalytic oxidation of phenol over iron modified zeolite L nanocrystals. *Chemical Engineering Journal*, **214**, 63-67.

[3-22] Lee, S.Y., Yoon, J. H., Kim, J.R. & Park, D.W. (2001) Catalytic degradation of polystyrene over natural clinoptilolite zeolite. *Polymer Degradation and Stability*, **74**, 297–305.

[3-23] Dawood, A. & Miura, K. (2002) Catalytic pyrolysis of γ-irradiated polypropylene (PP) over HY zeolite for enhancing the reactivity and the product selectivity. *Polymer*

*Degradation and Stability*, **76**, 45-52.

[3-24] Bagri, R. & Williams, P.T. (2002) Catalytic pyrolysis of polyethylene. *Journal of Analytical and Applied Pyrolysis*, **63**, 29-41.

[3-25] Lee, S.Y., Yoon, J.H., Kim, J.R. & Park, D.W. (2002) Degradation of polystyrene using clinoptilolite catalysts. *J. Anal. Appl. Pyrolysis*, **64**, 71–83.

[3-26] Ukei, H., Hirose, T., Horikawa, S., Takai, Y., Taka, M., Azuma, N. & Ueno, A. (2000) Catalytic degradation of polystyrene into styrene and a design of recyclable polystyrene with dispersed catalysts. *Catalysis Today*, **62**, 67-75.

[3-27] Jung, S.H., Kim, S.J. & Kim, J.S.(2013) The influence of reaction parameters on characteristics of pyrolysis oils from waste high impact polystyrene and acrylonitrile–butadiene–styrene using a fluidized bed reactor. *Fuel Processing Technology*, **116**, 123–129.

[3-28] Jung, S.H., Kim, S.J. & Kim J.S. (2012) Fast pyrolysis of a waste fraction of high impact polystyrene (HIPS) containing brominated flame retardants in a fluidized bed reactor: The effects of various Ca-based additives (CaO, $Ca(OH)_2$ and oyster shells) on the removal of bromine. *Fuel*, **95**, 514-520.

[3-29] Seo, Y.H., Lee, K.H. & Shin, D.H. (2003) Investigation of catalytic degradation of high-density polyethylene by hydrocarbon group type analysis. *J. Anal. Appl. Pyrolysis*, **70**, 383-393.

[3-30] Bozi, J., & Blazsó, M. (2009). Catalytic modification of pyrolysis products of nitrogen-containing polymers over Y zeolites. *Green Chemistry*, **11**, 1638–1645.

[3-31] Castaño a, P., Elordia, G., Olazara, M., Aguayoa, A., T., Pawelecb, B. & Bilbaoa, J. (2011). Insights into the coke deposited on HZSM-5, Hβ and HY zeolites during the cracking of polyethylene. *Applied Catalysis B: Environmental*, 104, 91–100.

# Chapter 4

# The $CO_2$ Gasification Kinetic Study of WEEE Plastic Char Derived from Medium Temperature pyrolysis by Thermogravimetric analyzer

## 4.1. Introduction

As mentioned in the above chapters and many other researchers, on the one hand, WEEE is a quite valuable and dangerous wastes, which is worthy recycling. On the other hand, the amount of WEEE is very enormous and also increases in an alarming rate [4-1]-[4-3]. Consequently, plenty of processes and methods have been intensively studies and developed in order to recover the useful and valuable resources, as well as prevent the environmental pollution and human health crisis from WEEE [4-4, 4-5], such as mechanical separation methods, combustion, supercritical fluids, pyrolysis and steam gasification [4-2]. Among of these process, the pyrolysis has been considered as one of most popular processes for recycling WEEE. Because, on the one hand, the cost and operation of pyrolysis process is relatively low and easy, On the other hand, the pyrolysis process not only can convert WEEE plastics into fuels and chemical feedstock but also easily separate metals and plastic fractions of WEEE [4-2]. Therefore, a large amount of attentions have been focused in the recycling of WEEE or WEEE plastics by pyrolysis and catalytic pyrolysis [4-6]-[4-12]. Whilst, plenty of effective catalysts and additives [4-6]-[4-12] also have been studied and developed for removing the bromine compounds in the derived oil products from WEEE pyrolysis, where the bromine compounds are derived from the brominated flame retardant, which was frequently added into WEEE plastics in attempt to reduce their flammability. In the chapter 2 and chapter 3 of this thesis, the low-cost and effective catalysts (red

mud, calcined limestone, natural zeolite, HY zeolite, $Fe_2O_3$ loaded HY zeolite, $Fe_2O_3$ loaded natural zeolites) were already studied and proved to successfully remove lots of bromine content from the oil products derived from the pyrolysis of brominated high impact polystyrene (Br-HIPS), especially the red mud, $Fe_2O_3$ loaded natural zeolite. The above research results indicated that the pyrolysis process could effectively convert the WEEE plastic into valuable, storable and transportable oil products used for fuel and chemical feedstock. In addition, they showed that metal recovery from the pyrolysis residues was relatively easy due to their friable and loose structure property [4-4, 4-5, 4-13].

However, after the low-medium temperature pyrolysis process, about 20 wt.% of WEEE plastic char remained [4-10, 4-11], which is worth recyclable resource in order to increase the recycle efficiency of WEEE plastics. On the other hand, the existence of the char would be a potential problem for the recycling of further metal screening and refinement. The gasification behaviors of pyrolysis coal char and biomass char have already been widely studied [4-14]-[4-19]. However, few attempts have been made to investigate the $CO_2$ gasification reactivity of WEEE plastic char derived from the medium-temperature pyrolysis [4-20]. Additionally, the $CO_2$ gasification reactivity of chars is lower than that of $O_2$ or $H_2O$ gasification, and consequently, it is regarded as the rate-determining step in the gasification process [4-19]. The $CO_2$ gasification of WEEE plastic char might prevent the oxidation of metals existing in the chars. To this end, it is of great significance to understand the $CO_2$ gasification reactivity of WEEE plastic char. The gasification behavior, reactivity and kinetic parameters are essential for the efficient and reliable design of the gasification system. Thermogravimetric analysis (TGA) is an ideal instrument for investigating the gasification characteristics of carbonaceous materials because of its high accuracy, simplicity of design and ease of operation [4-21]. By means of TGA, different models can be applied in order to evaluate the kinetic parameters and the activation energy.

With regard to biomass and coals, the intrinsic alkali (K and Na), alkaline (Ca and Mg) and transition (Fe) metal contents also play important roles on the char gasification rates [4-16, 4-22, 4-23]. In addition, the Si and Al metal content generally exert severe inhibition effect on the

gasification reaction [4-16, 4-17, 4-21]. Consequently, for different biomass and coals char containing various amount of alkali and alkaline metal contents, their gasification performance are totally different. Furthermore, in an attempt to further accelerate the reaction rates and considerably reduce the gasification temperature, various alkali (K and Na), alkaline (Ca and Mg) and transition (Fe) metal contents were added into the chars in order to enhance the gasification process. The Huang and co-workers [4-24] have investigated the effect of five metal catalysts (K, Na, Mg, Ca and Fe) on the promotion of fir char reactivity in $CO_2$ gasification process by using TGA. And their achieved results showed the significantly positive effect of metal catalysts on enhancing the reactivity of fir char with the order of K-char > Na-char > Ca-char > Fe-char > Mg-char > raw char. Zhou and co-workers [4-25] studied the catalytic effect of iron species on $CO_2$ gasification of high sulfur petroleum coke by using TGA. It was found that the catalytic activity of iron species followed the sequence of $FeCl_3$ > $Fe(NO_3)_3$ > $FeSO_4$. In addition, it was also clearly demonstrated that there exists a significant synergistic effect between calcium hydroxide and iron species during petroleum coke gasification [4-25]. Furthermore, Karimi et al. [4-26] studied the catalytic effects of $K_2CO_3$ and $Na_2CO_3$ on the steam gasification of bitumen coke by TGA and found that both catalysts accelerate the gasification reactivity and could significantly reduce the gasification activation energy of the bitumen coke. Vamvuku et al. [4-27] investigated the catalytic effect of $Na_2CO_3$, $Li_2CO_3$, $K_2CO_3$, $Rb_2CO_3$, $CaCO_3$, $Cs_2CO_3$, and $CaSO_4$, as well as their mixtures on $CO_2$ gasification of waste biomass chars. It was found that for different char, the optimum catalyst was different. For MSW, sewage sludge and waste paper, the optimum catalysts were $Na_2CO_3$, $CaCO_3$ and $Li_2CO_3$, respectively. And the mixtures of most effective catalysts exhibited gasification characteristics intermediate of those of the individual components. The blending of catalysts could obviously reduce the activation energy of char gasification [4-27]. Zhang and Kamo [4-13, 4-28] also conducted the steam gasification of phenolic circuit board and epoxy circuit board in the presence of equal weight mixture of $Na_2CO_3$, $Li_2CO_3$ and $K_2CO_3$. It was found that the mixture carbonates could decrease the gasification temperature and upgrade the steam gasification rate of phenolic circuit board and epoxy circuit board, and also could prevent the emission of organic brominated compounds.

In this study, the isothermal $CO_2$ gasification behaviors of three WEEE plastics (PB, HIPS and ABS) chars derived from the pyrolysis at 600 ℃ were investigated by using the thermogravimetric analysis (TGA) at the temperatures of 850-1050 ℃. Effects of the plastic char types, the reaction temperature and the $CO_2$ partial pressure on the char conversion, the reactivity index and the gasification rate were investigated in detail. Furthermore, the random pore model, the extended random pore model and the shifted extended random pore model were employed to fit with the gasification rate of three WEEE plastic char at different temperatures in order to determine their gasification correlation coefficients, kinetic parameters and activation energies, respectively. Furthermore, compared with biomass and coal, the amount instinct alkali and alkaline element in the WEEE plastic was minimal. In order to reduce the reaction time and lower the gasification temperature, the effect of carbonates (sodium carbonate, potassium carbonate and mixture of sodium carbonate and potassium carbonate) additives on gasification behaviors were also systematically studied. The activation energy was also calculated by the Arrhenius equation.

## 4.2. Experimental

### 4.2.1 Preparation of samples

Three char samples were collected from our previous pyrolysis experiments of three typical WEEE plastics, i.e. phenolic board (PB), brominated high impact polystyrene (HIPS) and acrylonitrile butadiene styrene (ABS), respectively. In brief, 30g of each WEEE plastic was pyrolyzed in a quartz fixed-bed reactor, which was heated to 600 ℃ at a heating rate of 100 ℃/min. The flow rate of the carrier gas ($N_2$) was 50 mL/min. After the reactor temperature reached 600 ℃, it was held at this temperature for 2 hours and was then cooled quickly. Subsequently, three chars were collected, ground and sieved to obtain the powder char sample with a size between 150 and 250 μm. Three char samples were denoted by PB char, HIPS char and ABS char, respectively. The proximate and ultimate analysis as well as the ash analysis of the char samples were presented in Table 4.1. The catalyst $K_2CO_3$, $Na_2CO_3$ and binary mixture

of $K_2CO_3$ and $Na_2CO_3$ loaded HIPS chars were prepared by the wetness impregnation method, as shown in Figure 4.1. And the loading amount of $K_2CO_3$, $Na_2CO_3$, binary mixture carbonate was 10 wt.% of char sample, respectively, and the binary mixture carbonate was prepared by mixing equal weights of $K_2CO_3$ and $Na_2CO_3$ (5wt.% $K_2CO_3$ and 5wt.%$Na_2CO_3$). The impregnation was conducted by mixing the char with appropriate amounts of carbonate in the deionized water. After that, the mixture was stirred for 24 hours in the water bath with the temperature of 50 ℃. Finally, it was dried in the oven at 110 ℃ until all of the water was removed.

Table 4.1. The proximate analysis, ultimate analysis and ash analysis of char samples

| **Sample** | **PB** | **HIPS** | **ABS** |
|---|---|---|---|
| *Proximate analysis (wt.%)* | | | |
| Moisture | 0.4 | 1.4 | 1.4 |
| Volatile matter | 21.5 | 19.1 | 15.5 |
| Fixed carbon | 76.8 | 53.1 | 73.8 |
| Ash | 1.3 | 26.5 | 9.3 |
| *Ultimate analysis (wt.%)* | | | |
| C | 90.7 | 94.6 | 95.3 |
| H | 2.2 | 2.8 | 1.4 |
| N | 0.3 | 0.3 | 1.7 |
| Br | 0.0 | 2.2 | 1.6 |
| O[a] | 6.8 | 0.0 | 0.0 |
| *Ash content (wt.% in ash)* | | | |
| Sb | 0.0 | 2.8 | 60.1 |
| Ti | 0.0 | 73.1 | 0.5 |
| Fe | 18.1 | 4.2 | 10.6 |
| Cr | 17.4 | 0.9 | 3.4 |
| Ca | 0.0 | 2.6 | 4.6 |
| Cu | 20.7 | 0.0 | 0.0 |
| Br | 0.0 | 13.4 | 12.0 |

[a] By difference

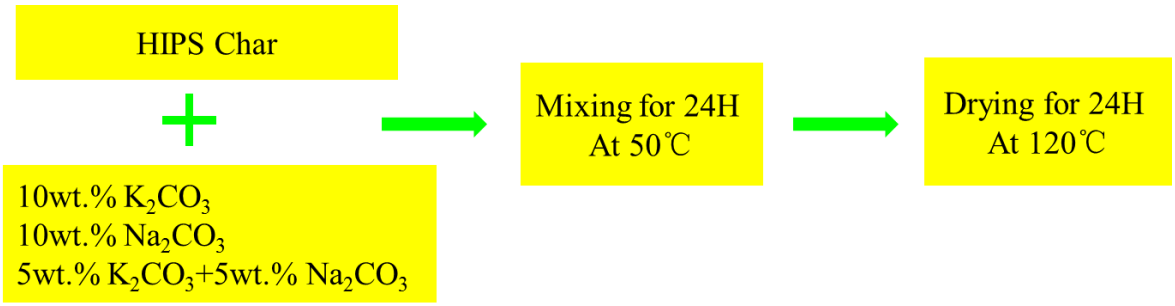


Figure 4.1. The schematic diagram of loading the carbonate catalysts on the char by the impregnation method.

### 4.2.2 Analytical Methods

The CHN element analysis was conducted by using a Micro Corder JM 10 Elemental Analyzer. The bromine content of the char was determined by using an air combustor coupled with Dionex ICS-1100 ion chromatography fitted with a Shodex ICS1-904E column according to JIS K 7392. The ash compositions of the char were determined by an energy dispersive X-ray fluorescence spectrometer (XRF) under vacuum mode for precise measurement. A powder X-ray diffraction (XRD) analysis was carried out for the verification of the crystallinity of the fresh additives and used additives. XRD measurements were performed using a Rigaku Ultimal V diffractometer with the CuKα radiation (λ = 1.540) at 40kV and 40 mA. The XRD patterns were accumulated in the range of 5–50° every 0.02° (2θ) with the counting time of 1 s per step. The surface structure property was analyzed by the SEM. Surface area and textural properties of the used catalysts were determined by $N_2$ physical adsorption at 77 K, applying the Brunauer–Emmett–Teller (BET) method, using a Micromeritics Tristar 3020 equipment.

### 4.2.3 Experimental procedure and reactivity measurements

The isothermal $CO_2$ gasification experiments were conducted using the Shimadzu DTG-50 thermogravimetric analyzer (TGA). The schematic diagram and photo of the TGA equipment are shown in Figure 4.2. 10 mg of each char sample was filled into a cylindrical alumina crucible and then was heated to the targeted temperature at the heating rate of 30 ℃/min under $N_2$ atmosphere

with a flow rate of 150 mL/min. After that, the temperature was kept at the targeted temperature for 10 minutes to maintain the thermal and weight equilibrium. Subsequently, the carrier gas was switched to $CO_2$ with the same flow rate to carry out the isothermal $CO_2$ gasification until the char sample weight became constant. The experimental conditions and the weight loss profile of PB char was shown in Figure 4.3. The time when $CO_2$ was injected was defined as t = 0. The carbon conversion (x) and the gasification rate (r) of chars in the gasification experiment were calculated by the following equation:

$$x = \frac{W_0 - W_t}{W_0 - W_a} \tag{4-1}$$

$$r = \frac{dx}{dt} \tag{4-2}$$

Where $W_0$ (mg) is the initial char weight at the gasification time $t = 0$. $W_t$ (mg) is the instantaneous sample weight at the gasification time of $t$, and $W_a$ (mg) is the left ash weight after finishing gasification. The reactivity index Rs has been widely used to compare the gasification reaction reactivity between different samples. It is given by $Rs = 0.5/t_{0.5}$ with $t_{0.5}$ being the time required for 50% carbon conversion [4-22].

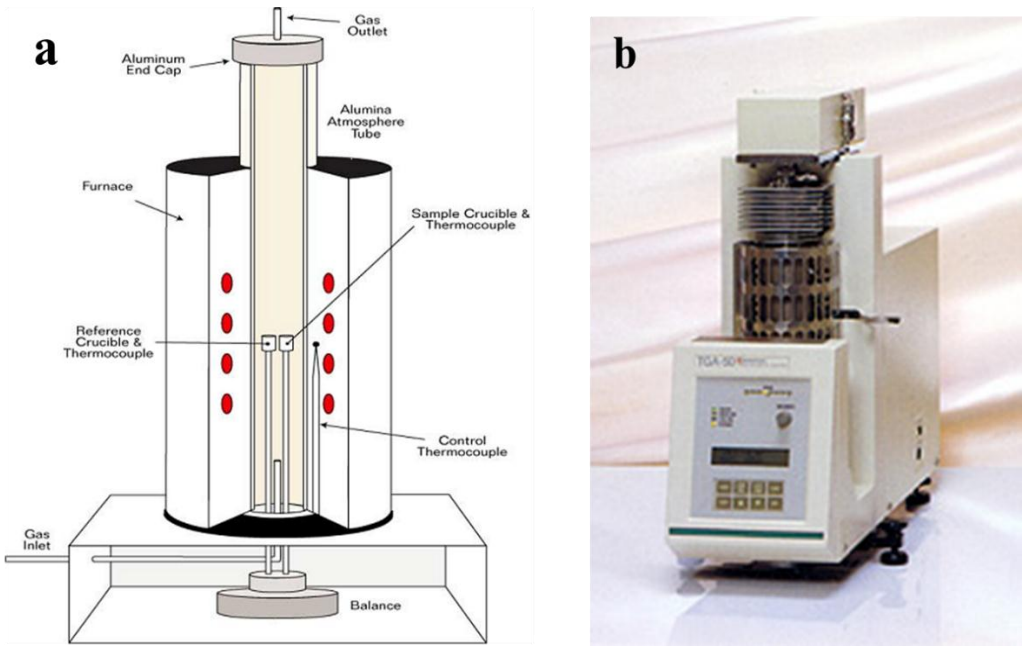


Figure 4.2. The schematic diagram (a) and photo (b) of the TGA equipment

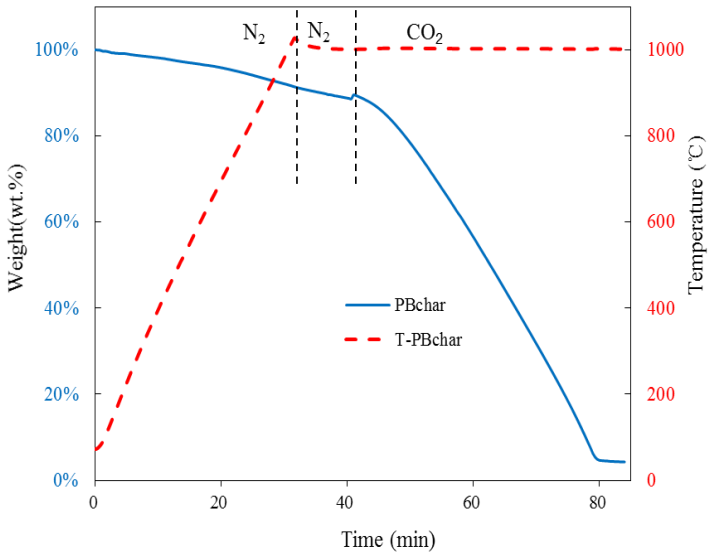


Figure 4.3. The weight loss profile and experimental conditions of $CO_2$ gasification of PB Char at temperature of 1000 ℃.

### 4.2.4 Kinetic models

The most widely used oxygen-exchange mechanism for the $CO_2$ gasification of char, proposed by Reif [4-29], can be summarized as

$$C_f + CO_2 \leftrightarrow C(O) + CO \tag{4-3}$$

$$C(O) \rightarrow CO + C_f \tag{4-4}$$

Where $C_f$ denotes a free carbon active site and C(O) denotes a carbon-oxygen complex. Additionally, in the presence of carbonates as catalysts, the following reaction mechanism have been proposed for the $CO_2$ gasification of char.

$$M_2CO_3 + 2C \rightarrow 2M + 3CO \tag{4-5}$$

$$2M + CO_2 \rightarrow M_2O + C \tag{4-6}$$

$$M_2O + CO_2 \rightarrow M_2CO_3 \tag{4-7}$$

Where M is an alkali metal, which can attack the carbon substrate causing extensive cracking [4-30, 4-31].

According to above mechanism, various kinetic models have been proposed and investigated to characterize the $CO_2$ gasification of char, such as the homogeneous model, the shrinking model, the random pore model and the extended random pore model and the shifted extended random pore model. In this work, three typical kinetic models, the random pore model (RPM), the extended random pore model (eRPM) and the shifted extend random pore model (s-eRPM) were used to characterize the $CO_2$ gasification of char in the absence and presence of carbonate catalysts. RPM, proposed by Bhatia and Perlmutter [4-32], was developed on the base of overlapping cylindrical pores mechanism, which means that there are arbitrary pore size distributions in the char particle and all pores grow and coalesce as the reaction progresses. The reaction rate is expressed as:

$$\frac{\mathrm{dX}}{\mathrm{dt}} = K(1-\mathrm{X})\sqrt{1-\Psi\ln(1-\mathrm{X})} \tag{4-8}$$

$$K = \mathrm{k_0 P_{CO_2}^n} \exp\left(-\frac{\mathrm{E_a}}{\mathrm{RT}}\right) \tag{4-9}$$

Where X is the char conversion, K is the rate constant for the reaction on the pore surfaces, Ψ is the pore surface parameter, $k_0$ ($min^{-1}$) is the pre-exponential factor, Ea (kJ/mol) is the activation energy, and $P_{CO2}$ (bar) is the $CO_2$ partial pressure. And the parameter Ψ can be calculated by the following equation:

$$\Psi = \frac{4\,\pi \mathrm{L_0}(1-\varepsilon_0)}{S_0^2} \tag{4-10}$$

Where $S_0$, $L_0$ and $\varepsilon_0$ denote the pore surface area, the pore length and the total volume of the solid porosity, respectively.

RPM have been successfully used for modeling the gasification reaction of chars. However, it failed to describe the reactivity profiles of biomass chars or alkali metals catalyzed char, for

which the reactivity increases with the increase of the conversion or exists a maximum gasification rate in higher or lower char conversion range [4-16, 4-17]. Therefore, the eRPM was proposed by Zhang et al [4-16] by introducing empirical parameters c and p to better fit the experimental data obtained from the alkali metal catalyzed gasification of coal char and biomass char. The eRPM is expressed in the equation 4-11.

$$\frac{dX}{dt} = K(1-X)\sqrt{1-\varphi \ln(1-X)}\,(1+(cX)^p) \tag{4-11}$$

Where c is a dimensionless constant, and p is a dimensionless power law constant. If c = 0, eRPM becomes the same as RPM. However, it was reported that when the maximum gasification rate appears in the lower char conversion interval, the eRPM also cannot perform well [4-19, 4-21]. The shifted extended random pore model (s-eRPM) was proposed by changing the conversion term $(1 + (cX)^p)$ of eRPM from multiplication to division in order to fit the gasification rate when maximum rate appears at lower char conversion (< 0.2) [4-19]. The s-eRPM could be written by the following equation.

$$\frac{dX}{dt} = \frac{K(1-X)\sqrt{1-\varphi \ln(1-X)}}{1+(cX)^p} \tag{4-12}$$

In this study, the rate constant K, the structure parameter Ψ and two semi-empirical parameters c and p are independent of the temperature and estimated by the nonlinear least-squares method in the MATLAB software.

## 4.3. Results and Discussions

### 4.3.1. Characteristics of char samples

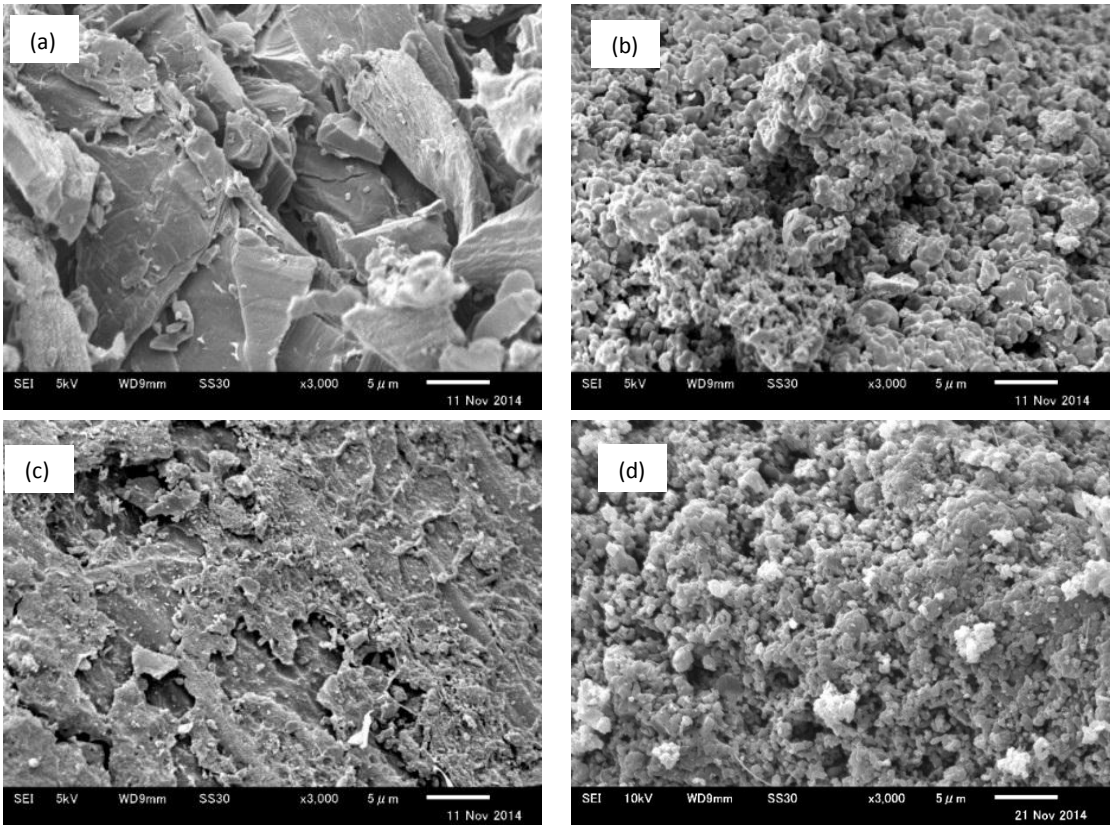


Figure 4.4. SEM micrographs (3,000X) of WEEE plastic chars: (a) PB Char, (b) HIPS Char, (c) ABS Char, (d) HIPS Char + 10wt.% $K_2CO_3$

From the proximate and ultimate analysis shown in Table 4.1, it is found that the three chars derived from the pyrolysis at 600 ºC still contained certain amount of volatile matter and various amount of ash and fixed carbon. For instance, the weight percent of fixed carbon in the PB char, HIPS char and ABS char is 76.8 wt.%, 53.1 wt.% and 73.8 wt.%, respectively. And the ash content of HIPS char is the highest (26.5 wt.%) while the ash content of PB char is the lowest (1.3 wt.%). The main compositions of HIPS char ash are Ti and Br elements. And the major components of the ABS char was the Sb and Br. The metal element, such as Ti and Sb, come from the synergist additives and the Br element mainly derived from the brominated flame retardant. The synergist additive and brominated flame retardant are often added into the WEEE plastics in an attempt to reduce their flammability [4-2, 4-10, 4-11]. Additionally, there are some Fe element exist in the ash fractions for three chars, which might come from the steel reactor when the WEEE plastics were pyrolyzed.

The surface morphology characteristics of chars could be a very important parameter to

evaluate the $CO_2$ gasification reactivity of char, which were observed by using SEM and are shown in Figure 4.4. The morphological structure of PB char showed irregular and sharp-edged property. The PB char exhibited porous and textural structure characteristics, which was in accordance with previous researches [4-33]. As for the HIPS char, it was observed that HIPS char consisted of small relatively uniform particles and each particle are smooth and compressed. There were some porosity structure during each particle. A significant difference in morphology can be seen for the ABS char. The surface of ABS char was smooth and compact. No obvious pore structure was found in the surface of ABS char, which might be attributed to the agglomeration and melting during the pyrolysis of ABS plastic. As for the 10 wt.% $K_2CO_3$ loaded HIPS char, it was observed that some loose twinkling white particles appeared on the surface of $K_2CO_3$ catalyst loaded char. The existence of $K_2CO_3$ catalyst particles would increase the active sites and improve the contact between the $CO_2$ reactant gas and char, which consequently enhance the gasification reactivity of char [4-19, 4-21, 4-30].

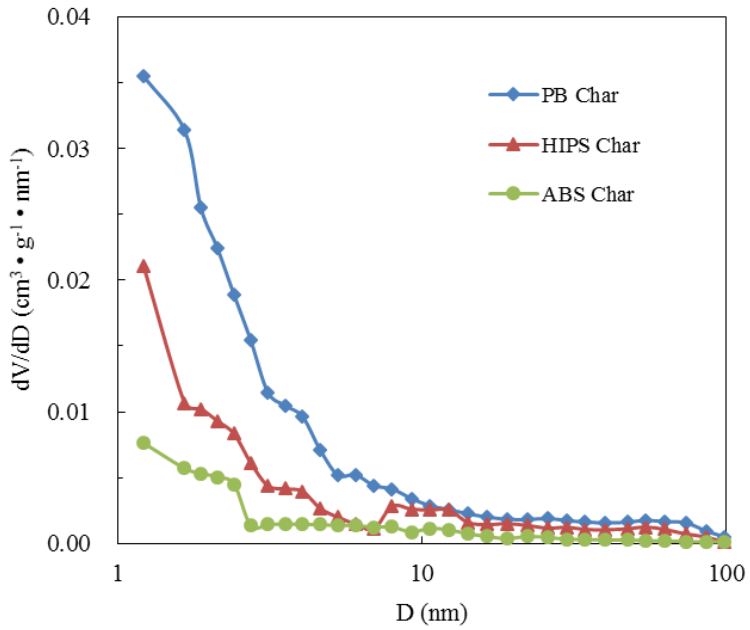


Figure 4.5. Pore size distribution of the WEEE plastic chars

The pore structure characteristics and pore size distribution of WEEE plastic chars were analyzed by $N_2$ adsorption-desorption whose results are shown in Table 4.2 and Figure 4.5, respectively. Table 4.2 indicated that the surface area and the pore volume reveal that the PB char

was more porous than the other two chars. For example, PB char has the largest BET surface area and micropore volume (309 $m^2/g$ and 0.136 $cm^3/g$, respectively), which are much larger than those of ABS char (30.16 $m^2/g$ and 0.04 $cm^3/g$, respectively). With regard to the surface area, it was considered to play a vital role in determining the gasification reactivity, which was attributed to the fact that the surface area could provide active sites and the char gasification reactivity was proportional to active sites and active surface area. For the pore size (Figure 4.5), it was reported that only the pores with diameters larger than 1.5 nm can contribute to the $CO_2$ gasification reaction [4-21]. Furthermore, the pore size distribution would influence the diffusion of reactants and products [4-19]. As shown in Table 4.2 and Figure 4.5, it was found that the average pore diameter of PB char was much smaller than those of HIPS char and ABS char, which indicated that PB char are richer in micro- and mesopores than those of HIPS char and ABS char. Therefore, the gasification reactivity of PB char is expected to be more active than those of HIPS char and ABS char.

Table 4.2. The pore structure properties of WEEE plastic chars

| **Char Samples** | **BET surface area ($m^2/g$)** | **Micropore volume ($cm^3/g$)** | **Average pore diameter (nm)** |
|---|---|---|---|
| PB Char | 309.32 | 0.136 | 4.47 |
| HIPS Char | 105.91 | 0.073 | 8.09 |
| ABS Char | 30.16 | 0.04 | 12.36 |

The carbon crystalline structure is another essential feature of char, which is closely associated with the char $CO_2$ gasification behavior. Liu and co-workers reported that the carbon crystalline structure exerted greater effect on the gasification reactivity than the porosity structure for the chars prepared at different pyrolysis conditions [4-18, 4-24]. In the studies by Jing et al.[4-18], the carbon crystalline structure performed better than the alkali index and BET surface area on the correlation with the gasification reactivity for the different coal chars. According to the XRD patterns in Figure 4.6, the crystal plane index C(002) peaks were observed at approximately 24 °in the all XRD spectrums of WEEE plastic chars. The C(002) diffraction peak represents the

degree of parallel and azimuthal orientation of the aromatic lamellae [4-24]. The disordering of carbon crystalline structure results in the broadening of the C(002) diffraction peak: the more disordering of carbon crystalline structure, the wider the diffraction peak of C(002). It was found that the C(002) diffraction peak of ABS char was narrow and sharp while the C(002) peak of PB char was flat and wide. The width and height of HIPS char were between those of PB char and ABS char. It indicated that the carbon crystalline degree in the three chars was in the sequence of ABS char > HIPS char > PB char. Therefore, it was predicted that the gasification reactivity of three was in the order of PB char > HIPS char > ABS char. Additionally, as for HIPS char, the sharp peaks at around 27.6 °, 36.5 ° and 41.9 ° represent $TiO_2$, while in the case of ABS char, the peaks at 28.9 °, 32.2 ° and 44.5 ° are related to the presence of $Sb_2O_3$. As mentioned above, the $TiO_2$ and $Sb_2O_3$ are commonly employed as synergist and added in WEEE plastic to reduce its flammability [4-2, 4-10, 4-11].

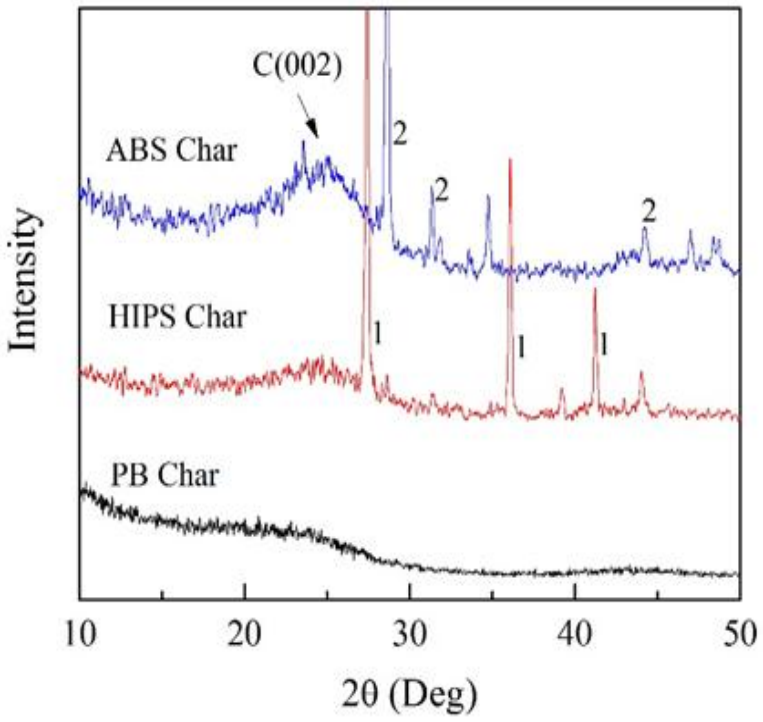


Figure 4.6. XRD patterns of WEEE plastic chars (1, $TiO_2$; 2, $Sb_2O_3$)

According to the analytical results discussed above, the conclusion could be drawn that the characteristics of three WEEE plastic chars are significantly different in the terms of the surface

area, pore structure and the carbon crystalline structure. The effect of these properties on the gasification reactivity will be investigated in detail in the following section.

### 4.3.2. Effect of the gasification temperature on the char conversion

It is well known that the gasification temperature is an essential parameter in controlling the gasification reactivity of char. Therefore, the isothermal $CO_2$ gasification of PB char, HIPS char and ABS char was firstly conducted in the range of 850 – 1050 $^oC$, and the result is shown in Figure 4.7. It indicated that, for all char samples, with the increase of the gasification temperature, the time for the total carbon conversion decreased. For instance, in the case of HIPS char, the gasification time required for the total carbon conversion was over 200 minutes at 850 $^oC$, while the gasification time decreased to 27 minutes at 1050 $^oC$. The gasification of HIPS at 1050 $^oC$ was approximately 7.3 times faster than that at 850 $^oC$. As for PB char, the gasification time at 1050 $^oC$ was 11.7 times shorter than that at 850 $^oC$. Meanwhile, in the case of ABS char, the gasification time at 850 $^oC$ was 3.8 times longer than that at 1050 $^oC$. It illustrated that the higher the gasification temperature is, the faster the char conversion becomes for all samples. Additionally, it indicated that the gasification behavior of the three samples were significantly different because of their various physicochemical properties. At the gasification temperature of 850 $^oC$, the time for the total char conversion of PB char, HIPS char and ABS char were 175.1, 204.7 and 238.2 minutes, respectively, while when the gasification was 1050 $^oC$, the time for the total char conversion of PB char, HIPS char and ABS char were 15.2, 28.1 and 63.6 minutes, respectively. It was found that under the same gasification temperatures, the gasification reactivity of PB char was found to be the highest, followed by that of HIPS char, and the gasification reactivity of ABS char was the lowest, which might be attributed to its smallest surface area and most compact pore structure property, as shown in Figure 4.4, Figure 4.5 and Table 4.2.

In order to compare the gasification reactivity of three WEEE plastic chars in detail, the reactivity index Rs, proposed by Takarada et al. [4-34], have been calculated in the temperature range of 850 $^oC$ – 1050 $^oC$. It is given by $Rs = 0.5/t_{0.5}$ with $t_{0.5}$ being the time required for 50% conversion of the fixed carbon. The results are listed in Table 4.3, which illustrates that the

reactivity index is in good agreement with the above mentioned result that the reactivity index of PB char was the highest, followed by that of HIPS char and the reactivity index of HIPS char was lowest for all of the temperatures. In addition, it could be found that, as the increase of the gasification temperature, the reactivity indexes for PB, HIPS and ABS chars also improved significantly.

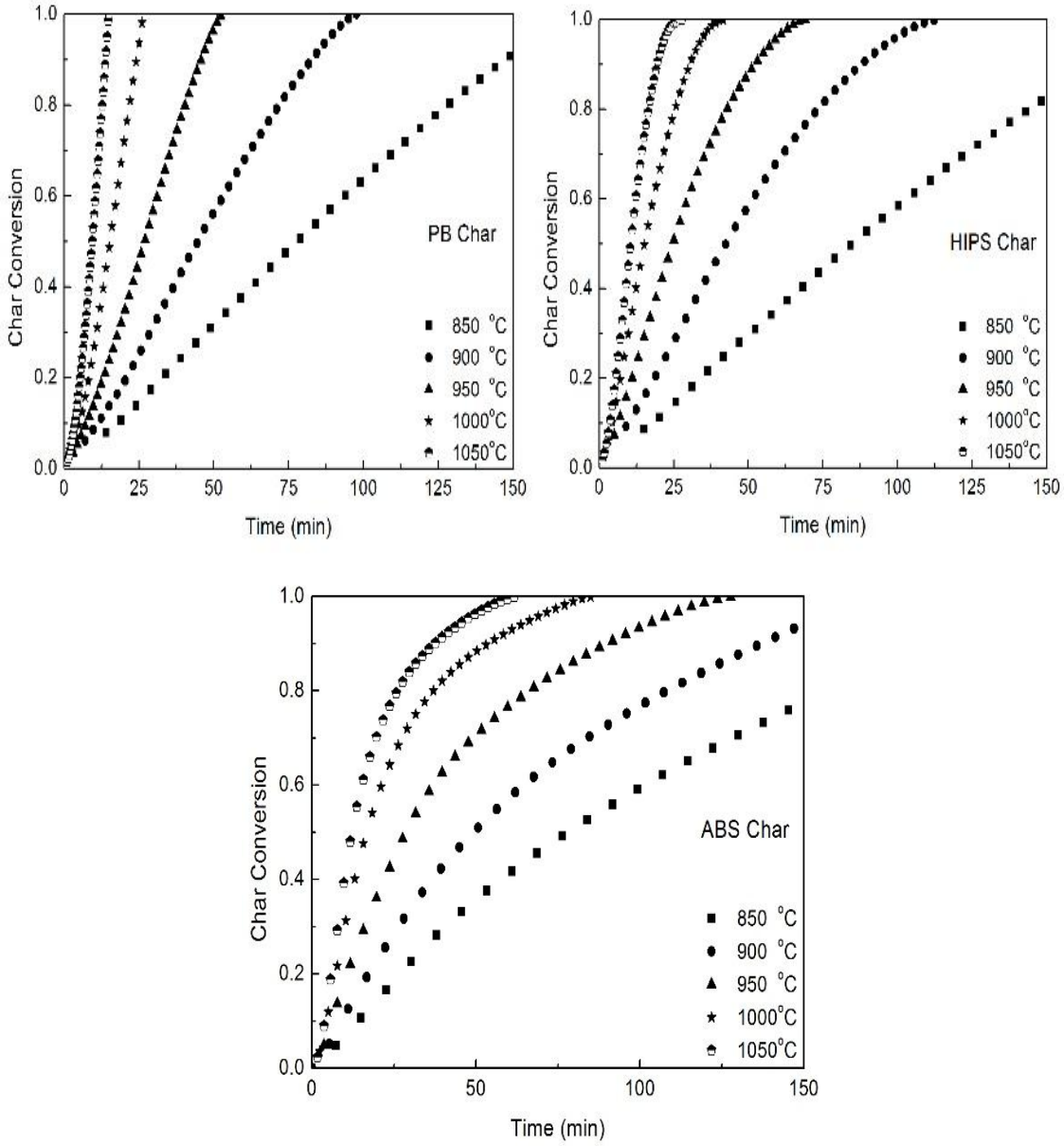


Figure 4.7. The effect of the temperature on the PB, HIPS and ABS char conversion curves

Table 4.3. The $CO_2$ gasification reactivity indexes of PB char, HIPS char and ABS char at different temperatures.

| **Rs** | **850 ºC** | **900 ºC** | **950 ºC** | **1000 ºC** | **1050 ºC** |
|---|---|---|---|---|---|
| PB Char | 0.00640 | 0.01171 | 0.02165 | 0.03373 | 0.05360 |
| HIPS Char | 0.00589 | 0.01157 | 0.02045 | 0.03216 | 0.04770 |
| ABS Char | 0.00569 | 0.01016 | 0.01745 | 0.03014 | 0.04115 |

### 4.3.4. Effect of the $CO_2$ partial pressure on the char conversion

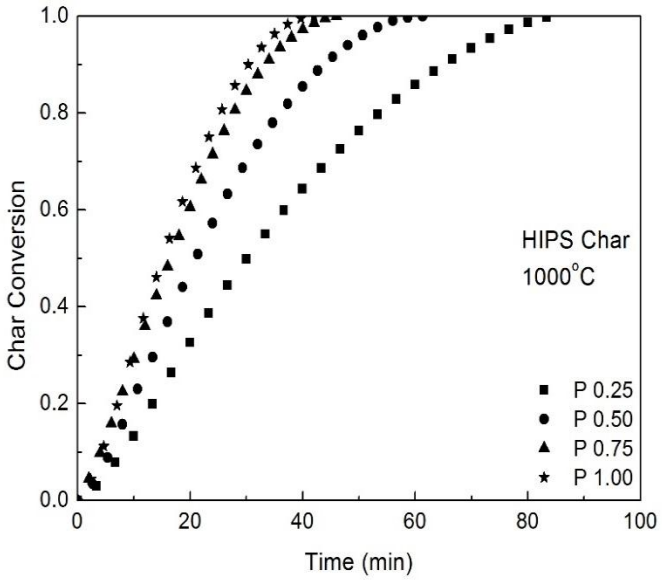


Figure 4.8. The effect of $CO_2$ partial pressure on the HIPS char conversion.

With regard to the $CO_2$ concentration, it was well known that during the $CO_2$ gasification, the partial pressure of $CO_2$ also play an important role in controlling the gasification reactivity of char. The effect of $CO_2$ partial pressure on the HIPS char conversion was shown in Figure 4.8. It indicated that as the increase in the partial pressure of $CO_2$ from 0.25 to 1, the required time for the total char conversion decreased significantly. For instance, when the partial pressure was 0.25, the required time for total char conversion was 84.67 minutes while that became 42.04 minutes at the partial pressure of 1, which was attributed to the fact that high $CO_2$ partial pressure means high $CO_2$ concentration, which could improve the oxygen exchange between $CO_2$ and char and then accelerate the gasification reaction, as shown in the equation 4-3. The reactivity index Rs of HIPS at various $CO_2$ partial pressure was presented in Table 4.4. It was found that the Rs of HIPS

was in accordance with the required time for total char conversion that the Rs increased with the increase of the partial pressure of $CO_2$. In addition, Table 4.4 also indicated that when the partial pressure increased from 0.25 to 0.75, the effect of the partial pressure on the Rs was obvious while when the partial pressure increased from 0.75 to 1, the influence was slight, which illustrated that the Rs was not proportional with the $CO_2$ partial pressure. Whiles, when the $CO_2$ partial pressure was higher than the atmosphere pressure, it might further upgrade the $CO_2$ gasification reactivity of char accompanied by an increase in the surface area, as reported by the Malekshahian et al. and Roberts et al. [4-35, 4-36].

Table 4.4. The $CO_2$ gasification reactivity indexes of HIPS char at different partial pressures

| Partial pressure | 0.25 | 0.50 | 0.75 | 1.00 |
|---|---|---|---|---|
| Rs | 0.01662 | 0.02384 | 0.03022 | 0.03216 |

### 4.3.5. Effect of the carbonates catalysts on the char conversion

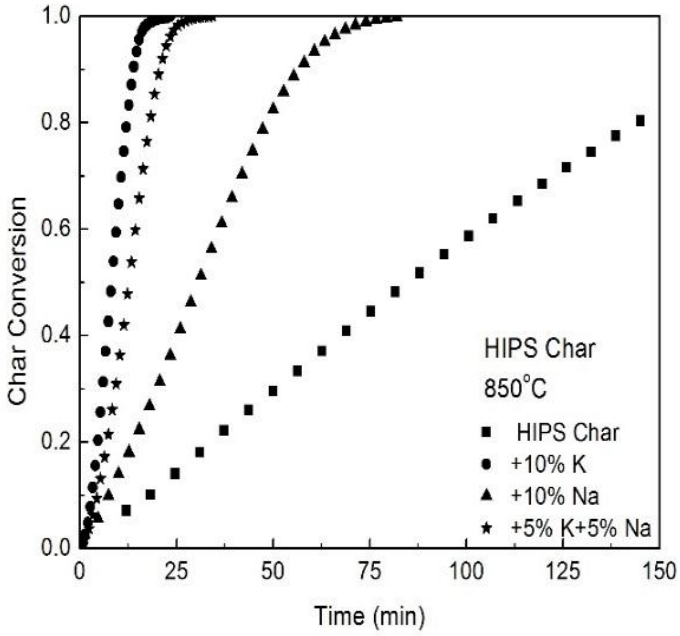


Figure 4.9. The char conversion curves of HIPS char with and without carbonate catalysts at 850 °C

Table 4.5. The $CO_2$ gasification reactivity indexes of HIPS char with and without carbonate catalysts at different temperatures

| **Rs ($min^{-1}$)** | **850 °C** | **900 °C** | **950 °C** |
|---|---|---|---|
| HIPS char | 0.0059 | 0.012 | 0.020 |
| HIPS char+10%K | 0.061 | 0.081 | 0.110 |
| HIPS char+10%Na | 0.016 | 0.030 | 0.049 |
| HIPS char+5%K+5%Na | 0.039 | 0.067 | 0.094 |

Figure 4.9 showed the effect of 10 wt.% $K_2CO_3$, 10 wt.% $Na_2CO_3$ wt.% and mixture of 5 wt.% $K_2CO_3$ + 5 wt.% $Na_2CO_3$ catalyst additions on the char conversion. It was indicated that the carbon conversion rate in the catalytic gasification was higher than that of non-catalytic gasification, which illustrated that all of three catalysts could accelerate the carbon conversion rate. The catalytic activity of the three catalysts followed the sequence of 10 wt.% $K_2CO_3$ > 5 wt.% $K_2CO_3$ + 5 wt.% $Na_2CO_3$ > 10 wt.% $Na_2CO_3$ wt.%. In order to compare the influences of three catalysts on the overall gasification reactivity of chars in detail, the reactivity index Rs has been calculated at 850 °C, 900 °C and 950 °C. It is given by $Rs = 0.5/t_{0.5}$ with $t_{0.5}$ being the time required for 50% conversion of the fixed carbon as shown in the equation. The results are shown in Table 4.5. It illustrates that, at 850 °C, when 10 wt.% $K_2CO_3$, 10 wt.% $Na_2CO_3$ and mixture of 5 wt.% $K_2CO_3$ + 5 wt.% $Na_2CO_3$ catalysts were added into HIPS char, respectively, the reactivity indexes increased 10, 2.8 and 6.7 times than that of HIPS char without the catalysts, respectively. Moreover, at 950 °C, the effect of addition of three catalysts decreased slightly but the gasification reactivity were 5.5, 2.5, and 4.7 times higher than that of HIPS without any catalysts, respectively. The K and Na element mapping of 5 wt.% $K_2CO_3$ + 5 wt.% $Na_2CO_3$ added HIPS char is shown in Figure 4.10, which illustrates that the impregnation method would almost make the K and Na elements uniformly distribute on the surface of HIPS char and thereby enhance the $CO_2$ gasification reactivity of HIPS char. The distributed $K_2CO_3$ and $Na_2CO_3$ particles could increase the reaction active sites which would play an important role in promotion of the gasification reaction [4-26]-[4-28]. The Kopyscinski and co-workers [4-35] have investigated the $K_2CO_3$ catalyzed $CO_2$ gasification of coal and ash-free coal. They concluded that $K_2CO_3$ was effective

catalyst to improve the $CO_2$ gasification reactivity of coal and ash-free coal. At 750 ℃, the $CO_2$ gasification of ash-free coal dry mixed with 20 wt.% $K_2CO_3$ was approximately 3 and 60 times faster than the raw coal and ash-free coal without catalyst, respectively.

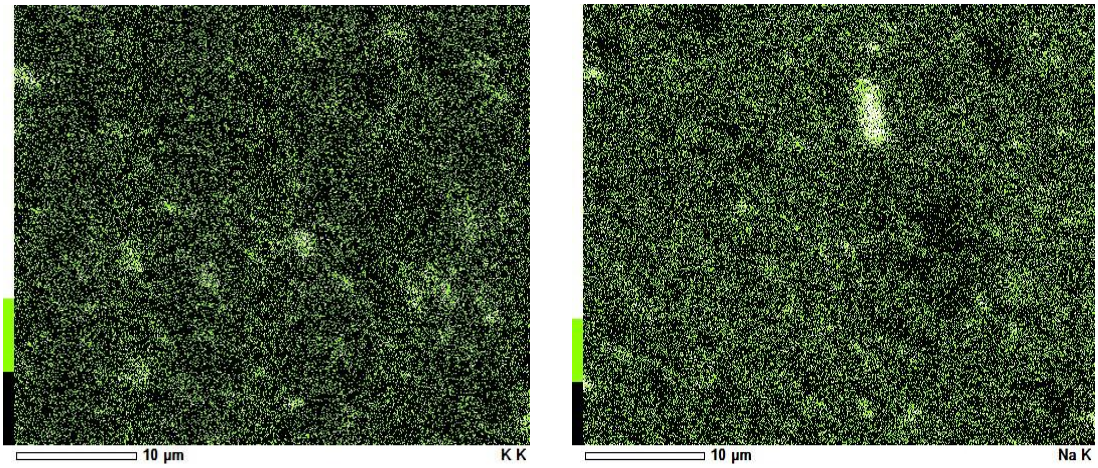


Figure 4.10. K and Na element mapping of 5wt.% $K_2CO_3$ and 5wt.% $Na_2CO_3$ added HIPS char

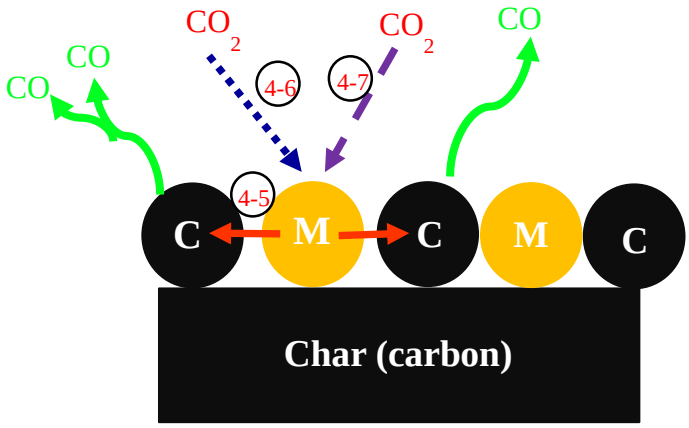


Figure 4.11. The mechanism of carbonate catalyzed $CO_2$ gaisfication of char.

In addition, the reaction equations were devided into three steps, as shown in the in the equations of 4-5, 4-6, 4-7. And each reaction equation correspond to the reaction schematic, which was proposed by McKee and co-worker in 1975 [4-30] In order to make the catalytic mechanism to be easily understood, the reaction schematic is drawn and shown in Figure 4.11, where, M respresents $M_2CO_3$, M and $M_2O$ in the three reactions,

respectively.

### 4.3.6. Kinetic analyses of $CO_2$ gasification of WEEE plastic chars

The effect of the temperature on the gasification reaction rate was investigated in the temperature range of 850 °C – 1050 °C, whose result is shown in Figure 4.13. It is worth mentioning that all of the gasification rates firstly increase to the maximum and then gradually decline with the char conversion. It was reported that this behavior may be attributed to char structure evolution during the reaction process. It is that in the initial stage, the porosity is lower and the original blocked pores are opened and grow, which can improve the surface area available for the reaction. Subsequently, the overlapping of pore structure occurs originating to collapse of the macropore and coalescence of the neighboring pores as gasification proceeds, which would lead to the reduction of the surface area available for the reaction [4-16]. However, with regard to the different chars, the maximum gasification rate appeared in different carbon conversion ranges. As for the PB char, the maximum gasification rate appeared at the char conversion of approximate 0.8. In the case of HIPS char and ABS char, the maximum gasification rate was obtained when the carbon conversion was about 0.45 and 0.2, respectively. In addition, as expected, the reaction rate results were consistent with that of char conversion, which was sensitive to the gasification temperature and the reactivity was improved as the temperature increased. The experimentally obtained $CO_2$ gasification rate results would be used for the kinetic study.

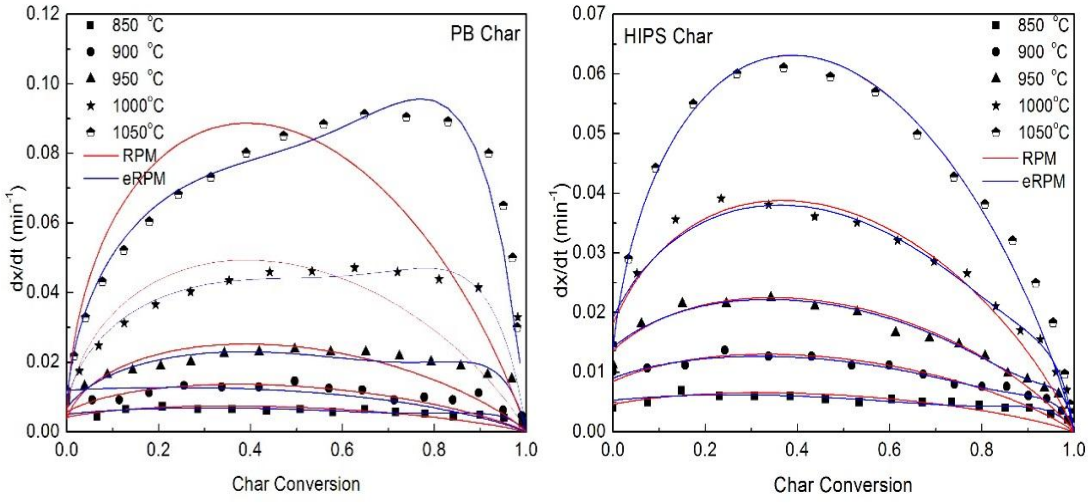

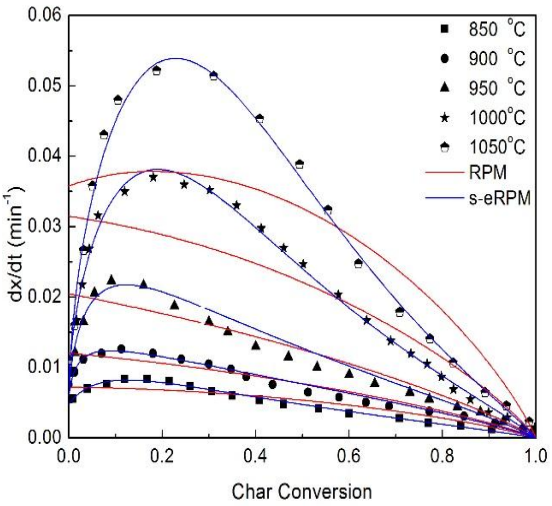


Figure 4.12. Gasification rates of PB char, HIPS char and ABS char (symbols) and fitting curves of RPM, eRPM and s-eRPM (lines)

Several kinetic models have been applied to simulate the gasification reactions and describe the relationship between the reaction rate and time, such as the homogeneous model, the shrinking core model, the normal distribution model, RPM, eRPM and s-eRPM. It could be obviously found that there was a maximum for the gasification rate of each char, as shown in Figure 4.12. In the above mentioned models, only RPM and eRPM are suitable to simulate this gasification behavior [4-16, 4-19]. The equations and the meanings of each parameters of RPM and eRPM have been shown and explained in the session 2.4. The reaction rate of three chars at different temperatures have been simulated by both RPM and eRPM, respectively. The MATLAB software was employed to fit experimental the reaction rate results by the nonlinear least-squares methods in order to estimate the kinetic parameters and the correlation coefficients ($R^2$).

The curve fitting results and the estimated kinetic parameters results are presented in Figure 4.12 and Table 4.6, respectively. From the curve fitting results, as for PB whose maximum gasification rate appeared at the char conversion of about 0.8, eRPM was better than RPM to predict the gasification rate. The maximum gasification rate of HIPS char was obtained at the char conversion of about 0.4. The curve fitting result of RPM and eRPM for the HIPS char gasification rate were almost comparable. Nevertheless, for ABS char, the RPM and eRPM could not simulate the gasification rate very well, because the maximum gasification rate of ABS char appeared at

the char conversion of less than 0.2 because of the smallest surface area [4-19]. It was reported that when the maximum gasification rate appeared at a lower char conversion, the s-eRPM, as shown in equation 10, was more suitable for the gasification rate curve fitting [4-19 ,4-21]. It was found that the s-eRPM could fit the gasification rate curve of ABS well with a higher $R^2$ valve over 0.99. The Jing and co-worker [4-19] reported that the better curve fitting results of eRPM and shifted eRPM than that of RPM illustrated that the gasification of coal char is not only affected by the initial pore structure but also the inherent minerals and variation of the pore structure in the gasification process.

Table 4.6. The kinetic parameters and regression coefficients estimated by the RPM and eRPM fitting

| Sample | **Kinetic Parameters** | | | | | | | | |
|---|---|---|---|---|---|---|---|---|---|
| | **T** | **RPM** | | | **e-RPM/s-eRPM[a]** | | | | |
| | ℃ | K | ψ | $R^2$ | K | ψ | c | p | $R^2$ |
| PB Char | 850 | 0.0042 | 14.7 | 0.931 | 0.005 | 7.67 | 1.2 | 9.85 | 0.993 |
| | 900 | 0.0057 | 29.0 | 0.972 | 0.012 | 1.70 | 0.6 | 0.95 | 0.994 |
| | 950 | 0.0035 | 286.9 | 0.951 | 0.007 | 62.18 | 1.2 | 8.89 | 0.991 |
| | 1000 | 0.0048 | 574.9 | 0.945 | 0.009 | 131.73 | 1.2 | 5.63 | 0.992 |
| | 1050 | 0.0035 | 572.1 | 0.944 | 0.009 | 384.52 | 1.3 | 4.45 | 0.994 |
| HIPS Char | 850 | 0.0046 | 8.8 | 0.989 | 0.005 | 5.00 | 1.1 | 10.47 | 0.993 |
| | 900 | 0.0084 | 10.8 | 0.991 | 0.009 | 8.49 | 1.1 | 15.71 | 0.994 |
| | 950 | 0.0137 | 12.6 | 0.987 | 0.014 | 11.15 | 1.0 | 25.50 | 0.998 |
| | 1000 | 0.0180 | 23.1 | 0.990 | 0.019 | 19.48 | 1.0 | 15.98 | 0.995 |
| | 1050 | 0.0139 | 110.2 | 0.987 | 0.014 | 110.20 | 1.0 | 117.42 | 0.996 |
| ABS Char | 850 | 0.0072 | 1.7 | 0.871 | 0.005 | 48.4 | 3.5 | 1.17 | 0.991 |
| | 900 | 0.0121 | 1.9 | 0.866 | 0.006 | 196.1 | 17.1 | 0.71 | 0.992 |
| | 950 | 0.0204 | 2.7 | 0.894 | 0.007 | 213.4 | 4.7 | 1.05 | 0.995 |
| | 1000 | 0.0315 | 3.4 | 0.887 | 0.0093 | 276.2 | 2.16 | 1.71 | 0.996 |
| | 1050 | 0.0358 | 4.4 | 0.853 | 0.0078 | 395.0 | 1.78 | 2.18 | 0.997 |

[a] For PB char and HIPS char, eRPM is used; For ABS char, s-eRPM is employed.

In addition, in the case of HIPS, The constant ψ has been used to try to fit the gasification experimental data, as shown in Table 4.7. It is found that basically both random ψ and constant ψ can be used to fit the experimental data. However, according to the simulation of MATLAB software, when ψ is random, the correlation coefficients ($R^2$) is higher. Therefore, the random ψ is more suitable to fit the gasification experimental data. And many other researchers also use the random ψ to obtain the optimum fitting kinetic parameters for the gasification of coal and biomass char [4-19,4-21].

Table 4.7 The kinetic parameters and regression coefficients estimated by eRPM fitting in the constant ψ

| HIPS char | Temperature (°C) | K | ψ | c | p | $R^2$ |
|---|---|---|---|---|---|---|
| | 850 | 0.006 | 10 | 1.1 | 8.99 | 0.814 |
| | 900 | 0.009 | 10 | 1.1 | 11.58 | 0.942 |
| **Constant ψ** | 950 | 0.014 | 10 | 1.1 | 15.12 | 0.972 |
| | 1000 | 0.024 | 10 | 1.0 | 5.34 | 0.922 |
| | 1050 | 0.030 | 10 | 1.0 | 0.98 | 0.958 |

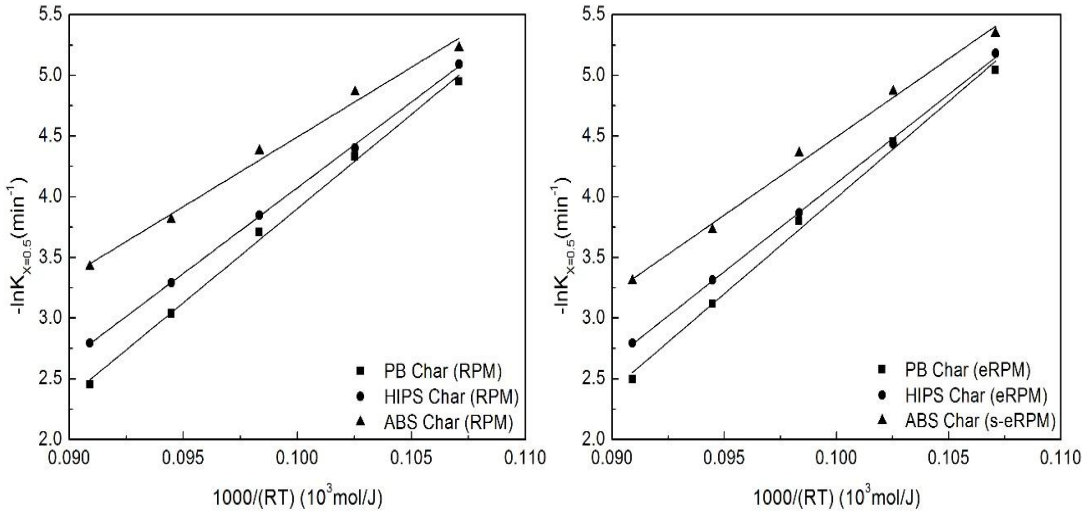


Figure 4.13. Arrhenius curves of WEEE plastic chars gasification reaction by employing RPM, eRPM and s-eRPM

It have been mentioned that the rate constant K in the above discussed models would become

the initial gasification rate d*X*/d*t* when char conversion X = 0. Nevertheless, it was reported that the switch of gas results for *dX/dt* (X = 0) obtained from the TGA is not accurate [4-14, 4-19, 4-21]. Consequently, in this study, the gasification rate at char conversion of 0.5 ($r_{0.5}$) was taken as the basis and the $lnr_{0.5}$ versus $1/(R \cdot T)$ is plotted in Figure 4.13. According to the RPM, eRPM and s-eRPM and Arrhenius curves. The activation energy $E_a$ and the pre-exponentional factor $k_0$ could be calculated by the Arrhenius equation, and the results are shown in Table 4.8. It can be observed that the values of activation energies of three chars obtained from eRPM and s-eRPM are a little higher than that of three chars obtained from RPM. According the best fitting model, the activation energies of PB char, HIPS char and ABS char are 158.44, 145.94 and 128.70 kJ/mol, respectively.

Table 4.8. Activation energy $E_a$ and the pre-exponentional factor $k_0$ calculated by Arrhenius equation

| | **RPM** | | **eRPM/s-eRPM** | |
|---|---|---|---|---|
| **Sample** | **$E_a$ (kJ/mol)** | **$k_0$ ($min^{-1}$)** | **$E_a$ (kJ/mol)** | **$k_0$ ($min^{-1}$)** |
| PB Char | 155.11 | $1.10 \times 10^5$ | 158.44 | $1.40 \times 10^5$ |
| HIPS Char | 141.18 | $2.30 \times 10^4$ | 145.94 | $3.56 \times 10^4$ |
| ABS Char | 114.77 | $1.08 \times 10^3$ | 128.70 | $4.34 \times 10^3$ |

### 4.3.7. Kinetic analyses of $CO_2$ gasification of HIPS chars in the presence of carbonate catalysts.

The reaction rates of carbonates catalyzed gasification of HIPS was also studied and the results are presented in Figure 4.14. It illustrates that after the addition of each carbonate catalyst, the reaction rate was significantly improved at 850 °C, 900 °C and 950 °C, especially, when 10 wt.% $K_2CO_3$ was added. It was consistent with the previous work that in the $CO_2$ gasification, the catalytic performance of potassium (K) was the strongest, followed by that of sodium (Na) [4-26, 4-27, 4-35]. The catalytic performance of the mixture of 5.wt.% $K_2CO_3$ and 5.wt.% $Na_2CO_3$, was between that of 10.wt.% $K_2CO_3$ and 10.wt.% $Na_2CO_3$, which means that the synergistic effect of

the mixture of carbonate catalysts was not very obvious. Additionally, the catalysts added reaction rates of HIPS char were simulated by RPM and e-RPM. The fitting curve and the estimated kinetic parameters are presented in Figure 4.14 and Table 4.9. From Table 4.9, it could be found that e-RPM was more suitable for fitting the experimental reaction rate data because the regression coefficients ($R^2$) of s-eRPM was higher than that of RPM. Therefore, it further comfirmed the above conclusion that when the maximum gasification rate appeared in the high char conversion range (> 0.4), eRPM was more suitable to fit the experimental gasification rate result than that of RPM, which was in accordance with the result reported by the Yung et al. and Jing et al. [4-19, 4-21].

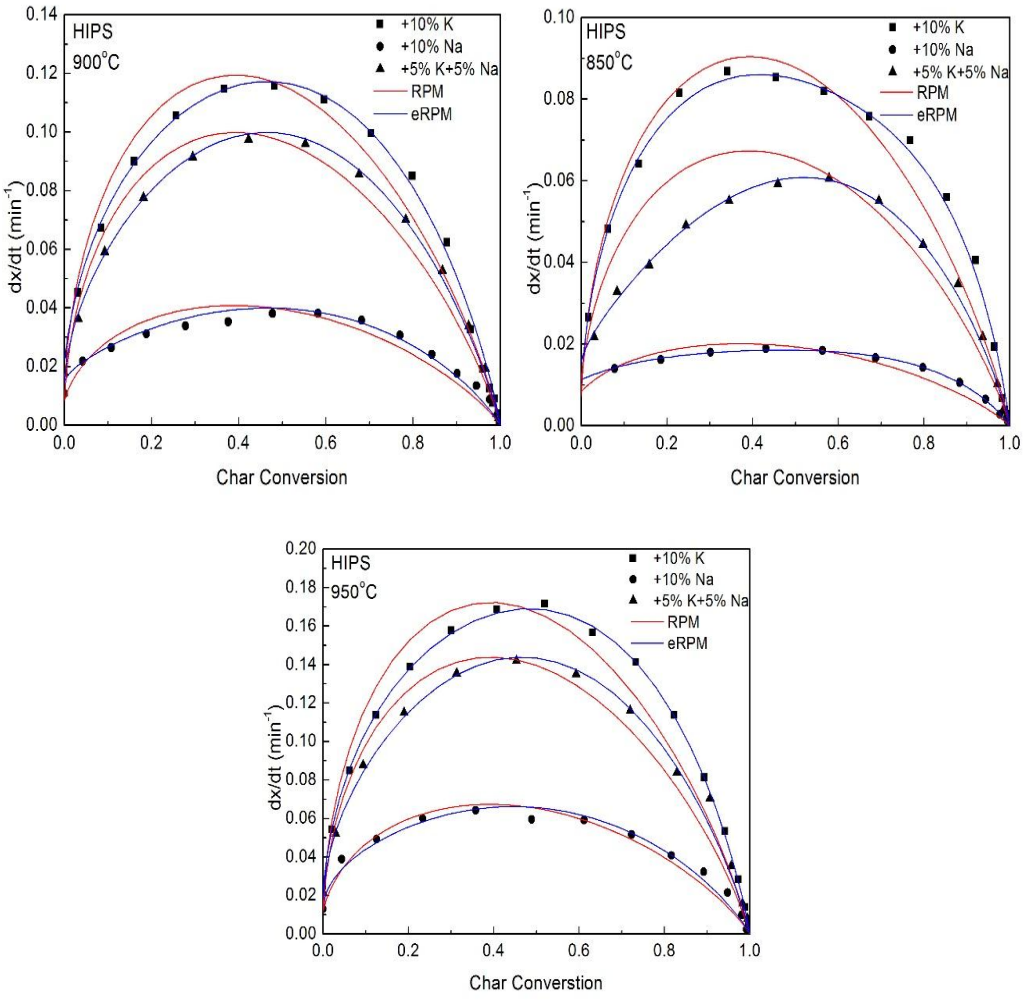


Figure 4.14. Gasification rates of HIPS char with carbonates catalysts at different temperatures and fitting curves of RPM and e-RPM (lines).

Table 4.9. The kinetic parameters and regression coefficients of carbonate catalyzed $CO_2$ gasification of HIPS char simulated by RPM and e-RPM

| Kinetic Parameters | | | | | | | | | |
|---|---|---|---|---|---|---|---|---|---|
| Sample | T | RPM | | | eRPM | | | | |
| | ℃ | $A_0$ | ψ | $R^2$ | $A_0$ | ψ | c | p | $R^2$ |
| HIPS+K | 850 | 0.0072 | 847.4 | 0.955 | 0.011 | 152.02 | 0.9 | 4.71 | 0.993 |
| | 900 | 0.0146 | 362.8 | 0.974 | 0.022 | 218.36 | 0.6 | 1.53 | 0.995 |
| | 950 | 0.0149 | 722.0 | 0.977 | 0.023 | 224.98 | 0.7 | 1.81 | 0.994 |
| HIPS-Na | 850 | 0.0084 | 29.2 | 0.933 | 0.011 | 10.56 | 1.0 | 2.68 | 0.989 |
| | 900 | 0.0085 | 124.6 | 0.958 | 0.015 | 3.07 | 6.2 | 0.63 | 0.995 |
| | 950 | 0.0115 | 186.1 | 0.936 | 0.012 | 2.79 | 88.2 | 0.45 | 0.991 |
| HIPS-NaK | 850 | 0.0115 | 186.1 | 0.961 | 0.016 | 3.34 | 10.0 | 0.73 | 0.990 |
| | 900 | 0.0090 | 659.9 | 0.952 | 0.014 | 1.43 | 76.1 | 0.60 | 0.989 |
| | 950 | 0.0124 | 726.1 | 0.986 | 0.018 | 1.73 | 111.3 | 0.57 | 0.991 |

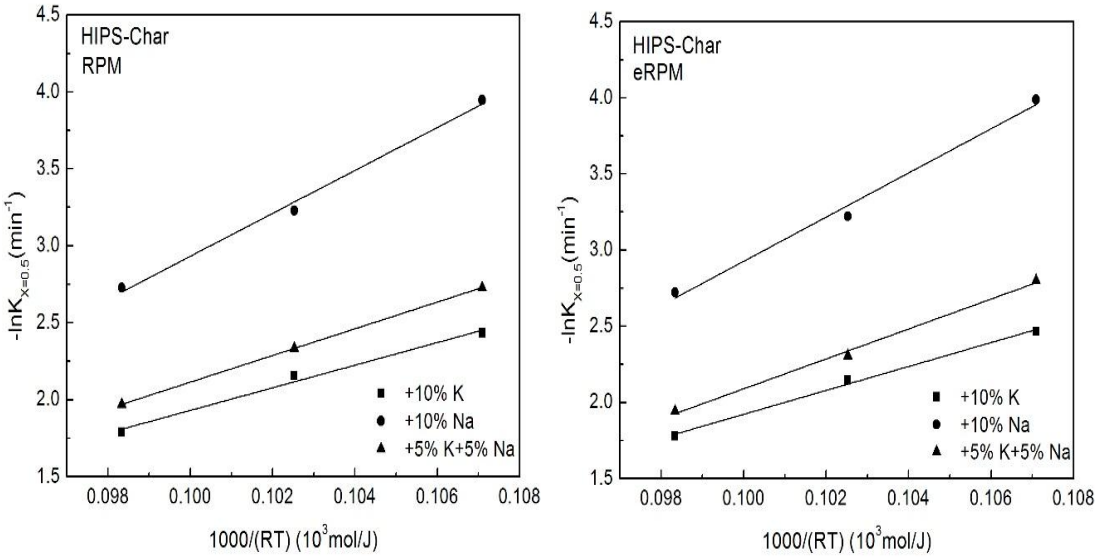


Figure 4.15. Arrhenius curves of gasification reaction of HIPS char carbonate catalysts by employing RPM and eRPM

Table 4.10. Activation energy $E_a$ and the pre-exponentional factor $k_0$ of $CO_2$ gasification of HIPS char with/without carbonate catalysts calculated by Arrhenius equation

| | RPM | | eRPM | |
|---|---|---|---|---|
| **Sample** | **Ea (kJ/mol)** | **$k_0$ (min-1)** | **Ea (kJ/mol)** | **$k_0$ (min-1)** |
| HIPS | 141.18 | $2.30\times10^4$ | 145.94 | $3.56\times10^4$ |
| HIPS+K | 73.46 | $2.25\times10^2$ | 78.50 | $3.75\times10^2$ |
| HIPS+Na | 119.44 | $6.06\times10^4$ | 125.00 | $1.06\times10^5$ |
| HIPS+NaK | 86.76 | $7.07\times10^2$ | 98.23 | $2.28\times10^3$ |

The Arrhenius equation was employed for the calculation of $CO_2$ gasification activation energy of HIPS char in the presence of carbonate catalysts. Here, the gasification rates at a conversion of 0.5 are taken as the basis, and the Arrhenius curves of ln $r_{0.5}$ versus 1000/RT by employing RPM and s-eRPM are shown in Figure 4.15, which indicates that for HIPS char with carbonate catalysts, the eRPM is better than that of RPM because of its higher regression coefficients ($R^2$). In addition, the Activation energy $E_a$ and the pre-exponentional factor $k_0$ were calculated by the Arrhenius equation and are shown in Table 4.10. From Table 4.10, it was found that the addition of carbonates catalytic could obviously reduce the $CO_2$ gasification activation energy of HIPS char. The activation energy of HIPS char decreased from 145.94 KJ/mol to 78.50, 125.00, 98.23 KJ/mol, respectively when the 10 wt.% $K_2CO_3$, 10 wt.% $Na_2CO_3$, 5 wt.% $K_2CO_3$ + 5 wt.% $Na_2CO_3$ carbonate catalysts was added, respectively. Zhou and co-worker [4-25] reported that the $CO_2$ gasification activation energy of petroleum coke was 198.05 kJ/mol, which decreased to 168.06 kJ/mol when the 5 wt% $FeCl_3$ catalyst was added. Karimi et al. [4-26] conducted the steam gasification of coke in the presence of $Na_2CO_3$ and $K_2CO_3$ as catalysts and found that the activation energy decreased from 210 kJ/mol to 120 and 130 kJ/mol, respectively. It was concluded from their studies that this considerable effect of catalysts on reducing the activation energy was consistent with some changes in the reaction pathway rather than simply increasing the number of active sites. However, the result reported by Kopyscinski and co-worker [4-35] that the gasification of ash-free coal dry mixed with 20 wt.% $K_2CO_3$ was approximately 3 and 60 times faster than the raw coal and ash-free coal without catalyst, respectively. However,

the activation energy for the catalyzed ash-free coal gasification was approximately 100 kJ $mol^{-1}$ larger than for raw coal and the uncatalyzed ash-free coal, which was explained by the reason that this increase of the activation energy might be due to the energy required for the potassium (i.e., catalyst) transfer to a new carbon site or caused by the pyrolysis process, because the formed char might have different properties.

## 4.4. Summary

The $CO_2$ gasification of PB char, HIPS char and ABS char were conducted at the temperature range of 850-1050 $^oC$ in the TGA. The main conclusions from this work are summarized as follows: (1) As expected, for all three char samples, with the increase of the gasification temperature, the time for the char conversion decreased while the reactivity index and the gasification rate significantly increased. The reactivity indexes of PB char, HIPS char and ABS char at 1050 $^oC$ became 8.4, 8.1 and 7.2 times higher than that of them at 850 $^oC$, respectively. (2) At the same gasification temperature, the gasification reactivity of three WEEE plastic chars was in the order of PB char > HIPS char > ABS char, which was attributed to the fact that the surface area of PB char is the largest and lowest carbon crystalline degree. (3) For PB char, its maximum gasification rate appears in the char conversion of approximate 0.8 and the best fitting curve model was eRPM with the highest $R^2$ (> 0.991). As for HIPS char, RPM and eRPM are comparably suitable to fit with the gasification rate curve, and $R^2$ of RPM and eRPM are > 0.985 and > 0.993, respectively. In the case of ABS char, the maximum gasification rate presents in the lower carbon conversion (< 0.2), and s-eRPM was the most suitable model for predicting the gasification rate with the highest $R^2$ (> 0.991). (4) The $CO_2$ gasification activation energies of PB char, HIPS char and ABS char are 158.44, 145.94 and 128.70 kJ/mol, respectively. (5) The addition of carbonate catalyst could obviously increase the gasification rate and the reactivity index of the char samples. At 850 $^oC$, the addition of 10wt.%$K_2CO_3$, 5wt.%$K_2CO_3$ 5wt.%$Na_2CO_3$, 10wt.%$Na_2CO_3$ into HIPS char could increase the reactivity index 10, 6.7 and 2.8 times,

respectively. Therefore, the catalytic activity of the three catalysts followed the sequence of 10 wt.% $K_2CO_3$ > 5 wt.% $K_2CO_3$ + 5 wt.% $Na_2CO_3$ > 10 wt.% $Na_2CO_3$. (6) eRPM with a higher $R^2$ (> 0.99) was more suitable for fitting with the carbonate catalyzed $CO_2$ gasification rate of HIPS char than the RPM. (7) According to eRPM and Arrhenius curve, the addition of 10 wt.% $K_2CO_3$, 10 wt.% $Na_2CO_3$, 5 wt.% $K_2CO_3$ + 5 wt.% $Na_2CO_3$ carbonate catalysts could reduce the activation energy of HIPS char from 145.94 KJ/mol to 78.50, 125.00, 98.23 KJ/mol, respectively.

## References


[4-1] United Nations Environment Programme [UNEP]. (2009). Retrieved from

[4-2] Yang, X. N., Sun, L., S., Xiang, J., Hu, H. & Su, S. (2013). Pyrolysis and dehalogenation of plastics from waste electrical and electronic equipment (WEEE): A review. *Waste Management*, **33**, 462–473.

[4-3] Ongondo, F., O., Williams, I., D. & Cherrett, T., J. (2011). How are WEEE doing? A global review of the management of electrical and electronic wastes. *Waste Management*, **31**, 714–730.

[4-4] Quan, C., Li, A., Gao, N. & Dan, Z. (2010). Characterization of products recycling from PCB waste pyrolysis. *Journal of Analytical and Applied Pyrolysis*, **89**, 102–6.

[4-5] Long, L., Sun, S., Zhong, S., Dai, W., Liu, J. & Song, W. (2010). Using vacuum pyrolysis and mechanical processing for recycling waste printed circuit boards. *Hazardous Material*, **177**, 626–32.

[4-6] Bhaskar, T., Matsui T., Uddin, Md. A., Kaneko, J., Muto, A. & Sakata, Y. (2003). Effect of $Sb_2O_3$ in brominated heating impact polystyrene (HIS-Br) on thermal degradation and debromination by iron oxide carbon composite catalyst (Fe-C). *Applied Catalysis B: Environmental*, **43**, 229–241.

[4-7] Bhaskar, T., Matsui, T., Kaneko, J., Uddin, Md. A., Muto, A. & Sakata, Y. (2002). Novel calcium based sorbent (Ca-C) for the dehalogenation (Br, Cl) process during halogenated mixed plastic (PP/PE/PS/PVC and HIPS-Br) pyrolysis. *Green Chemistry*, **4**, 372–375.

[4-8] Terakado, O., Ohhashi, R. & Hirasawa, M. (2011). Thermal degradation study of tetrabromobisphenol A under the presence metal oxide: Comparison of bromine fixation ability. *Journal of Analytical and Applied Pyrolysis*, **91**, 303–309.

[4-9] Terakado, O., Ohhashi, R. & Hirasawa, M. (2013). Bromine fixation by metal oxide in pyrolysis of printed circuit board containing brominated flame retardant. *Journal of Analytical and Applied Pyrolysis*, **103**, 216-221.

[4-10] Hall, W. & Williams, P., T. (2008). Removal of organobromine compounds from the pyrolysis oils of flame retarded plastics using zeolite catalysts. *Journal of Analytical and Applied Pyrolysis*, **81**, 139-147.

[4-11] Hall, W., J., Miskolczi, N., Onwudili, J. & Williams, P., T. (2008). Thermal Processing of Toxic Flame-Retarded Polymers Using a Waste Fluidized Catalytic Cracker (FCC) Catalyst. *Energy & Fuels*, **22**, 1691–1697.

[4-12] Bozi, J. & Blazsó, M. (2009). Catalytic modification of pyrolysis products of nitrogen-

containing polymers over Y zeolites. *Green Chemistry*, **11**, 1638–1645.

[4-13] Zhang S., Z., Yoshikawa K., Nakagome, H. & Kamo, T. (2013). Kinetics of the steam gasification of a phenolic circuit board in the presence of carbonates. *Applied Energy*, **101**, 815–821.

[4-14] Kajitani, S., Hara, S. & Matsuda, H. (2002). Gasification rate analysis of coal char with a pressurized drop tube furnace. *Fuel*, **81(5)**, 539–546.

[4-15] Kajitani, S., Zhang, Y., Umemoto, S., Ashizawa, M. & Hara. S. (2010). Co-gasification Reactivity of Coal and Woody Biomass in High-Temperature Gasification. *Energy & Fuels*, **24**, 145-151.

[4-16] Zhang, Y., Ashizawa, M., Kajitani, S. & Miura, K. (2008). Proposal of a semi-empirical kinetic model to reconcile with gasification reactivity profiles of biomass chars. *Fuel*, **87**, 475-481.

[4-17] Zhang, Y., Hara, S., Kajitani, S. & Ashizawa, M. (2010). Modeling of catalytic gasification kinetics of coal char and carbon. *Fuel*, **89**, 152-157.

[4-18] Jing, X., L., Wang, X., Q., Zhang, Q., Yu, Z., L., Li, C., Y., Huang, J., J. & Fang, Y. (2013). Evaluation of $CO_2$ Gasification Reactivity of Different Coal Rank Chars by Physicochemical Properties. *Energy & Fuels*, **27**, 7287−7293.

[4-19] Jing, X., L., Wang, Z., Q., Yu, Z., L., Zhang, Q., Li, C., Y. & Fang, Y., T. (2013). Experimental and Kinetic Investigations of $CO_2$ Gasification of Fine Chars Separated from a Pilot-Scale Fluidized-Bed Gasifier. *Energy & Fuels*, **27**, 2422-2430.

[4-20] Gil, M., V., Fermoso, J., Pevida, C., Pis, J., J. & Rubiera, F. (2010). Intrinsic char reactivity of plastic waste (PET) during $CO_2$ gasification. Fuel Processing Technology, 91, 1776–1781.

[4-21] Yuan, S., Chen, X., L., Li, J. & Wang, F., C. (2011). $CO_2$ Gasification Kinetics of Biomass Char Derived from High-Temperature Rapid Pyrolysis. *Energy & Fuels*, **25**, 2314–2321.

[4-22] Lahijania, P., Zainala, Z., A. & Mohamedb, A., R. (2012). Catalytic effect of iron species on $CO_2$ gasification reactivity of oil palm shell char. Thermochimica Acta, 546, 24-31.

[4-23] Lahijani, P., Zainal, Z., A., Mohamed, A., R. & Mohammadi, M. (2013). $CO_2$ gasification reactivity of biomass char: Catalytic influence of alkali, alkaline earth and transition metal salts. *Bioresource Technology*, **144**, 288-295.

[4-24] Huang, Y., Yin, X., Wu, C., Wang, C., Xie, J., Zhou, Z., Ma, L. & Li, H. (2009). Effects of metal catalysts on $CO_2$ gasification reactivity of biomass char, *Biotechnology Advances*, **27**, 568–572.

[4-25] Zhou, Z., J., Hu, Q., J., Liu, X., Yu, G., S. & Wang, F., C. (2012). Effect of iron species and calcium hydroxide on high-sulfur petroleum coke $CO_2$ gasification, *Energy & Fuels*, **26** 1489–1495.

[4-26] Karimi, A., Semagina, N. & Gray, M., R. (2011) Kinetics of catalytic steam gasification of bitumen coke. *Fuel*, **90**, 1285–1291.

[4-27] Vamvuka, D., Karouki, E., Sfakiotakis, S. & Salatino, P. (2011). Gasification of Waste Biomass Chars by Carbon Dioxide via Thermogravimetry-Effect of catalysts. Combustion Science and Technology, 184, 64-77.

[4-28] Zhang S., Z., Yoshikawa K., Nakagome, H. & Kamo, T. (2012). Steam gasification of epoxy circuit board in the presence of carbonates. *Journal of Material Cycles and Waste Management*, **14**, 294-300.

[4-29] Reif, A., E. (1952). The mechanism of the carbon dioxide-carbon reaction. J. Phys. Chem., 56,785.

[4-30] McKee, D.W. & Chatterji, D. (1975). The catalytic behavior of alkali metal carbonates and oxides in graphite oxidation reactions. *Carbon*, **13**, 381.

[4-31] Kpteijn, F. & Mouliji, J. (1983). Kinetics of the potassium carbonate-catalyzed $CO_2$ gasification of activated carbon. *Fuel*, **62**, 221.

[4-32] Bhatia, S. & Perlmutter, D. (1980). A random pore model for fluid-solid reactions: I. Isothermal, kinetic control. *AIChE*, 26 (3), 379−386.

[4-33] Ke, Y., H., Yang, E., T., Liu, X., Liu, C., L. & Dong, W., S. (2013). Preparation of porous carbons from non-metallic fractions of waste printed circuit boards by chemical and physical activation. New Carbon Materials, 28 (2), 108-114.

[4-34] Takarada,T., Tamai, Y.&Tomita, A. (1985). Reactivities of 34 coals under steam gasification. Fule, 64 (10), 1438-1442.

[4-35] Kopyscinski, J., Habibi, R., Mims, C., A. & Hill, J., M. (2013). $K_2CO_3$-Catalyzed $CO_2$ Gasification of Ash-Free Coal: Kinetic Study. Energy & Fuels, 27, 4875−4883.

[4-36] Roberts, D., G., Harris, D., J., & Wall, T., F. (2003). On the Effects of High Pressure and Heating Rate during Coal Pyrolysis on Char Gasification Reactivity. *Energy & Fuels*, **17**, 887-895.

[4-37] Malekshahian, M. & Hill, J., M. (2011). Effect of Pyrolysis and $CO_2$ Gasification Pressure on the Surface Area and Pore Size Distribution of Petroleum Coke. *Energy & Fuels*, **25**, 5250-5256.

[4-38] Ochoal, J., Cassanello, M., C., Bonelli, P., R. & Cukierman, A., L. (2001). $CO_2$ gasification of Argentinean coal chars: a kinetic characterization. Fuel Processing Technology, 74, 161-176.

[4-39] Kopyscinski, J., Rahman, M., Gupta, R., Mims, C., A. & Hill, J., M. (2014). $K_2CO_3$ catalyzed $CO_2$ gasification of ash-free coal. Interactions of the catalyst with carbon in $N_2$ and $CO_2$ atmosphere. *Fuel*, **117**, 1181-1189.

# Chapter 5

# Conclusions and Recommendations

## 5.1. Conclusions

It was well known that there are not only a large amount of valuable metals and plastics contained in WEEE, but also some dangerous and hazardous substances [5-1]-[5-3]. Therefore, in this thesis, certain cost-effective, feasible processes and catalysts were studied and developed in attempt to effectively recover the WEEE into bromine-free fuel oil and valuable metal. Briefly speaking, first of all, the catalytic pyrolysis of Br-HIPS (typical WEEE plastic) was conducted in the presence of red mud, natural zeolite and limestone. Furthermore, from an industrial implementation point of view, the two-stage pyrolysis and catalytic reforming process was applied into the feedstock recycling of Br-HIPS in the presence of four kinds of zeolite catalysts. Last but not the least, in order to separate metals from the char and completely utilize the char resource, $CO_2$ gasification and carbonate catalyzed $CO_2$ gasification were proposed to recycle the chars derived from the medium-temperature pyrolysis of WEEE plastics.

According to the mentioned and conducted experiments and studies above, the main conclusions can be drawn as following:

★ In the thermal pyrolysis of Br-HIPS without catalyst, the optimum pyrolysis temperature for the maximum oil production (84.4 wt.%) was 500 ℃. Nevertheless, there were lots of inorganic and organic brominated compounds existing in the oil products, such as (1-Bromoethyl)benzene and $SbBr_3$ compounds. And the effect of the pyrolysis temperature on the bromine content of the oil products was slight.

★ In the catalytic pyrolysis of Br-HIPS with red mud, limestone and natural zeolite, it was found that the main compositions of oil products were styrene, ethylbenzene, 1,3-diphenylpropane, toluene etc.. And the addition of three catalysts could significantly reduce the amount of bromine and antimony content of oil products and hereby upgraded oil products.

★ In the catalytic pyrolysis of Br-HIPS, compared with limestone and natural zeolite, red mud was the most effective additives used in this research. Because, on the one hand, red mud played a cracking catalyst effect on destroying the organobrominated compounds. On the other hand, it could work as a sorbent to fix HBr formed by the Br-HIPS degradation. In addition, from the XRD and SEM-EDAX analysis of the residues, it was found that there were lots of metal bromides compounds existing in the residues, which confirmed that the reaction between bromine and metal oxides was the dominant mechanism of the bromine fixation.

★ In the two- stage combined pyrolysis and catalytic reforming of Br-HIPS with natural zeolite (NZ), HY-zeolite (YZ), iron oxide loaded natural zeolite (Fe-NZ) and iron oxide loaded HY-zeolite (Fe-YZ), respectively, it was found that all catalysts could effectively reduce the bromine content in the oil products, especially Fe-NZ and Fe-YZ.

★ In the two-stage combined pyrolysis and catalytic reforming of Br-HIPS, compared with Fe-HY, Fe-NZ did not greatly alter the yield and composition of oil products and therefore preserved the valuable single-ring aromatic compounds, such as styrene, ethylbenzene, toluene. Consequently, Fe-NZ was more effective and feasible for the feedstock recycling of Br-HISP by the pyrolysis process. The mechanism of bromine removal from the oil product was mainly attributed to the zeolite pore capture of produced $SbBr_3$ and $FeBr_3$, the catalytic reforming of the organobrominated compounds, as well as the neutralization reaction of the iron oxide with HBr derived from the decomposition of Br-HIPS.

★ As for the spent Fe-NZ, the debromination performance became weaker, which was attributed to the formation of coke and the reduction of the amount of $Fe_2O_3$. Whilst, the debromination performance of regenerated Fe-NZ was comparative with that of fresh Fe-NZ. It

illustrated that the synthesized Fe-NZ catalyst was cost-effective and recyclable for the production of valuable and low bromine content oil products from the pyrolysis and catalytic reforming of Br-HIPS.

★ In the $CO_2$ gasification of phenolic board (PB), brominated high impact polystyrene (HIPS) and acrylonitrile butadiene styrene ABS chars, as the increase of the gasification temperature and the $CO_2$ partial pressure, the time for the char conversion decreased while the reactivity index and the gasification rate significantly increased. In addition, at the same gasification temperature and $CO_2$ partial pressure, the gasification reactivity of three WEEE plastic chars was in the order of PB char > HIPS char > ABS char, which was attributed to the fact that the surface area of PB char was the largest with the lowest carbon crystalline degree.

★ In the $CO_2$ gasification of PB, HIPS and ABS chars, because their maximum gasification rate appeared in the different char conversion region (0.8, 0.45, 0.2, respectively), for PB and HIPS chars, their best fitting model was the extended random pore model (eRPM). And the shifted extended random pore model (s-eRPM) was the most suitable model to predict the $CO_2$ gasification rate of ABS char. According to the best fitting model for each char and the Arrhenius curve, the activation energy of $CO_2$ gasification of PB char, HIPS char and ABS char were 158.44, 145.94 and 128.70 kJ/mol, respectively.

★ In the catalytic $CO_2$ gasification of HIPS char with 10 wt.% $K_2CO_3$, 10wt.% $Na_2CO_3$ and mixture of 5 wt.% $K_2CO_3$ and 5 wt.% $K_2CO_3$, respectively, the addition of these three carbonate catalysts could significantly increase gasification rate and the reactivity index of the char samples, especially the addition of 10 wt.% $K_2CO_3$ could increase the reactivity index 10 times. The catalytic activity of the three catalysts for the $CO_2$ gasification of HIPS char followed the sequence of 10 wt.% $K_2CO_3$ > 5 wt.% $K_2CO_3$ + 5 wt.% $Na_2CO_3$ > 10 wt.% $Na_2CO_3$.

★ In the carbonate catalyzed $CO_2$ gasification of HIPS char, it was found that eRPM with higher regression coefficients ($R^2 > 0.99$) was more suitable for fitting than RPM. And according to eRPM and the Arrhenius curve, the addition of 10 wt.% $K_2CO_3$, 10 wt.% $Na_2CO_3$, 5 wt.%

$K_2CO_3$ + 5 wt.% $Na_2CO_3$ carbonate catalysts could reduce the activation energy of HIPS char from 145.94 KJ/mol to 78.50, 125.00, 98.23 KJ/mol, respectively.

## 5.2. Recommendations

### 5.2.1 The plant scale pyrolysis - catalytic reforming of Br-HIPS

The lab-scale two-stage pyrolysis-catalytic reforming of pure Br-HIPS plastics was conducted and the low-bromine content valuable oil products were successfully obtained. However, there are still some interesting problems and questions needed to be solved in the plant-scale pyrolysis-catalytic reforming reactor. For instance, in the above mentioned experiments, just 30 grams pure Br-HIPS plastics were tested in the lab-scale reactor. However, in the plant-scale reactor, the real Br-HIPS plastics obtained from discarded television, washing machine and refrigerator would be used. Therefore, the effect of some impurities in the used Br-HIPS plastics on the product yield and composition, as well as the debromination performance should be confirmed. In addition, the optimum pyrolysis temperature and reforming temperature should be investigated. Furthermore, the amount and the particle size of spent Br-HIPS plastics will also be expanded, therefore, whether this upgrading of sample will impact the product yield and composition should be investigated together with the debromination performance of the used catalysts. Last but not the least, the performance and cost of the catalysts, and the life time, regeneration and dispose of catalysts are still some interesting and severe problems needed to be studied and solved before the real commercial application.

### 5.2.2 The utilization of the derived oil products from the pyrolysis-catalytic reforming of Br-HIPS plastics

There are a large amounts of experiments and results reported by many researches about the application of bio-oil and plastics oil derived from the pyrolysis/ catalytic pyrolysis of biomass

and plastics, respectively [5-4] – [5-7]. Here, the real application of oil products is one of the most essential topics. One of the most popular applications for plastic oils is engine fuel. In our lab., the application of oil products derived from the catalytic pyrolysis of waste polyethylene and polypropylene plastics for the engine test have been successfully done [5-7]. Therefore, the oil products derived from the pyrolysis and catalytic reforming of real Br-HIPS plastics need to be used for the engine test.

### 5.2.3 The problem of denitrogen from the pyrolysis and catalytic pyrolysis of ABS plastics

Acrylonitrile butadiene styrene (ABS), as one of the most popular thermoplastics, is also widely used in WEEE. Because of containment of the nitrogen element in ABS plastics, high nitrogen contents in the oil product derived from the pyrolysis and catalytic pyrolysis of ABS plastics have been reported by many researchers [5-9] – [5-13]. It would hinder the usage of pyrolysis oil from the pyrolysis of ABS, and then would prevent the pyrolysis or catalytic pyrolysis process being applied for the feedstock recycling of WEEE plastics containing the ABS plastics.

In our group, we have try to utilize different pyrolysis conditions and various catalysts (HY zeolite, HZSM-5, NiO loaded HZSM-5, zeolite, red mud, dolomite, natural zeolite, $Fe_2O_3$ loaded natural zeolite and HY zeolite) in the catalytic pyrolysis and two-stage pyrolysis and catalytic reforming process, although certain catalyst could slightly reduce the nitrogen content in the oil products when compared with that of pyrolysis oil without catalysts. Especially, when ABS polymer was mixed with HIPS and was catalytic pyrolyzed in the presence of Fe-NZ, the nitrogen content in the derived oil products was reduced over 50 wt.%. Nevertheless, there are still certain amount of organic nitrogen compounds existing in the oil products, which is still a serious problem for their further utilizing. Therefore, in the future, how to remove nitrogen content from the derived pyrolysis and catalytic pyrolysis oil is still an interesting problem needed to be solved. In the case of catalytic pyrolysis process, maybe some novel and effective denitrogen catalysts are necessary to be developed.

### 5.2.4 The effect of metals contained in the WEEE on the pyrolysis and gasification processes and products

It was well known that, except for some precise and rare metals (Au, Ag, Pt, Ni, etc.) contained in WEEE, there are certain dangerous metals included in WEEE, such as lead, beryllium, mercury, arsenic and cadmium. During the pyrolysis and gasification process, if these dangerous metals was released into the environment, it will pose a serious risk for human health and environment. It was reported by Lin and co-worker that the liquid oil products derived from the pyrolysis of printed circuit board still contained certain amount of copper, lead, chromim and manganese, which would hinder the reuse of oil products [5-14]. Therefore, the controlling of dangerous metals in WEEE released into the environment and products will also be important and necessary to be considered before the industrialization and commercialization of pyrolysis feedstock recycling of WEEE.

## References


[5-1] Yang, X. N., Sun, L., S., Xiang, J., Hu, H., & Su, S. (2013). Pyrolysis and dehalogenation of plastics from waste electrical and electronic equipment (WEEE): A review. *Waste Management*, **33**, 462–473.

[5-2] Bhaskar, T., Matsui, T., Uddin, M., A., Kaneko, J., Mutoa, A., & Sakata, Y. (2003).Effect of $Sb_2O_3$ in brominated heating impact polystyrene (HIPS-Br) on thermal degradation and debromination by iron oxide carbon composite catalyst (Fe-C). *Applied Catalysis B: Environmental*, **43**, 229-241.

[5-3] Jakab, E., Uddin, M., A., Bhaskar, T., & Sakata, Y. (2003). Thermal decomposition of flame-retarded high-impact polystyrene. *Journal of Analytical and Applied Pyrolysis*, **68-69**, 83-89.

[5-4] Masimalai, S. & Venkatesan, K., (2014). Experimental Investigations on a Diesel Engine Using Coconut Shell Pyro Oil (CSPO) - Diesel Blends as Fuel. *SAE Technical*, **01**, 1377.

[5-5] Vedharaj, S., Vallinayagam, Yang, R., W., M., Chou, S., K., Chua, K., J., E. & Lee, P., S. (2014). Experimental and finite element analysis of a coated diesel engine fueled by cashew nut shell liquid biodiesel. *Experimental Thermal and Fluid Science*, **53**, 259-268.

[5-6] Yang, S., I., Hsu, T., C., Chen, K., H., Hsu, Y., L. & Li, Y., H. (2014). Application of biomass fast pyrolysis part II: The effects that bio-pyrolysis oil has on the performance of diesel engines. *Energy*, **66**, 172-180.

[5-7] Syamsiro, M., Saptoadi, M., Cheng, S., Alimuddin, Z. & Yoshikawa, K. (2013). Pyrolytic Oil Production from Municipal Plastic Waste and its Performance in a Diesel Engine. Research Association for Feedstock Recycling of Plastics (Japan). Conference proceeding.

[5-8] Hall, W., & Williams, P., T. (2008). Removal of organobromine compounds from the pyrolysis oils of flame retarded plastics using zeolite catalysts. *Journal of Analytical and Applied Pyrolysis*, **81**, 139-147.

[5-9] Bozi, J., & Blazsó, M. (2009). Catalytic modification of pyrolysis products of nitrogen-containing polymers over Y zeolites. *Green Chemistry*, **11**, 1638–1645.

[5-10] Hall, W., J., Miskolczi, N., Onwudili, J., & Williams, P., T. (2008). Thermal Processing of Toxic Flame-Retarded Polymers Using a Waste Fluidized Catalytic Cracker (FCC) Catalyst. *Energy & Fuels*, **22**, 1691–1697.

[5-11] Brebua, M., Bhaskara, T., Muraia, K., Mutoa, A. Sakata, Y. & Uddin, Md.A. (2005). Removal of nitrogen, bromine, and chlorine from PP/PE/PS/PVC/ABS-Br pyrolysis liquid products using Fe- and Ca-based catalysts. *Polymer Degradation and Stability*, **87**, 225-230.

[5-12] Jung, S., H., Kim, S., J. & Kim, J., S. (2012). Thermal degradation of acrylonitrile–butadiene–styrene (ABS) containing flame retardants using a fluidized bed reactor: The effects of Ca-based additives on halogen removal. *Fuel Processing Technology*, **96**, 265–270.

[5-13] Jung, S., H., Kim, S., J. & Kim, J., S. (2013). The influence of reaction parameters on characteristics of pyrolysis oils from waste high impact polystyrene and acrylonitrile–butadiene–styrene using a fluidized bed reactor. *Fuel Processing Technology*, **116**, 123–129.

[5-14] Lin, K., H. & Chiang, H., L. (2014). Liquid oil and residual characteristics of printed circuit board recycle by pyrolysis. *Journal of Hazardous Materials*, **271**, 258-265.

# Acknowledgement

Foremost, I would like to express my sincere gratitude to my advisor Professor Kunio Yoshikawa for his continuous support and guidance in my Doctor Period, for his patience, motivation, enthusiasm, and immense knowledge. His guidance helped me in all the time of research and writing of this thesis.

Besides my advisor, I would like to appreciate Professor Tohru Kamo and Professor Takanori Fukushima, Associate Professor Fumitake Takahashi, Koji Tokimatsu and Shiro Kajitani, as well as Assistant Professor Kiyoshi Tsuji for their valuable helps and discussions in my Doctor period.

I would like to thank Mrs. Eriko Ohno, laboratory secretary for her sincere efforts in all official works. Also thank all the research colleagues for their help and suggestion. Special thanks to my junior Mr. Noboru Harada and Mr. Qi An, who help me a lot and provided me with their precious experiences and discussion.

Last but not the least, I would like to express my special gratitude to my parents and younger sister for their unwavering support and encouragement for my study in Japan, without which I could not have persevered until now. I believe this thesis will be a good blessing and a gift to my family.

Hu Wu

February-6th-2015